Mitteilungen 101

Friction at the base of a glacier

Jürg Schweizer

Zürich, 1989

Preface

Any sliding process depends on the driving and the retaining forces. If the sliding mass is clearly defined and its motion is only due to gravity, the driving forces can easily be determined i.e. the component of weight parallel to the sliding interface. The retaining forces, however, are more difficult to evaluate, since only crude empirical relations for the assessment of the friction exist.

In modern glaciology a lot of work is involved in investigating the conditions at the glacier bed and determining the sliding motion of a glacier. The nature and the physical processes 'down at the base give rise to many questions: Which sort of friction is adequate? What is the influence of the subglacial hydraulics and what role does the debris concentration of the basal ice play?

The author of the present report, Dr. Jürg Schweizer, deals with these questions. He establishes different types of friction for typical bed characteristics and, to a certain extent, derives qualitative analytical solutions. The application of the friction model of Hallet requires a numerical treatment using the finite element method. The results show that the debris concentration in the basal ice and the subglacial water pressure dominate the sliding process.

Accordingly this study follows the extensive field observations, carried out during the last years by the glaciological section of the VAW, investigating the relation between the sliding velocity and the subglacial water pressure. The report helps to fill the gap between measurements and empirical relationships on one hand and the physical theories on the other.

The study was performed with support from the Swiss National Science Foundation and supervised by Dr. Almut Iken.

Prof. Dr. D. Vischer

CONTENTS

Abstract

The motion of glaciers and ice sheets due to gravity consists of two components: the flow and the sliding motion. The flow of an ice mass is the internal deformation. The sliding is the motion at the interface between ice mass and substratum existing only if the temperature at the interface is at the pressure melting point. The roughness of the glacier bed prevents the ice mass from slipping away: the ice is forced to flow around the bed obstacles. The classic theories usually assume that this sort of motion occurs in a frictionless way, since a very thin water film does exist between ice and underlying substratum, i.e. there is no local shear stress. This assumption may be true for clean ice, however, basal ice is debris loaden and friction occurs between the substratum and rock particles embedded in the basal ice, as can be seen from striaes on rock bumps.

The aim of this study is to investigate the influence of debris concentration on the sliding process. The actual conditions where certain types of friction apply are defined and the consequences for the sliding law are formulated. The classic Coulomb friction is modified according to the notion that a glacier is rubbing over its bed like a piece of sandpaper. For small debris concentrations the concept of Hallet applies where the friction depends on the sliding velocity. Hence a numerical approach is required. The numerical modelling of the sliding of an ice mass over an undulating bed, including the effect of both the subglacial water pressure and the friction, is done by solving the problem by the finite element method using an existing two-dimensional code.

Friction between a dirty basal layer and the glacier bed is a relevant process and can be seen as a reduction of the driving shear stress. The frictional drag can therefore be included into existing sliding laws which should contain as an important variable the critical pressure. A functional relationship between the sliding velocity, the effective basal shear stress and the subglacial water pressure is given. Considering the seasonal velocity variations, valley glaciers

may be classified according to the glacier bed characteristics and probably vice versa. A more detailed classification and the simulation of the dynamic movement of an actual glacier are two possible directions of further investigations outlined.

Zusammenfassung

Die Bewegung der Gletscher und Eisschilder beruht auf der
Schwerkraft. Man unterscheidet das Fliessen und das Gleiten.
Mit Fliessen bezeichnet man den Vorgang der internen Verfor-
mung. Ist die Temperatur am Grund des Gletschers gleich dem
Druckschmelzpunkt, so beginnt das Eis über den Untergrund zu
gleiten. Die Rauhigkeit des Gletscherbettes verhindert, dass
der Gletscher abstürzt, da das Eis die Unebenheiten umflies-
sen muss, so dass eine in der Regel gleichförmige Bewegung
entsteht. In den klassischen Theorien wird davon ausgegangen,
dass die Gleitbewegung reibungsfrei sei als Folge eines Was-
serfilms zwischen Eis und Untergrund. Somit existiert lokal
gesehen keine Scherspannung, was unter Umständen bei sauberem
Eis zutrifft. Tatsächlich aber ist das basale Eis eine ge-
schichtete Mischung aus Eis und Felspartikeln. Schliffspuren
auf Felsbuckeln zeugen von der Reibung zwischen dem felsigen
Untergrund und im Eis eingefrorenen Steinen.
Ziel dieser Arbeit ist es, den Einfluss unterschiedlicher
Schuttkonzentrationen des basalen Eises auf die Gleitbewegung
zu untersuchen. Verschiedene Arten der Reibung werden charak-
terisiert, und es werden die Auswirkungen auf das Gleitgesetz
besprochen. Die Coulomb-Reibung wird modifiziert im Hinblick
auf die Idee, dass der Gletscher wie ein Stück Sandpapier den
felsigen Untergrund abschmirgelt. Für geringe Schuttkonzen-
tration wird das Modell von Hallet verwendet: die Reibung
hängt von der Gleitgeschwindigkeit ab. Somit drängt sich eine
numerische Behandlung auf. Mit der Methode der finiten Ele-
mente wird das entstehende Differentialgleichungssystem zur
Simulation der Gleitbewegung gelöst, wobei verschiedene Para-
meter wie Schuttgehalt und subglazialer Wasserdruck, die das
Gleiten beeinflussen, variiert werden können.
Die Reibung erweist sich als ein für die Gleitbewegung mass-
geblicher Faktor. Die Wirkung der Reibung kann durch die Ein-
führung einer verminderten, effektiven Scherspannung berück-
sichtigt werden. Auf diese Weise lassen sich die für reines
Eis gültigen Gleittheorien formal auf den Fall schutthaltigen
Eises übertragen. Ein funktionaler Zusammenhang zwischen der

Gleitgeschwindigkeit, der basalen Schuttkonzentration und dem subglazialen Wasserdruck bei gegebener Schubspannung wird ermittelt. Aus der Art der saisonalen Schwankungen der Oberflächengeschwindigkeit von Talgletschern lassen sich Rückschlüsse ziehen auf die Natur des Untergrundes und die Art der Reibung. Eine detailiertere Klassifikation und die Simulation der dynamischen Bewegung eines bestimmten Gletschers sind mögliche zukünftige Forschungsvorhaben.

Chapter A

I N T R O D U C T I O N

Glaciers are moving. This fact, well known by the inhabitants of the Alpine regions, was a source of scientific controversy in the past century. The mountain-dwellers experienced the moving force of a glacier at the beginning of the Little Ice Age, when advancing Alpine glaciers passed over meadows and forests and destroyed huts (Vögele, 1987). With the awakening interest in nature in the 16th and 17th century a series of travel books appeared describing the glacierized regions with a mixture of horror and awe. In the 18th centuries the description of natural phenomena became more realistic, accurate and scientific. Horace Bénédict de Saussure (1740-1799), one of the first glaciological investigators in the modern scientific sense, held the view that glaciers slide due to gravity. One of the first very remarkable overviews of this topic was written by Bernhard Friedrich Kuhn (1762-1825), a lawyer and statesman, who grew up in the vicinity of glaciers in Grindelwald. In the 19th century major interest was concentrated on the mechanism of glacier motion. In addition to the sliding theory, the dilatation theory and the viscous flow theory were proposed and fiercely defended.

The exponent of the latter was James D. Forbes. Inspired by Louis Agassiz (1807-1873) he investigated the Mer de Glace during the same period as Agassiz did his pioneering work on the Unteraargletscher. In those times the different ideas were in strong competition with each other and it was incredible to think that both sliding and viscous flow could contribute to the motion of glaciers. A further confusing fact was that ice is brittle and viscous. Even nowadays the material properties are not fully understood and the search for a creep law forms a branch of glaciology (Clarke, 1987).

John Nye established the glacier flow mechanics, mathematically formulated, and together with John Glen's flow law, adopted from metallurgy, his studies are the fundamental base of the present research work. Finally, the recent era of investigation on the sliding problem was opened in 1957 by Hans Weertman. He proposed two sliding processes: regelation and ice flow around obstacles. John Nye and Barclay Kamb developed Weertman's idea further by introducing more realistic bed topographies. Louis Lliboutry brought up a third mechanism: the formation of subglacial cavities.

In the last thirty years extensive field observations and numerical modelling made possible by computer facilities growing at a fantastic rate have broadly enlarged the view on the sliding problem.

Sliding is not restricted to temperate glaciers where it can account for 50% or more of the total movement, but exists also under cold glaciers or ice sheets where the ice is not at the melting point. The effect is of course minimal, but not negligible in a paleoglaciological sense. Seasonal and shorter-term variations in surface velocity must result from sliding, because ice deformation depends on parameters such as ice thickness, surface slope and temperature, which do not change rapidly. Velocity variations are strongly related to the amount of water beneath a glacier, as could be shown by water pressure measurements in boreholes. Hence the subglacial hydraulic system seems to control the sliding motion. Furthermore it is now obvious that not all glaciers and ice sheets are lying on a hard rock bed as is implicitly as-

- 13 -

sumed in current sliding theories. Deformable and permeable sediment beds are widespread and certainly affect the glacier motion (Paterson, 1987).

As a result a great deal of scientific energy was and still is being concentrated on the lower boundary between the ice and its substrata. The relevant physical processes occur at this level, controlling the motion, and the complex interactions between ice, water, rock and sediment also take place there. Yet in spite of the growing knowledge the definition of a complete basal boundary condition seems to be further away than ever. However, in order to predict the behaviour of

Figure A.1   The fact that glaciers are moving can be mainly perceived by studying crevasses and moraines. Serac zone at the junction of Pers- and Morteratschgletscher.

a glacier, for instance whether, a water intake will be over-run, a sliding law is essential as a basis for modelling. An understanding of processes of glacial erosion or deposition is only possible provided it is based on a comprehensive the-ory of glacier motion.

Observations in accessible subglacial cavities (e.g. Vivian and Bocquet, 1973) and borehole photography (Engel-hardt, Harrison and Kamb, 1978) suggest that the classic sliding theories, based on the assumption of clean ice, should be modified to allow for the effect of basal debris.
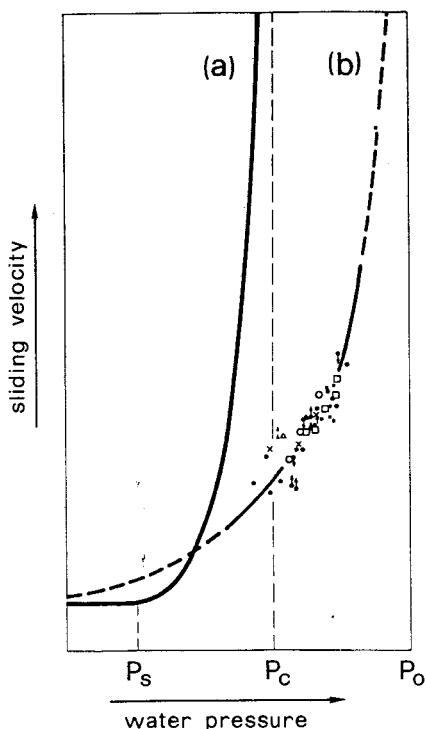

Figure A.2   Sliding velocity versus subglacial water pres-sure showing the discrepancy between theory (a) and observation (b) modified from Iken and Bindschadler (1986).

Detailed measurements of velocity and subglacial water pres-
sure at the Findelengletscher were done by Iken and Bind-
schadler (1986). Their results agree qualitatively with cur-
rent sliding theories. However, the measured water pressure
values are too large as compared to the observed sliding ve-
locities. According to theory the glacier should in some
cases have reached the state of accelerated motion (Figure
A.2). This, in fact, is not the case. It is supposed that
friction between the dirty basal ice and the glacier bed pre-
vents the glacier from slipping off.

       Only a few attempts were made to include friction in
the sliding law. Morland (1976b) studied a sort of Coulomb
friction, but without regard to the actual physical processes
at the sole. Bindschadler (1983) made implicitly the same as-
sumption by defining a bed separation index $I \sim \tau/N$ which is
equivalent to the friction coefficient. Boulton (e.g. 1976)
has dealt in full with the problem of friction in connection
with abrasion and erosion, especially in the case of soft
sediment beds. He argues that the normal load of the ice is
the relevant variable, an assumption probably true if the de-
bris concentration is very large. Hallet (1981) developed a
physical model based on what really could happen at the ice-
rock interface, if the debris concentration is small.

       This study investigates the influence of the debris
concentration in the basal ice on the sliding velocity of a
glacier for various debris concentrations. The actual condi-
tions where certain types of friction apply are defined and
the consequences for the sliding law are formulated. The
classic Coulomb friction is modified in accordance with the
notion that a glacier is rubbing over its bed like a piece of
sandpaper (Drewry, 1986). The main objective then is to ex-
tend Hallet's concept to the general case of sliding on an
undeformable bed, including both debris friction and the ef-
fect of subglacial water pressure. Hallet assumes that fric-
tion occurs due to rock particles which, embedded in the bas-
al ice, are pressed against the rigid, unpermeable rock bed
and dragged along. This process acts on the upstream side of

bed undulations. As the frictional force depends on the local velocity field, a numerical approach is required. The numerical modelling of the sliding of an ice mass over a undulating bed, including the effect of both the subglacial water pressure and the friction, is done by solving the problem by the finite-element method using the existent, well established two-dimensional code: RHEO-STAUB (Fritz and Arn, 1983). It is not possible to give a simple sliding law, but the present study can provide an idea of which variables are relevant and how they could be included in a realistic relation.

In **Chapter B** the model with assumptions, basic equations and boundary conditions is presented. The only closed form solution, the laminar flow, is derived.

The classic theories on sliding are reviewed in **Chapter C** and a relation for the amount of bed separation is developed.

Chapter D deals with debris friction. Coulomb, sandpaper and Hallet friction are compared and implications for the separation process are studied.

Details on numerical modelling including Hallet friction and bed separation, are discussed in **Chapter E.** Numercial values for the modelling are chosen on the basis of field observations and the FE-code is tested.

In **Chapter F** the results of the numerical simulations with varying flow law, bed geometry, subglacial water pressure and basal debris concentration are given.

Chapter G contains a detailed summary, conclusions and some future perspectives.

Chapter B

I C E   D Y N A M I C S

B.1   Introduction

The motion of glaciers and ice sheets consists of
two components: the **flow** and the **sliding** motion.

The flow of an ice mass is the deformation due to
the gravitational force. The critical point for the flow is
the sort of constitutive relation called flow law which means
the relation between stress and strain rate, that is, the
rheological properties of ice. The deformational process is
also called creep (continuous deformation under steady load).

Sliding is the motion at the interface between ice
mass and substratum existing only if the temperature at the
interface is at the pressure melting point. That is the clas-
sic definition. Nowadays one knows that sliding can occur
well below the freezing temperature (Shreve, 1984; Echelmeyer
and Zhongxiang, 1987), yet exercise little effect on the
large-scale motion.

The temperature of the ice is involved in the ice
dynamics too, influencing primarily the constitutive relation

and as mentioned the basal boundary condition. There is production of heat due to deformation and transport of heat within the ice mass also partly by migrating water.

Glacier ice is not an isotropic, homogenous medium. There are different sorts of ice (fabric, grain size, impurities, grain boundaries etc.), different temperature zones and cracks, crevasses and moulins; thus glacier ice is furthermore a porous medium, but usually considered to be impermeable.

In temperate glaciers where the ice is at the melting point there exists a lot of water in cracks, in crevasses and in the ice itself. The water is partially drained by the subglacial water system which, characterized by subglacial water pressure, plays a significant role in the sliding process. The state of the subglacial drainage system is supposed to be the critical point for the sort of sliding probably responsible for the surge phenomena (a tremendous glacier advance of some kilometers in some months).

Whether a glacier will advance or retreat, one of the most striking and popular features, is the effect of changing environmental conditions. Accumulation - ablation and the thermal boundary conditions control this process.

The brief discussion above has touched on some aspects involved in the problem of moving glaciers and ice sheets. The response of a glacier or an ice sheet to gravitational forces and external environmental conditions is a complicated thermo-mechanical problem (Hutter, 1983).

B.2   Assumptions and Boundary Conditions

In consideration of the great number of phenomena surrounding a glacier or an ice sheet, some simplifying assumptions must be made in order to obtain a mathematical formulation.

First of all, ice is to be considered as an imperme-
able, viscous, isotropic, incompressible fluid at constant
temperature.

The assumption of impermeability is justified since the pos-
sible water flow between grain boundaries is negligible com-
pared to the water flow through the subglacial drainage sys-
tem. Berner, Stauffer and Oeschger (1978) studied ice samples
from Griesgletscher (Switzerland) and found water flow values
between 0.02 to 0.04 m/a.

The most simple rheological law is that of constant viscosity
(Newtonian fluid). A better description of the flow of ice is
a power law, Glen's flow law, which is popular but controver-
sial. Other relations such as polynoms were proposed (Smith
and Morland, 1982) concurring more effectively with the ex-
perimental creep data. There are efforts to adapt the flow
law to the effect of impurities, different ice fabrics and
other inhomogeneities introducing, for example, an enhance-
ment factor (Dahl-Jensen, 1985). Furthermore, the question of
accelerating or tertiary creep due to recrystallization is
not clear. Aspects of ice rheology are discussed in detail by
Hutter (1983) and Lliboutry and Duval (1985).

The temperature is not regarded as independent variable and
therefore temperature and velocity field can be decoupled - a
great but unavoidable simplification. Nevertheless, in a num-
erical analysis the temperature can be taken into account
through the flow law parameter by an iterative scheme.

The boundary condition at the glacier surface is
free surface, which means free of stress, and velocity compo-
nents normal to the surface are balanced by accumulation or
ablation. Thus the glacier is in a steady state. The basal
boundary condition is the crucial one in ice dynamics. For a
cold glacier (ice temperature below the melting point) the
problem is still easy to solve. There is no sliding and the
boundary condition is the no-slip condition. Perfect-slip is
the most common condition for temperate glaciers. The basal
ice and the substratum in the following called "bed" (unde-
formable and impermeable) are therefore not in contact with
each other but separated by a very thin layer of water pre-

venting the transfer of any shear stress. Hence there is no friction at the interface. The velocity vector is parallel to the non-deformable bed since vertical components due to melting and refreezing are neglected. This is of course a small-scale view, but physically correct. Nevertheless of major interest is the large-scale view where the no-friction condition is no longer valid. At this scale one needs as bottom boundary condition a relation between basal shear stress and basal velocity, a so-called sliding law. To find an easy-to-use sliding law for large-scale glacier motion is one of the main objectives of glaciological research work.

B.3   **Basic Equations**

The assumptions from Section B.2, in particular considering ice as being an impermeable, viscous, incompressible fluid at constant temperature, result in the following set of equations for a mathematical ice flow model:

$$u_{i,i} = 0 \qquad\qquad (B.1)$$

$$\rho\, u_{i,t} = t_{ij,j} + \rho\, g_i \qquad\qquad (B.2)$$

$$\varepsilon_{ij} = f(\, t'_{ij}) \qquad\qquad (B.3)$$

expressing the mass conservation (B.1), the balance of momentum (B.2) and the constitutive relation between strain rate tensor and deviatoric stress tensor (B.3). The Einstein convention for vectors, tensors and deviations was used in the above. Stated in more detail:

u_i: velocity vector
ρ :   density of ice
t_{ij}:   stress tensor

g_i : vector of external forces (gravity)

$\dot{\varepsilon}_{ij}$: strain rate tensor

$$\dot{\varepsilon}_{ij} = 1/2 \ (u_{i,j} + u_{j,i})$$

t'_{ij}: deviatoric stress tensor

$$t'_{ij} = t_{ij} - p\delta_{ij}$$

p : hydrostatic pressure

$$p = 1/3 \ t_{ii}$$

δ_{ij}: Kronecker symbol

The upper boundary condition (stress free surface) is

$$t_{ij} \ m_j = 0 \qquad . \tag{B.4}$$

The basal boundary condition for the case of no ice-bedrock separation is either the no-slip condition

$$u_i = 0 \tag{B.5a}$$

or the perfect-slip condition

$$t_{ij}n_j - (t_{kl}n_k n_l)n_i = 0 \tag{B.5b}$$

together with a kinematic boundary condition (neglecting melting and refreezing)

$$u_i \ n_i = 0 \tag{B.5c}$$

where m_j and n's are unit vectors normal to the surface and to the bed respectively. For the case of not vanishing tangential stress, that means if there is friction between the ice and the bed, Eq. B.5b turns to

$$t_{ij}n_j - (t_{kl}n_k n_l)n_i = \tau_{fi} \tag{B.5d}$$

where τ_{fi} is the vector of the tangential traction or the frictional drag.

For the case of bed separation the boundary in the separated area is

$$t_{ij}n_in_j + p_w = 0 \quad .$$

(B.5e)

where p_w is the water pressure in the subglacial hydraulic system.

A general solution to the above equations for any given glacier geometry has not yet been found because of the nonlinearity of the constitutive relation and the complexity of the boundary conditions, and is probably not worth seeking. The alternative is to introduce more or less reasonable omissions and approximations which simplify the system. This traditional procedure established by Nye, especially the restriction to two-dimensional problems, has thrown light on quite a lot of glaciological phenomena. Another more modern approach is to try to solve the problem numerically yet offering the same sort of complications, but allowing to choose more complex domains.

An analytical solution for a cold glacier adhering at its bed is briefly presented below. Chapter C reviews some known solutions for the sliding motion problem.

B.4   Laminar Flow

The ice flow problem Eq. (1 - 5a) can be solved for a parallel, infinitly wide ice slab on an inclined plane assuming that there is no sliding: the ice is frozen to the bedrock (Figure B.1).

The infinite width leads to a two-dimensional problem. The stress tensor reduces to the components σ_x, σ_y and τ_{xy}. u and v are the velocity vector components in x and y direction respectively. From the infinite length it follows that the solution is independent of x. Thus for the stress
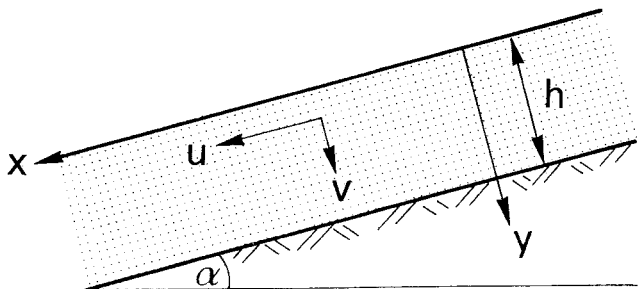
Figure B.1   Coordinate system of parallel-sided slab.
h glacier thickness, α bed slope, u,v velocity
vector components.

field one obtains

$$\sigma_x(y) \;=\; \sigma_y(y) \;=\; \rho\, g\, y\, \cos\alpha$$

$$\tau_{xy}(y) \;=\; \rho\, g\, y\, \sin\alpha$$

and the velocity is

$$u(y) \;=\; \frac{2\,A}{n+1}\, (\rho\, g\, \sin\alpha)^n\, (h^{n+1} - y^{n+1}) \qquad (B.6)$$

assuming that the constitutive relation is a power law of Glen's type

$$\dot{\varepsilon}_{ij} \;=\; A\left(t'^2_{II}\right)^{\frac{n-1}{2}} t'_{ij} \,. \qquad (B.7)$$

The flow law parameters are A: a constant including the temperature dependence of the creep, and n: the exponent in the flow law usually taking values between 2 and 4 (for n = 1 a linear relation results). $t'_{II} = 1/2\, t_{ij}t_{ij}$ is the second invariant of the deviatoric stress tensor.
The vertical velocity component is v = 0; thus the flow lines are parallel to the surface of the slab: the flow is laminar.

The velocity u_s at the surface $(y = 0)$ is

$$u_s = \frac{2\,A}{n+1}\,(\tau_b)^n\,h \qquad (B.8)$$

where τ_b is the shear stress at the bed $(y = h)$:

$$\tau_b = \rho\,g\,h\,\sin\alpha \quad . \qquad (B.9)$$

The basal shear stress is independent of the flow law. The above formula is fundamental and can explain several glaciological features as, for instance, the fact that a glacier is thin where the surface is steep, and thick where the surface slope is small (Paterson, 1983).
On the other hand, the laminar flow model is often too primitive. Some factors limit the use of Eq. (B.6) and Eq. (B.8) (Drewry, 1986):

- (a) The temperature gradient through the ice mass affecting the flow law parameter A is not taken into account.
- (b) In the case of valley glaciers, Eq. (B.8) for the shear stress has to be corrected by a shape factor (Nye, 1965).
- (c) Changes of accumulation and ablation influence the ice flux and therefore the velocity and stress field.
- (d) Longitudinal stress gradients exist but are not considered.

Nevertheless, the laminar flow model is the first consistent mathematical formulation of the glacier flow problem and therefore of broad interest.

Chapter C

G L A C I E R   S L I D I N G

C.1   Introduction

In Chapter B, a solution to the flow problem was presented whereby all motion takes place within the glacier. The ice mass is frozen to the bed and motion is due only to deformation. This is the case within cold glaciers, Alpine glaciers at high altitudes, or polar ice sheets.

Most of the measured surface velocities on Alpine glaciers are essentially larger than only the corresponding creep velocity determinable simply by surface slope and ice thickness. Findelengletscher in the Zermatt area (Swiss Alps) (Figure C.1) is, in the most intensively studied area (about 2730 m.a.s.l.), about $h = 180$ m thick and the mean surface slope is $\alpha = 6.5°$ (Iken and Bindschadler, 1986). Taking flow law parameters $A = 0.16$ bar^{-3}a^{-1} and $n = 3$, and a shape factor $f = 0.6$, a creep velocity (Eq. B.8) at the surface $u_s = 18$ m/a results. Summer velocities at Findelengletscher are in the range of 0.5 m/d, corresponding to an annual velocity of 180 m/a.
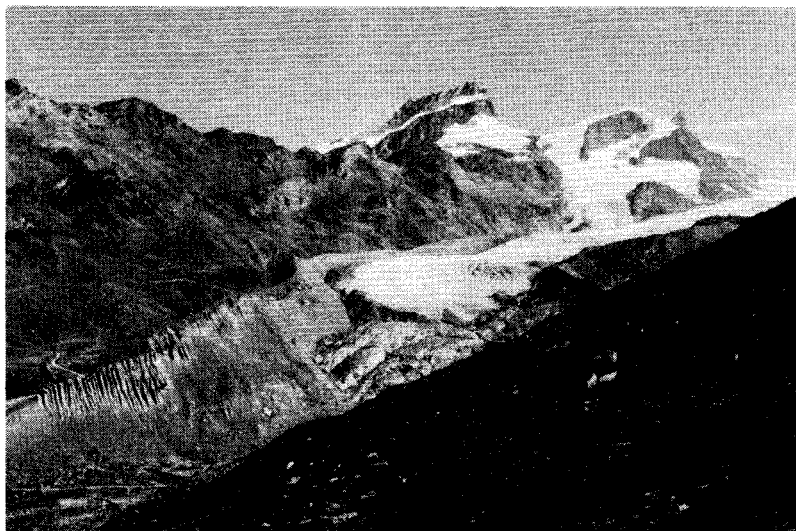
Figure C.1   Findelengletscher in 1985. Study area is above
              the first ice fall. 1985 was the end of an active
              advancing phase of the temperate, 9 km long valley
              glacier.

The difference between observed and calculated surface veloc-
ities accounts for basal sliding. Thus it is quite possible
that 90% of the motion of a glacier is due to sliding at the
ice/bed interface. Sliding velocities of some 100 m/a are not
exceptional. Jacobshavn Glacier in Greenland, a fast-flowing
ice stream, moves in the lower part at speeds of 7 km/a, yet
it is not clear whether these high speeds are mainly due to
sliding. The contribution of the sliding to the overall mo-
tion may vary temporarily and spatially on a glacier. This is
probably an effect of a different amount of water at the gla-
cier bed, an assumption based on the fact that the surface
velocity increases at the beginning of the melt season (Iken,
1978). Basal sliding is likely responsible for a large part
of the erosive effect of glaciers.
        Yet glacier sliding is one of the least understood
glaciological phenomena. Paterson (1981) writes:

"Obtaining a better understanding of sliding is
the major unsolved problem in glacier physics."

This lack of knowledge is not hard to comprehend and follows
from the difficulty to directly observe the glacier bed. Such
observations are possible in man-made ice tunnels (Figure
C.2), subglacial water intakes of hydroelectric power stati-
ons and through boreholes. Moreover, the theoretical treat-
ment of the sliding problem is complex, in particularly the
formulation of the basal boundary condition. The present
state of knowledge derives from a few contributions of a
small number of investigators: Weertman (1957), Lliboutry
(1968, 1975, 1987), Nye (1969, 1970), Kamb (1970, 1987) Mor-
land (1976a, 1976b), Hallet (1979, 1981) and Fowler (1981,
1987).

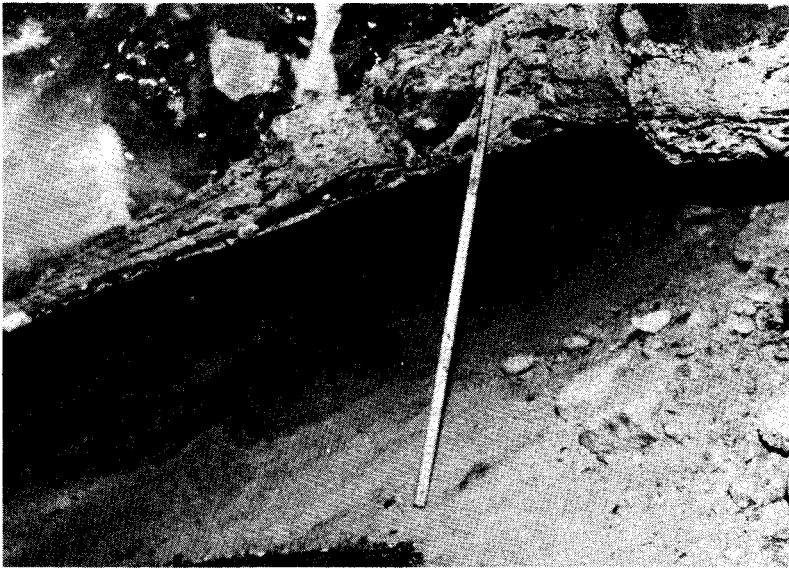Before attempting to solve the sliding problem one

Figure C.2   Basal ice and glacier bed in an ice tunnel at
the snout of Findelengletscher. The ice containing a
basal layer of debris and regelation ice is separa-
ted from the bed.

should take stoke of what is or could be going on at the base
of a glacier and then decide which phenomena one will include
in the model. An incomplete list:

- plastic deformation

- regelation (melting/refreezing around bed irregu-
  larities)

- water from   · regelation
              · geothermal heat
              · frictional heat
              · deformational heat
              · meltwater from surface ablation

- cavities, particulary in the lee (downstream
  side) of bed irregularities

- debris loaden basal ice

- friction between basal ice and substrata

- special rheology of basal ice (different
  fabric and chemical composition)

- temperature at the melting point

- different substrata (deformability, permeability)

- plucking

- etc.

Modelling means to choose the relevant factors and to neglect
the unimportant ones and simultaneously to ensure that the
resulting fluid dynamic problem is well posed.

The aim of all investigators is to find a realistic,
but simple bottom boundary condition involving some variables
describing to a certain extent the phenomena listed above.
The pertinent variables are the shear stress on the bed τ_b,
the normal stress p_n, the sliding velocity u_b, in the case of
bed separation the water pressure P_w in the cavities, and
some parameters describing roughness of the bed, and several
physical properties of ice and possibly of the glacier bed.

A review follows of some known analytical and semi-analytical solutions to the sliding problem, distinguishing between sliding without and with formation of water filled cavities leading to bed separation. The presentation follows partly the one of Raymond (1980) and Paterson (1981), but always with a critical look at the original literature and with the particular situation of Findelengletscher in mind. A special focus is on theories relating to friction between rock particles embedded in the ice and the glacier bed. Chapter D deals principally with friction.

C.2   **Sliding without bed separation**

A temperate ice mass, that is, one not frozen to the bed, can only rest stably on an inclined plane if irregularities of the bed balance out the gravitional driving force, provided there is no friction between the basal ice and the glacier bed. The upstream side of rock bumps has to be steeper than the mean bed slope (Figure C.3), otherwise the glacier is accelerating and may fall as a catastrophic ice avalanche. Thus an irregular or rough bed is one of the basic conditions.

Sliding, meaning real material motion at the icerock interface, is possible by means of two physical processes proposed by Weertman (1957): **regelation** and **creep**. Both of them enable the ice mass to overcome the obstacles at the bed. Since the ice is at the pressure melting point at the base, regelation follows from the fact that on the upstream side of rock bumps the pressure is higher than on the downstream side, leading to a difference in the pressure melting point. Thus the ice melts on the upstream side of an obstacle and is transferred as water in a very thin, only a few microns thick, layer to the lee side where it refreezes. The latent heat flows back through the rock bump to the melting
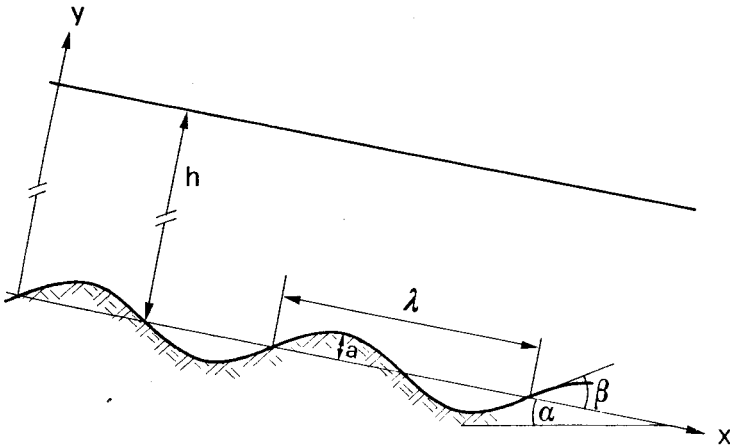
Figure C.3   Ice mass sliding over undulating bed. For stable
motion β must be larger than α.

plane in the upstream side. The thermal conductivity of the
bedrock is therefore one of the parameters controlling the
regelation process. Regelation takes place also in the exper-
iment where a weighted loop of wire slowly passes through a
block of ice without splitting the ice. The second mechanism
is enhanced plastic deformation produced by local stress con-
centrations on the upstream side of rock bumps giving rise to
enlarged strain rates and accordingly to increased flow.

    Considering these two processes, an exact analytical
solution for the sliding problem exists, if the following as-
sumptions are made:

(1)   Clean, impermeable ice is sliding over an un-
      deformable and impermeable rock surface.

(2)   There is no friction between basal ice and sub-
      stratum, which means the sole is free of local
      shear stress. In other words: the perfect-slip
      condition is assumed.

(3) No ice/bed separation. The ice sole is entirely
     in contact with the rock surface through a very
     thin water layer.

(4) Small slope and roughness of the rock bed.

(5) The ice deforms as Newtonian fluid with con-
     stant viscosity η.

     The first solution was presented by Weertman (1957)
modelling the glacier bed as an inclined plane with cubical
bumps on it. He also included a Glen type power law for the
ice rheology and determined the sliding velocity due to each
of the two sliding mechanisms alone.
The velocity u_1 is the result of the regelation process:

$$u_1 \sim \frac{\tau_b}{a \, r^2}$$

where τ_b: the average shear stress at the bed, a: the side
length of the cubical obstacles, $r = a/\lambda$:   the so-called
roughness parameter and λ : generally the wavelength of the
bed undulations or in Weertman's model of the bed the dis-
tance between cubical obstacles (from center to center of the
cubes). u_1 is inversely proportional to the obstacle length
a, thus regelation is most effective for small bumps.

The second mechanism, enhanced deformation, causes a contri-
bution u_2 to the sliding velocity u_b:

$$u_2 \sim a \left[\frac{\tau_b}{2 \, r^2} \right]^n$$

where in the above n is : the exponent in the Glen type flow
law. u_2 increases with increasing obstacle size a.

The two mechanisms, regelation and deformation, therefore
compete with each other at an intermediate obstacle size

where the two contributions u_1 and u_2 are equal. Weertman calls such an obstacle a controlling one.

The sliding velocity u_b is now derived as the sum of the processes, assuming that the controlling obstacle size completely determines the sliding velocity:

$$u_b \sim \frac{(\tau_b)^{\frac{n+1}{2}}}{r^{n+1}} \quad . \tag{C.1}$$

For the most common value of the exponent $n = 3$ the sliding velocity is proportional to the square of the basal shear stress τ_b 'and inversely proportional to the fourth power of the roughness r. The above relation is the first so-called sliding law connecting the basal shear stress, the bed topography and the sliding velocity. It is possible now to determine the basal velocity by macroscopic values such as surface slope, glacier thickness and geometry of the bed.

Lliboutry (1968), Nye (1969,1970) and Kamb (1970) improved Weertman's solution. They developed sliding theories with a more realistic model of the glacier bed for linear viscous deforming ice. The bed topography is expressed in terms of a spectral decomposition by Fourier transformation methods rendering it possible to choose an arbitrary periodic bed profile, yet many of the results were found for so called white roughness, in other words the roughness (the amplitude to wavelength ratio) is independent of wavelength.

Again they all found a characteristic wavelength called by Kamb transition wavelength λ_*, for which the contributions of regelation and deformation are equal. For wavelengths greater than λ_* the creep process dominates and regelation can be neglected, and for smaller ones accordingly vice versa. A typical value for the transitional wavelength is $\lambda_* = 0.5$ m, thus of the order of magnitude 10^{-1} m.

Kamb's definition in the case of linear flow law is:

$$\lambda_*^2 = 2 \eta (k_i + k_b) \frac{C}{\rho L}$$

where in the above k_i, k_b are: thermal conductivity of ice and bedrock respectively, C : Clausius-Clapeyron constant and L : specific latent heat of fusion.

Nye and Kamb found as a sliding law with linear rheology the relation

$$u_b \sim \frac{\tau_b}{r^2} \qquad \text{(C.2)}$$

corresponding to Weertman's solution, yet with a flow law exponent n = 1.

Lliboutry (1975) derived a simpler formula for the sliding law yet with a different representation of the bed profile (in form of spectral power density):

$$u_b = \frac{\tau_b}{m_*^2 \sqrt{\Gamma \eta}}$$

where m_* is a measure of roughness, η the ice viscosity and Γ a constant arising from the regelation process containing ice density, latent heat of fusion, thermal conductivity of both bedrock and ice, and the Clausius-Clapeyron constant.

For a sinusoidal bed with only one wavelength the sliding velocity can be given neglecting regelation as (Nye, 1969):

$$u_b = \frac{\lambda \, \tau_b}{8 \, \pi^3 \, \eta \, r^2} \qquad \text{(C.3a)}$$

or

$$u_b = \frac{\lambda^3 \, \tau_b}{8 \, \pi^3 \, \eta \, a^2} \qquad \text{(C.3b)}$$

or

$$u_b = \frac{\tau_b}{\eta \, a^2 \, k^3} \qquad \text{(C.3c)}$$

where k is the wave number $k = 2\pi/\lambda$

A numerical example is considered:

$$
\begin{aligned}
\text{glacier thickness:} \quad & h = 200 \text{ m} \\
\text{surface slope:} \quad & \alpha = 6.5° \\
\text{shape factor:} \quad & f = 0.68 \\
\text{basal shear stress:} \quad & \tau_b = 1.2 \times 10^5 \text{ Pa} \\
\text{wavelength:} \quad & \lambda = 20 \text{ m} \\
\text{roughness:} \quad & r = 0.05 \\
\text{viscosity:} \quad & \eta = 1 \times 10^{13} \text{ Pa s}
\end{aligned}
$$

producing a sliding velocity

$$
u_b = 3.87 \times 10^{-7} \text{m/s} = 12.2 \text{ m/a}
$$

a value of reasonable order of magnitude: 10^1 m/a.
The surface velocity u_s due to internal deformation of the ice

$$
u_s = \frac{1}{2 \, \eta} \, \tau_b \, h \qquad\qquad (C.4)
$$

would be

$$
u_s = 37.8 \text{ m/a}
$$

assuming the same numerical values as above. Thus the whole motion at the surface is $U = u_b + u_s = 50.0$ m/a consisting of 24% sliding and 76% deformation. The portion of sliding varies as the wavelength and inversely as the square of roughness.

In detail with Eq.(C.3) and Eq.(C.4) for sliding and surface velocity respectively, one obtains the portion of sliding on the total motion:

$$
\frac{u_b}{u_b + u_s} = [u_b] = \frac{\lambda}{4 \, \pi^3 \, r^2 \, h + \lambda} \quad .
$$

Figure C.4 shows the dependence on roughness and wavelength for the above numerical example with wavelengths of $\lambda = 5$, 10, 20, 50 m. However, the important elements are not the absolute values of λ, but the magnitude of λ relative to the glacier thickness. Since the considered glacier thickness is $h = 200$ m, the four curves in Figure C.4 correspond to the
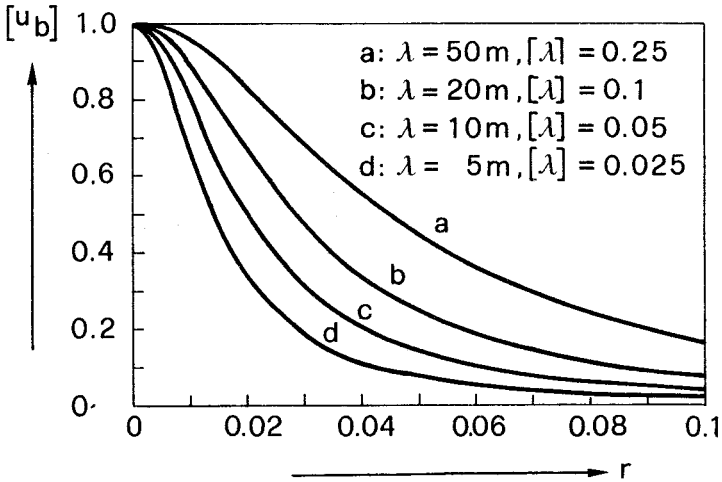
Figure C.4   Portion of sliding at the whole motion at the
             surface depending on roughness r and on wavelength
             of bed undulations. Glacier thickness is h = 200 m.
             For details see text below.

dimensionless wavelengths $[\lambda] = \lambda/h = 0.025, 0.05, 0.1, 0.25$.
Thus for a glacier 500 m thick with bed undulation wavelength
of 50 m the same curve results as for h = 200 m and a wave-
length of λ = 20 m. The curve with $[\lambda] = 0.25$ represents a
rather unrealistic case and is more an uppermost boundary be-
cause a wavelength only four times smaller than the glacier
thickness describes large-scale bed topography and no longer
bed roughness. Therefore, one can say that a high proportion
of sliding always indicates a small bed roughness or in more
general terms, a glacier bed offering not too much drag to
motion.

        The above considerations are made for the case of
linear viscosity, but are probably also true for non-linear
deforming ice, since the viscosity affects both the sliding
and the deformational surface velocity in the same way. If
there is friction at the sliding interface due to debris in
the basal ice, the sliding velocity decreases and thus the
above statement is even reinforced. The case where water

filled cavities are forming can be interpreted as a smoothing
of the bed leading to a smaller roughness, which in turn
leads to a larger sliding velocity. Again, a high proportion
of sliding corresponds to small roughness.

Kamb (1970) and Lliboutry (1975) attempted to expand
their theories to include nonlinear rheological properties.
It was only possible to reach this aim by the use of approxi-
mation methods. The second invariant of the stress deviator
called effective viscosity in the Glen type power law depends
on the strain rate itself, thus the stress distribution can-
not be determined directly, unless with iterative methods. To
avoid this complication Kamb assumes that for a given sliding
velocity and a given bed the pattern of local motion and
strain rate are approximately the same for the linear and the
nonlinear case. The effective viscosity therefore depends
only on the distance from the ice-rock interface. Lliboutry
made another simplification. In his derivation the effective
viscosity is the same for all spectral components of the bed.
The component of the transition wavelength from the solution
of the linear problem determines the value of the effective
viscosity as a lower bound.
Both authors again found a transition wavelength; it is no
longer constant, but dependent on roughness and stress dis-
tribution as a consequence of the variable effective viscosi-
ty. The sliding velocity varies in the case of white rough-
ness (constant roughness independent of wavelength) with the
shear stress as Weertman (1957) has proposed:

$$u_b \sim \tau_b^{\frac{n+1}{2}} .$$

If the short wavelengths were absent, as in a case called by
Kamb "truncated white roughness" the sliding velocity is pro-
portional to the n-th power of the basal shear stress:

$$u_b \sim \tau_b^n .$$

It makes sense to neglect the short wavelengths with regard to the well-polished rock bumps beneath former glaciers. Furthermore, the sinusoidal bed, which has only one wavelength, provides an interesting case for comparison. In addition, it is assumed that the considered wavelength is much greater than the transition wavelength ($\lambda \gg \lambda_*$), so plastic deformation dominates the sliding process. Starting with Kamb's Eqs.(92) and (96) (Kamb, 1970, p. 703) one obtains from the above simplifications a relatively simple expression for the sliding velocity:

$$u_b = \frac{[1 + \pi^2 e^2 r^2]^{\frac{n-1}{2}}}{(2\pi)^{n+2} e^{n-1} r^{n+1}} \quad \lambda \quad \left[\frac{\tau_b}{\bar{N}}\right]^n \qquad (C.5a)$$

The coefficient e is the base of natural logarithm and $\bar{N}$ originates from Kamb's definition of the nonlinear flow law and corresponds to the more usual flow law parameter A:

$$A = \frac{1}{(2\bar{N})^n}$$

or vice versa

$$\bar{N} = \frac{1}{2} A^{-\frac{1}{n}} .$$

Eq.(C.5a) can therefore be written as:

$$u_b = \frac{[1 + \pi^2 e^2 r^2]^{\frac{n-1}{2}}}{4 \pi^{n+2} e^{n-1} r^{n+1}} \quad \lambda A \tau_b^n \qquad (C.5b)$$

In the case of linear rheology where n=1 Kamb's Eq.(C.5a) is merged in Nye's Eq.(C.3a):

$$u_b = \frac{1}{(2\pi)^3 r^2} \lambda \frac{\tau_b}{\bar{N}}$$

where the parameter $\bar{N}$ in the nonlinear flow law is just equal to the linear viscosity η, so the two theories are consistent.

Kamb tested his theory with eight well-studied field examples where both basal shear stress and sliding velocity had been estimated from field mesurements of e.g. surface slope, velocity and from borehole measurements. From these values the roughness needed for agreement with the theory was calculated and compared with the expected roughness from observations of the glacier forefield. The predicted values were lower than the expected ones by a factor of 2 to 4, particulary in the examples of relatively high sliding velocity (u_b > 20 m/a) where creep dominates. From a different point of view that means that for the actual observed bed roughness a sliding velocity that is too slow would result. A possible explanation for this discrepancy would be ice-bed separation leading to an effective smoothing of the bed and therefore to a larger sliding velocity.

How does Findelengletscher, the example considered above, fit into Kamb's theory? From the numerical values given below (proposed by Iken and Bindschadler, 1986):

$$\tau_b = 1.2 \text{ bar} \quad (= 1.2 \times 10^5 \text{ Pa})$$
$$\bar{N} = 0.92 \text{ bar a}^{1/3} \text{(equivalent to A} = 0.16 \text{ bar}^{-3}\text{a}^{-1})$$
$$\lambda = 20 \text{ m}$$
$$r = 0.05$$
$$n = 3$$

follows (Eq. C.5) a sliding velocity for the case of a sinusoidal bed:

$$u_b = 114 \text{ m/a}.$$

This is an intermediate value midway between the summer and the winter sliding velocity. In 1982 the surface velocity in the summer was about 0.5 m/d and in the winter about 0.3 m/d. The extent of deformation is about 20 m/a, thus summer and winter sliding velocities of 160 m/a and 90 m/a respectively are to be assumed. If one takes a roughness of 0.02, which is a rather low value but nevertheless a reasonable one, regarding the exposed former glacier bed in front of the tongue of
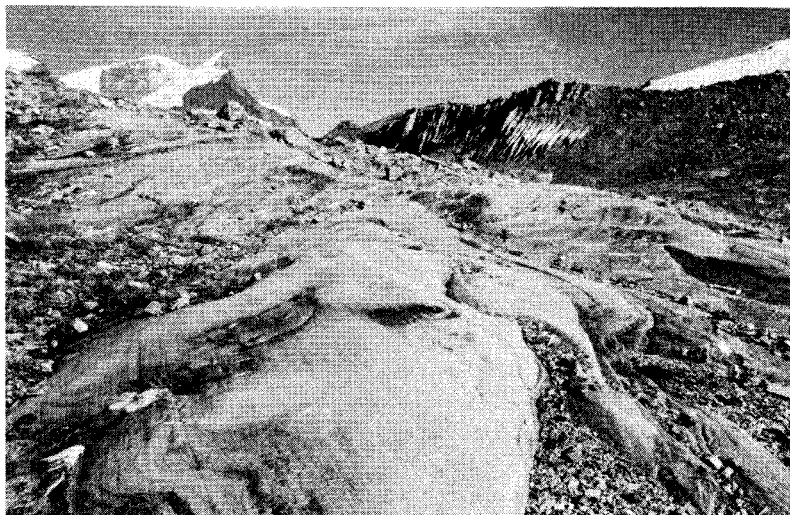
Figure C.5   Former glacier bed of Findelengletscher. Small-
            scale roughness in the centimeter range is absent.
            Glacier bed with well-polished rock bumps gives the
            impression of being very smooth. Also visible via
            chemical deposition is the extent of cavities.

Findelengletscher (Figure C.5), one obtains a sliding veloci-
ty of

$$u_b = 3860 \text{ m/a} \quad (!)$$

which really is a tremendously high, unrealistic speed.

Thus it seems that in contrary to the statement above, Eq.C.5
produces sliding velocities that are too large. It is not at
all easy to say under what sort of conditions the Kamb formu-
la for nonlinear sliding over a sinusoidal bed is appropriate
and gives reasonable values. There are several knotty ques-
tions involved:

  (1)   Wavelengths of 10, 20 m are very large compared
        to the transition wavelength which is two orders
        of magnitude smaller (in the centimeter range).

(2) An idealized sinusoidal bed has to be of about
     double roughness compared to the roughness of
     the actual bed topography. This doubling seems
     necessary to account for the fact that the gla-
     cier bed consists of several different wave-
     lengths and three-dimensional as well. Refer to
     Kamb (1970, p. 706, Table 2) where the roughness
     calcuated from a bed with truncated white spec-
     trum is about half the roughness determined from
     theory for a bed with a single wavelength.
     Therefore, if the observations suggest a low
     roughness value of 0.02, it could be appropriate
     to choose for the calculation an intermediate
     value of 0.05 to achieve agreement with field
     measurements.

(3) The dependence of the sliding velocity with the
     n+1-th power on the inverse roughness is doubt-
     ful and should be reduced (Figure C.6). The num-
     erator in Eq.(C.5) would be responsible for the
     reduction, but is not sufficiently effective as
     it is nearly independent of roughness.

The last point gives rise to an improvement made by Raymond
(1978). He proposed to take for the numerator in Eq. C.5 just
a dimensionless constant K to be determined by numerical
methodes:

$$u_b = \frac{K^n}{k \ (ka)^{n+1}} \left(\frac{\tau_b}{\bar{N}} \right)^n$$

$$= \frac{K^n}{(2\pi)^{n+2} r^{n+1}} \lambda \left(\frac{\tau_b}{\bar{N}} \right)^n \quad . \tag{C.5c}$$

For n = 1 and for low roughness (as in all theories) Nye's
formula (C.3) follows K = 1.
Raymond solved the sliding problem over a sinusoidal bed num-
erically using the finite element method, and calculated the
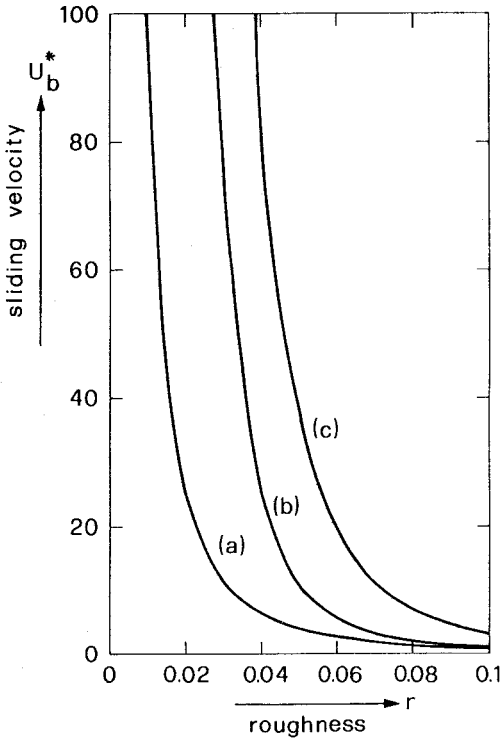
Figure C.6   Dependence of the sliding velocity (calculated
after Nye [1969] and Kamb [1970]) on the roughness
(constant wavelength λ = 20 m) for linear and non-
linear viscous flow law (n = 3). Normalized repre-
sentation:

(a) : Linear sliding velocity normalized to the value
where r = 0.1

(b) : Nonlinear sliding velocity normalized to the
value where r = 0.1 showing the much stronger
dependence on the roughness than in the linear
viscous case.

(c) : Nonlinear sliding velocity normalized to the
linear value where r = 0.1, showing the depend-
ence on the roughness compared to the linear
viscous case.

constant K from the solution for the sliding velocity. Values
of K with n = 3 are in the range of 0.5.
Kamb's numerator in Eq.(C.5) is about equal to one, thus one
order of magnitude larger than Raymond's value. Hence sliding
velocities in the km-range are no longer possible. The strong
dependence on the inverse roughness is diminshed due to Ray-
mond's improvement. But the problem is that the value of K is
known only for a very few different combinations of wave-
length and roughness.

However, the sophisticated derivation by Kamb pro-
vides the only possibility to get an idea of the effect of
the nonlinear rheology of ice. In the example of Findelen-
gletscher the sliding velocity in the nonlinear case is about
ten times larger then the one calculated by the linear theory
of Nye, a fact that can be seen well in Figure C.6. Local
stress concentrations due to bed undulations cause a soften-
ing of the ice through the stress dependent effective visco-
sity and thus lead to larger basal sliding velocities.

Members of a new generation of investigators, Mor-
land (1976a) and Fowler (1981), have reformulated the sliding
problem from a more mathematical point of view. Morland's
derivation of the sliding velocity for linear rheology veri-
fies the solution of Nye. In his theory the gravitational
force and therefore surface slope α and glacier thickness h
enter explicitly.
Again a simple solution for the sliding over a sinusoidal bed
is presented (Morland, 1976a, eq.(92)):

$$u_b = \frac{\rho g h \sin\alpha}{\eta} \frac{\omega^2 + 1}{\omega} \frac{\tilde{\lambda}_*}{r^2}$$

where $\omega = \tilde{\lambda}/\tilde{\lambda}_*$. For wavelengths $\tilde{\lambda}$ (= 1/k) much greater than
the transition wavelength $\tilde{\lambda}_*$ ($\omega \gg 1$) the above relation can
be simplified:

$$u_b = \frac{\rho g h \sin\alpha}{\eta} \frac{\tilde{\lambda}}{r^2} \quad .$$

This differs from Nye's result (a factor $8\pi^3$) in that it follows from a different definition of the wavelength. Morland furthermore presents a second order solution of the velocity and stress field for the case of a sinusoidal bed. Hence he developed a simple criterion for the onset of formation of water filled cavities which will be studied thoroughly in the next section.

Fowler introduces the idea of matched asymptotic expansions, a well known method in fluid dynamic boundary layer theory. Thus the problem is split into the flow in a basal boundary layer and the outer large scale or bulk glacial flow. The so-called sliding law is therefore the boundary condition of the outer flow at the smoothed bed and the somewhat ill-defined terms basal shear stress and basal velocity became clear from this point of view. Ill-defined because the real boundary condition at the ice-rock interface is the perfect-slip condition, thus the shear stress immediately at the base equals zero. Fowler formulates the sliding problem properly in nondimensional units. A priori assumptions as small roughness and surface slope are not necessary. The regelation process is neglected, since it is only important at the millimeter scale as is shown by scaling arguments. However, to solve the whole system (stress and velocity field) for a nonlinear flow law and an arbitrary undulating bed proves to be impossible. Nevertheless Fowler succeeds in deriving the following dimensionless form of the sliding law:

$$u_b^* = \bar{C} \, \tau_b^{\,n}$$

very similar to the ones already known. u_b^* is the dimensionless velocity and $\bar{C}$ is a function of bed topography.

In contrast to Lliboutry (1976) who argues that the Weertman type sliding law can be obtained by a simple dimensional consideration, since there would exist only four physically relevant constants: basal velocity, basal shear stress, viscosity and a constant describing the regelation process, Fowler

is convinced that a further physical parameter, the glacier
depth h, enters the sliding law. The thickness is essential
for matching the inner to the outer flow and appears in the
dimensional form of the sliding law:

$$u_b = \frac{\lambda}{h} \frac{\bar{C}}{r^{n+1}} \tau_b^n \quad .$$

Untill now all theories were based on the basal per-
fect-slip condition. As a matter of fact, friction exists at
the ice-rock interface mainly due to debris in the basal ice.
Friction occurs at single points where rock particles embedd-
ed in the ice and dragged along are in contact with the bed.
But to get a treatable analysis one must assume that the mean
effect of the individual debris contacts can be described by
friction laws which apply continously over the bed surface.
There has to exist a tangential traction τ_f at the interface.
The boundary condition (B.5bb) is modified as follows:

$$t_{ij} n_i m_j = \tau_f \quad .$$

The friction law is hence a relation between tangential trac-
tion (also called frictional shear stress or frictional drag)
and another quantity like normal stress (known as Coulomb
friction) or, for example a power of the sliding velocity.

Morland (1976b) has studied the possible effects of
friction on the sliding over a sinusoidal bed assuming linear
rheology for two different friction laws. The solution he
constructed for the Coulomb law of friction proved to be in-
valid for all possible ranges of bed inclination α, since for
all values of α extended cavity formation occurs due to ten-
sile normal tractions at the base. The tangential traction
τ_f has to be smaller than the mean downward component of the
gravity force, but is in the mathematical solution of the
same order of magnitude as the normal stress. Morland con-
cludes that the Coulomb friction is only applicable if sig-

nificant cavity formation takes place.

The second friction law Morland considers is a velocity power law producing smaller sliding velocities than one would expect and a different stress distribution at the glacier bed. The latter is important for the onset of bed separation.

Fowler (1981) also has included in his theory on sliding over a wavy bed in the absence of cavity formation the possibility of a non vanishing tangential traction. If there is friction ($\tau_f > 0$) the sliding law is:

$$u_b^\star = \bar{C} \tau^n (1 - \tau_f^\star)^n \qquad (C.6a)$$

where asterisks denote dimensionless values: $\tau_f^\star = \tau_f/\tau$. The above equation can be written in the form

$$\tau = \bar{R} u_b^{\star \, 1/n} + \tau_f \qquad (C.6b)$$

where $\bar{R} = \bar{C}^{-1/n}$ is a measure of the bedrock roughness; this implies that the shear stress τ is additively dependent on the ice flow and the frictional drag under the limiting assumption of small roughness. Seen from another viewpoint this means that in the presence of friction the driving basal shear stress is reduced:

$$\tau_b = (\tau - \tau_f)$$

and accordingly the basal sliding velocity:

$$u_b^\star = \bar{C}' (\tau - \tau_f)^n \qquad (C.6c)$$

The above result is one of the basal assumptions of Hallet's (1981) sliding theory. The principal aim of Hallet was the development of a model of bedrock abrasion by rock fragments dragged against the ice-rock interface. His general model for linear ice rheology starts just from the assumption

that the average shear stress at the base τ (due to gravity) consists of two components: the ice flow and the frictional drag (Figure C.7):

$$\tau = R\, u_b + \tau_f \quad . \tag{C.7}$$

The proportionality factor is a function of bedrock roughness and ice viscosity.

The second improvement of Hallet's theory lies in the sort of friction he is postulating. In contrast to a wide-spread assumption that friction depends on the normal so-called ice overburden pressure, hence primarily a function of the glacier thickness, he adopts the results of an early theory on abrasion by Gilbert (1910). Gilbert recognized that abrasion depends on the basal sliding velocity, the pressure exerted by rock particles on the bed, the concentration of rock fragments, the bed topography and the hardness of both the rock fragments and the bedrock.
Hallet's general model writes as follows (Hallet, 1981, Eq.(1)):

$$\tau = \xi\, \eta\, u_b + \mu\, c\, F \tag{C.8}$$

where ξ : coefficient of bed geometry
η : ice viscosity
μ : coefficient of friction
c : aeral concentration of rock particles
F : contact force between rock fragment and the bed (proportional to the ice velocity v_n normal to the bed)

Hallet's model appears appropriate for glaciers with rather small concentrations (<15% in volume) of rock fragments in the basal layer. For glaciers with a dominately debris-containing basal layer a different approach for determing the friction term in the sliding law would be required. For more details see Chapter D.

There exist no results which indicate to what extent friction of the Hallet type would slow down the glacier sliding. Hallet concentrates on the calculation of abrasion rates.

        The foregoing represents the state of the art in sliding theories without bed separation. For some years research interest has been concentrated mainly on the subglacial hydraulics and related phenomena as formation of water-filled cavities or particulary as surging glaciers.

C.3   **Sliding with bed separation**

C.3.1   Subglacial water pressure

        Fast glacier flow can be explained on the basis of the sliding theories presented above, at least insofar as surface velocities larger than the velocity due to internal deformation follow from sliding motion at the ice/rock interface. In the sliding theories mentioned, the sliding velocity u_b is a function of the basal shear stress τ_b, a fixed value for a given glacier geometry. Hence it is impossible to interpret variations of the surface velocity. As a matter of fact, there are changes, seasonal and diurnal, in glacier flow as many observations illustrate (e.g. Aellen and Iken, 1979).

Increased velocity after heavy melting or rain suggests that water at the base influences the sliding velocity. This occurs mainly from surface meltwater penetrating through the glacier to the bed, and not by means of water originating from geothermal heating or from the regelation process. At the base the water flows partially delayed through a system of passageways, channels and connected cavities, forming in

the lee of bed undulations, to the terminus, where often only
one, or a few, large tunnels exist. Thus the water pressure
P_w in this complex subglacial hydraulic system can be chosen
as a further relevant variable in a realistic sliding law.
Since the cavities are interconnected, the water pressure is
the same in all cavities, neglecting differences in altitude,
described by Lliboutry (1976) as interconnected hydraulic re-
gime.
However, the hydraulic system itself is varying, for instance
at the beginning of the melt season: the cavities are grow-
ing, passageways between cavities are forming, tunnels are
reopening. Iken (1981) and Iken et al. (1983) calculated and
observed that the sliding velocity is a maximum when the cav-
ities are growing. Probably both the water pressure and the
state of the subglacial hydraulic system influence the slid-
ing velocity.

Lliboutry (1958) was the first to point out that in
addition to the two processes, introduced by Weertman (1957),
regelation and deformation, a third one, that is, flow with
cavitiy formation, should be considered.

Figure C.7   Cavity in an ice tunnel near the tongue of
              Findelengletscher

The compressive stress $p_n(x,y)$ normal to the bed due to gravity varies according to the varying geometry along the glacier bed. At locations where p_n becomes tensile, most likely on the downstream side of rock bumps, the ice will separate from the rock to form a cavity. Wherever the water pressure P_w is larger than the normal stress p_n water will intrude between ice and rock to form a water-filled cavity. There exist many observations of air and water-filled cavities (Figure C.7).

Hence the formation of water-filled cavities depends on the difference between p_n and P_w. As soon as

$$P_w > p_n(x,y) \tag{C.9}$$

the condition for cavities to form is given. To get a more handy relation the local varying stress $p_n(x,y)$ is substituted by the pressure P_0, the average normal stress $p_n(x,y)$ and equal to the weight per unit area of the ice. P_0 is usually called ice overburden pressure. A new parameter can be given by

$$N = P_0 - P_w \tag{C.10}$$

where N is known in the literature as effective normal pressure. The smaller the effective pressure N, the more extended is the bed separation.

Cavities in the lee of bedrock bumps reduce the roughness and so increase the sliding velocity. By introducing the effective pressure N in the sliding law it seems to be possible to explain velocity fluctuations.

C.3.2   Classic theories

Lliboutry (1958, 1968, 1979, 1987a,b) has with great effort studied in detail the problem of sliding with forma-

tion of subglacial cavities. In 1968 he published a paper en-
titled "General theory of subglacial cavitation and sliding
of temperate glaciers". Nearly twenty years later (1987a) he
wrote in the conclusions, p. 9109, of the paper "Realistic,
yet simple bottom boundary conditions for glaciers and ice
sheets": "We have tried to expose clearly the main concepts
which have been successively introduced in sliding theory ...
The most important ones are (1) a sliding law holds for some
space scale only, and (2) for a given space scale, the law
may be completely different according to the models which are
adopted for the microrelief and for the subglacial hydrau-
lics." In other words, a general sliding law fiercely claimed
by modellers and by applied glaciologists is not yet in
sight. In the following section some steps in the development
indicated are pointed out.

In 1958 Lliboutry found that the friction due to the
process of flow with cavity formation varies as $u_b^{-1/2}$, a
result corrected in 1959 to $u_b^{-1/n+2}$. Assuming that the fric-
tion of the three processes contributing to sliding are addi-
tive a total friction results

$$\tau_b = \frac{1}{2} \pi r N$$

independent of the speed of sliding u_b. In this case sliding
is reduced to a simple Coulomb friction relation, in which
the ratio τ_b/N gives the equivalent coefficient of friction.

In 1979 he derived the following general relation between τ_b,
u_b, and N :

$$\tau_b = k N f \left(\frac{N^n}{u_b} \right)$$

where k is a constant. For the case of a bed profile of ran-
dom bumps of similar rather large wavelengths (compared to
the transition wavelength), he found:

$$\tau_b = k_1 u_b^{1/n} + k_2 N\tilde{F} + k_3 u_b^{2/n+1}$$

where $\tilde{F}$ is a function of the properties of the bed profile, and k_1, k_2, k_3 are constants.

In Lliboutry (1987a,b) the sliding problem is split for different length scales: a decimetric scale corresponding to the transition wavelength and usually included in the classic theories, a decametric scale yielding sliding laws to be used in mountain glacier modelling and thirdly, a kilometric scale relevant for ice sheet modelling. At the intermediate scale for a gently undulating profile with random roughness, an asymptotic sliding law can be given:

$$\tau_b = k_4 N + k_5 u_b N^{1-n}$$

where k_4 and k_5 denote constants depending on the distribution of the bump heights and on typical bed and ice properties respectively. The asymptotic sliding applies in case of extended bed separation and therefore large sliding velocity. When no bed separation occurs a different sliding law,

$$u_b = k_6 \tau_b^n + k_7 \tau_b$$

not consistent with the above one, is postulated. It is not clear how the transition between the two sliding laws operates.

Fowler (1986) reformulated the sliding with bed separation as a Hilbert problem and presented a solution for the particular case of a periodic bedrock. The deduced sliding law for ice as linear viscous material can be written dimensionlessly in the form

$$\tau_b^{\star} = p^{\star} f\left(\frac{u_b^{\star}}{p^{\star}}\right)$$

where asterisks denote dimensionless variables. Given in more detail, the values are $\tau_b^* = \tau_b/[\tau]$, $u_b^* = u_b/[u_b]$ and $p^* = \bar{r}\, N/[\tau]$, where $[\tau]$ and $[u_b]$ are typical values for basal velocity and shear stress and $\bar{r}$ is a sort of roughness. The dimensional sliding law is therefore

$$\tau_b = \bar{r}\, N\, f\left(\frac{u_b}{N}\right) \quad .$$

Generalized for a non-Newtonian flow law

$$\tau_b = \bar{r}\, N\, f\left(\frac{N^n}{u_b}\right) \quad ,$$

a relation strongly resembling the one developed by Lliboutry (1979). Thus Fowler partially reproduced Lliboutry's results.

Fowler's basic result is that, for the sort of bedrock profiles studied, the sliding law is multi-valued as illustrated by Hutter (1982) (Figure C.8). The surge behavior suggests
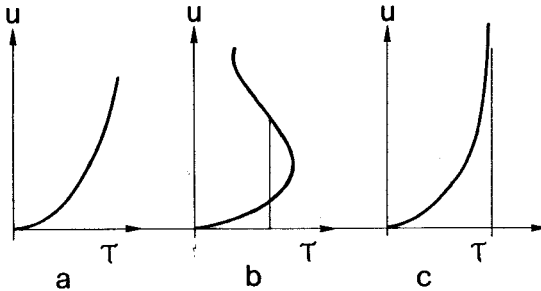

Figure C.8   Sliding velocity as a function of basal shear stress (from Hutter 1982b).
      a) Regular "Weertman-type" sliding law
      b) Sliding law with a range of basal shear stress for which the sliding velocity is multi-valued
      c) For a critical value of the shear stress sliding velocity grows fast.

such a solution. Fowler nevertheless expects that for a gen-
eral bedrock profile a single-valued sliding law would result
and that the surge phenomenon could be explained by the
different state of the subglacial hydraulic system, an as-
sumption based on recent results of the 1982-1983 surge of
Variegated Glacier (Kamb et al. 1985, Kamb 1987).

Fowler doubts whether the often used "generalized Weertman
law" of the form

$$\tau_b = u_b^{\alpha} N^{\beta}$$

is appropriate to describe fast sliding. However, the results
of an experimental study by Budd et al. (1979) and an analys-
is by Bindschadler (1983) support the above relation. They
propose $\alpha = \beta = \frac{1}{3}$. Thus the sliding law can be given in the
popular form

$$u_b = k \frac{\tau_b^3}{N} \tag{C.11}$$

The sliding law (Eq. C.11) is frequently used in ice sheet
models as shown in an overview by Bentley (1987).
Hence no sophisticated law, but a very crude relation between
some of the relevant parameters, is used without any regard
for the recent development. The above relation (C.11) can
perhaps be matched with field data but has less to do with
the physics down at the glacier base. The sliding law de-
scribed is a simple empirical relation between sliding veloc-
ity and subglacial water pressure.

C.3.3   Sliding over a sinusoidal bed

The sliding over a perfectly lubricated sinusoidal
bed is a well-studied particular case of the sliding problem
(e.g. Lliboutry, 1968). It is therefore worthwhile to focus

on it more closely and develop some details such as separation and critical pressure. In the section below only the process of enhanced creep is considered; regelation is neglected.

C.3.3.1 Stress distribution without bed separation

On a sinusoidal bed the stress distribution normal to the bed is principially given by the vertical and horizontal force balance (e.g. Raymond, 1980, eq.46a,46b). Here horizontal means parallel, vertical means perpendicular to the average bed slope (Figure C.3). The direction perpendicular to the local (oscillating) bed is considered "normal".
The pressure which the sliding ice mass exerts vertically on the bed is on the average equal to the ice overburden pressure $P_0 = \rho gh \cos\alpha$, but due to the undulating bed, it is oscillating: larger than the ice overburden pressure on the upstream faces of bed undulations and smaller on the downstream faces. In the down-glacier direction the force balance requires that the sum of components in x-direction of the normal stress $p_n(x)$ is equivalent to the average shear stress $\tau = \rho gh \sin\alpha$. In detail for a two-dimensional model (Figure C.3)

$$\tau = \frac{1}{\lambda} \int_0^\lambda p_n(x) \frac{\partial y_b(x)}{\partial x} \, dx \qquad (C.12)$$

and

$$P_0 = \frac{1}{\lambda} \int_0^\lambda p_n(x) \sqrt{1 - \left(\frac{\partial y_b(x)}{\partial x}\right)^2} \, dx \qquad (C.13)$$

In the above equations an approximation for small roughness $(r \leq 0.1)$ is already included

$$\sin \beta \approx \tan \beta = \frac{\partial y_b(x)}{\partial x} \quad .$$

where β is the angle of the local bed compared to the mean bed (see Figure C.3) and $y_b(x)$ describes the bed geometry

$$y_b(x) \quad = \quad a \, \sin \, (\frac{2\pi x}{\lambda}) \quad .$$

Since the normal stress $p_n(x)$ is undulating as mentioned above it can be given as

$$p_n(x) \quad = \quad p \quad + \quad \Delta p(x)$$

where p is a constant and $\Delta p(x)$ a fluctuating contribution. It is reasonable to choose the following expression for the normal stress:

$$p_n(x) \quad = \quad p \quad + \Delta p_{max} \cos \, (\frac{2\pi x}{\lambda}) \qquad (C.14)$$

assuming that the normal stress is varying with the same wavelength as the glacier bed.
The two unknowns, p and Δp, can be determined by the balance conditions (Eq. C.12 and C.13)

$$\tau \quad = \quad \frac{1}{\lambda} \int_0^\lambda \Delta p_{max} \, \cos \, (\frac{2\pi x}{\lambda}) \, \frac{\partial y_b(x)}{\partial x} \, dx \quad (C.12a)$$

$$P_0 \quad = \quad \frac{1}{\lambda} \int_0^\lambda [p + \Delta p(x)] \, \sqrt{1 - \left[\frac{\partial y_b(x)}{\partial x}\right]^2} \, dx \qquad (C.13a)$$

Usually it is tacitly assumed that

$$\sqrt{1 - \left[\frac{\partial y_b(x)}{\partial x}\right]^2} \quad = \quad 1$$

and with

$$P_0 \quad = \quad \frac{1}{\lambda} \int_0^\lambda p \, dx$$

it follows that the constant contribution is equal to the ice overburden pressure

$$p = P_0 \quad .$$

The usual assumption as given above is only valid for small roughness. The integral in Eq.(C.13a) can be solved numerically, which was done for the special case of a sinusoidal bed profile with $\lambda = 2\pi$ and different values of the wave amplitude to
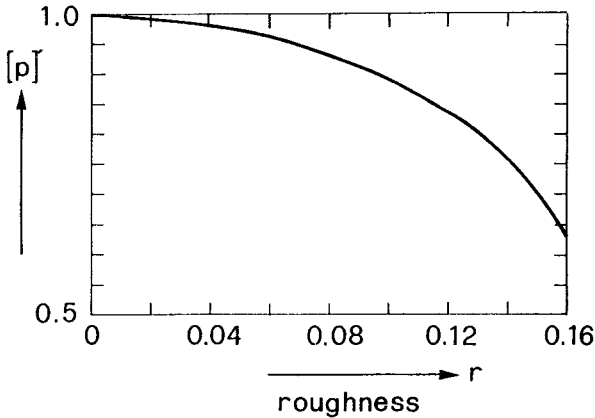

Figure C.9   Constant contribution [p] to the fluctuating normal stress p_n in dependence on the roughness r. For $r \leq 0.01$, $p \approx P_0$ follows. [p] is dimensionless and normalized [p] = p/P_0 .

take into account different roughness. The result for a quarter of a wavelength varies between $\pi/2$ and 1 for an amplitude range of $0 \leq a \leq 1$. Figure C.9 shows that the assumption $p = P_0$ is justified for a roughness $r \leq 0.1$ (the deviation is in this case less than about 10%).
The balance condition parallel to the mean bed slope requires

$$\tau = \frac{2\pi a}{\lambda^2} \Delta p_{max} \int_0^\lambda \cos^2(\frac{2\pi x}{\lambda}) \; dx \quad .$$

The integral expression is equal to $\lambda/2$ and therefore

$$\Delta p_{max} = \frac{\lambda\tau}{a\pi} \quad . \tag{C.14}$$

Thus finally the local normal stress which the ice exerts on the bed can be expressed (for small roughness only) as

$$p_n(x) = P_0 + \frac{\lambda\tau}{a\pi} \cos(\frac{2\pi x}{\lambda}) \tag{C.15}$$

C.3.3.2 Bed separation: separation and critical pressure

For large values of the fluctuating contribution to the normal stress

$$\Delta p_{max} > P_0$$

the normal stress becomes tensile, that means the ice will separate from the glacier bed without any effect of basal water: an air-filled cavity is forming unless water exists at the base. The condition for tensile stresses at the bed is

$$\tan \alpha \geq \pi r$$

where α is the mean bed slope and r $(= a/\lambda)$ the roughness. The above relation can be deduced considering that

$$\tau = P_0 \tan \alpha \quad .$$

If the normal stress is compressive everywhere, bed separation takes place only at a sufficiently large subglacial water pressure. If the water pressure reaches the minimum normal stress bed separation starts and water-filled cavities form. The so-called separation pressure P_s is well established and has been introduced in the classic sliding theories (Lliboutry 1958, Nye 1969, Kamb 1970, Morland 1976a). The separation condition can be given as

$$P_w = P_s = P_0 - \frac{\lambda \tau}{a \pi} \qquad (C.16)$$

or with $\tau = P_0 \tan \alpha$

$$P_s = P_0 - \frac{\tau}{\pi \, r}$$

The water pressure at which the sliding ice mass attains the state of unstable motion is called critical pressure P_c. It is well-known that usually the critical pressure is below the ice overburden pressure. Therefore, it is probably preferable to introduce the critical pressure rather than the effective one in a possible sliding law. A derivation is presented by Iken (1981) and Iken and Bindschadler (1986) regarding an ice mass resting on a rectangular stepped bed profile. In this special case the critical pressure corresponds to the force moving the ice mass upward along the stoss faces with accelerating velocity. Details are given in Section D. Independent of the sort of bed profile the critical pressure can be written as (Iken, 1981)

$$P_c = P_0 - \frac{\tau}{\tan \beta} \qquad (C.17)$$

where in the above P_0: the overburden pressure, τ: the basal shear stress and β: the angle which the stoss faces make with the mean downstream slope.

For the special case of a sinusoidal bed, the steepest tangent of the stoss face is

$$(\tan \beta)_{max} = \frac{2\pi a}{\lambda}$$

and thus

$$P_c = P_0 - \frac{\lambda \, \tau}{2\pi a} \qquad (C.17a)$$

or

$$P_c = P_0 - \frac{\tau}{2\pi r} \qquad .$$

This means in general that the critical pressure is always halfway between the ice overburden and the separation pressure
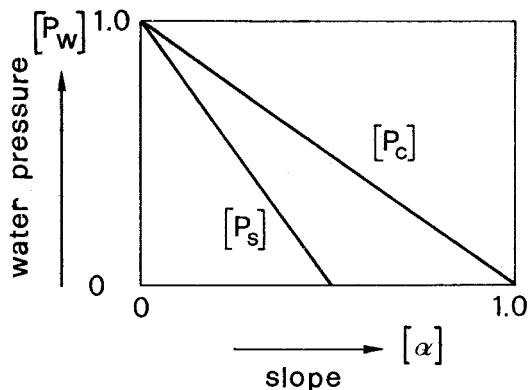
$$P_C = \frac{1}{2}(P_0 + P_s) \quad .$$

Figure C.10 Dependence of dimensionless, normalized critical pressure $[P_C] = P_C/P_0$ on dimensionless slope parameter $[\alpha]$.

Figure C.10 shows that on a horizontal bed the glacier is afloat only if the water pressure exceeds the ice overburden pressure: $P_s = P_C = P_0$.

In Figure C.10 a measure for roughness and average bed slope is introduced defined as follows

$$[\alpha] = \frac{\tan \alpha}{(\tan \beta)_{max}} = \frac{\tan \alpha}{2\pi r} \quad .$$

The critical pressure varies as roughness and inversely as bed slope. One can easily see that for a very smooth, perfectly lubricated glacier bed only a small amount of water pressure is necessary to initiate the accelerating motion, an effect even enlarged for increasing slope. In other words, as one would expect a glacier is most stable on a gentle and rough slope.

C.3.3.3 **Bed separation: stress distribution and cavity length**

If the water pressure exceeds the minimum normal stress the ice exerts on the bed, the ice separates from the bed and water-filled cavities will form. This happens in the lee of bed undulations. The stress distribution (Eq. C.15) which determines the bed separation is changed itself by the bed separation. Hence, the formation of water-filled cavities is distinctly a dynamic process. The subsequent balance considerations describe only a singular transient state and can help to understand the process of bed separation, but cannot fully describe the dynamics.

It is assumed that a cavity forms symmetrically around the inflexion point ($x = \lambda/2$) on the lee side of a rock bump. The length of the separated zone is 2l (see Figure C.11). The bed separation is described by the bed separation parameter $s = 2l/\lambda$. To determine the stress distribution after the separation and to give the cavity length at a certain water pressure, we make the assumption that the force balance parallel and perpendicular to the mean bed slope has to be fulfilled. Otherwise an accelerating force would arise, which is not allowed, since glaciers move with constant velocity (at constant water pressure) even when the ice is partly separated from the bed. The movement becomes unstable only if the water pressure exceeds the critical pressure.

The stress distribution along one wavelength of the sinusoidal bed can be given as follows:

$$
\begin{aligned}
p_n'(x) &= p' + \Delta p' \cos\left(\frac{2\pi x}{\lambda}\right) &&\text{for } -\frac{\lambda}{2}+l \leq x \leq \frac{\lambda}{2}-l \\
&&&\qquad\qquad\qquad\text{(C.18)} \\
p_n'(x) &= P_w &&\text{for } \frac{\lambda}{2}-l \leq x \leq \frac{\lambda}{2}+l \quad .
\end{aligned}
$$

The continuity at the end of the cavity requires

$$
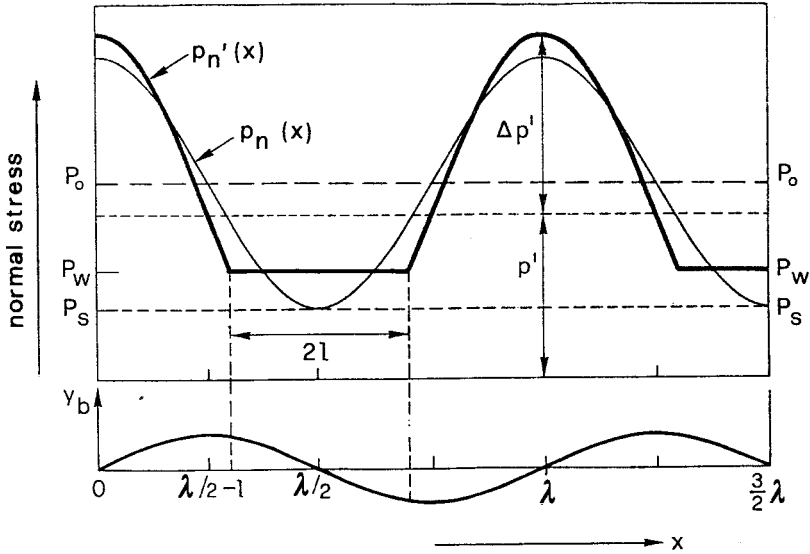P_w = p' + \Delta p' \cos\left(\frac{2\pi}{\lambda}\left(\frac{\lambda}{2} + l\right)\right) \quad .
$$

Figure C.11 Bed geometry and stress distribution before $(p_n(x))$ and after $(p_n'(x))$ bed separation

Hence the constant contribution p' is

$$p' = P_w + \Delta p' \cos(\frac{2\pi l}{\lambda})$$

and thus

$$p_n'(x) = P_w + \Delta p'[\cos(\frac{2\pi l}{\lambda}) + \cos(\frac{2\pi x}{\lambda})] \ . \qquad (C.19)$$

This expression reduces to equation C.15 when bed separation ceases ($l = 0$, $P_w = P_s = P_o - \Delta p_{max}$).

The amplitude of the fluctuating contribution can be deter-
mined considering the force balance. In y-direction the mean
stress perpendicular to the bed has to be equal to the ice
overburden pressure P_o. As the stress distribution is symmet-
rical to the inflexion point in the lee of the bed undula-
tion, only half a wavelength is considered.

$$P_o \lambda/2 = \int_{\lambda/2}^{\lambda} p_n'(x) \, dx$$

$$P_o \lambda/2 = \int_{\lambda/2}^{\lambda/2+1} P_w \, dx + \int_{\lambda/2+1}^{\lambda} p_n'(x) \, dx$$

$$= P_w 1 + \int_{\lambda/2+1}^{\lambda} \left[P_w + \Delta p' [\cos(\frac{2\pi 1}{\lambda}) + \cos(\frac{2\pi x}{\lambda})] \right] dx$$

It follows that

$$P_o = P_w + \Delta p'[\frac{1}{\pi} \sin \pi s + \cos \pi s (1 - s)]$$

or

$$\Delta p' = \frac{\pi (P_o - P_w)}{\pi (1 - s) \cos \pi s + \sin \pi s} \qquad (C.20)$$

The stress distribution is not yet determined, since we do not know the bed separation parameter s, nor the water pressure P_w. To find a relation between these two variables the force balance in x-direction (parallel to the mean bed) is considered. The sum of the stress components in x-direction has to be equal to the driving shear stress:

$$\tau \lambda = \int_{-\lambda/2+1}^{\lambda/2-1} \left[P_w + \Delta p' [\cos(\frac{2\pi 1}{\lambda}) + \cos(\frac{2\pi x}{\lambda})] \right] \frac{\partial y_b}{\partial x} \, dx$$

$$+ \int_{-\lambda/2+1}^{\lambda/2-1} P_w \frac{\partial y_b}{\partial x} \, dx \quad .$$

It follows that

$$\tau = \frac{a}{\lambda} \Delta p' [\cos \pi s \sin \pi s + \pi(1 - s)] \quad . \qquad (C.21)$$

In Equation C.21 the water pressure no longer appears. So $\Delta p'$ can be given by choosing a value of the bed separation parameter s. Together with Equation C.20 the corresponding water pressure can be calculated. Hence, by combining Equations

C.20 and C.21 one gets a functional relationship between the subglacial water pressure and the bed separation

$$P_w = P_o - \frac{\lambda\tau}{\pi a} \left(\frac{\sin \pi s + \pi(1 - s)\cos \pi s}{\sin \pi s \cos \pi s + \pi(1 - s)}\right) \quad (C.22)$$

or otherwise

$$\tau = \pi r (P_o - P_w) \frac{\sin \pi s \cos \pi s + \pi(1 - s)}{\sin \pi s + \pi(1 - s)\cos \pi s}$$

In order to make the expression independent of the geometry a new dimensionless water pressure $[\bar{P}_w]$ is introduced

$$[\bar{P}_w] = \frac{\Delta p_{max} - (P_o - P_w)}{\Delta p_{max}} = \frac{P_w - P_s}{P_o - P_s} \quad . \quad (C.23)$$

At the separation pressure $[\bar{P}_w] = 0$, at the critical pressure $[\bar{P}_w] = 0.5$ and the ice overburden pressure corresponds to $[\bar{P}_w] = 1$. With $[\bar{P}_w]$ it follows that
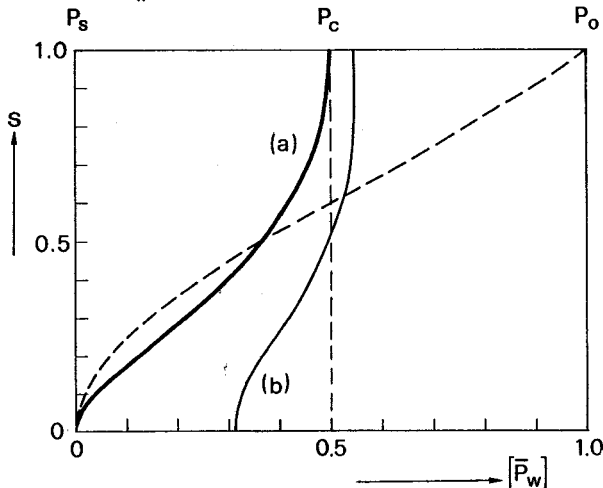

Figure C.12   Bed separation as a function of the subglacial water pressure for a sinusoidal bed: (a) without friction, (b) with sandpaper friction ($\mu = 0.1$, Eq. D.22). Broken line indicates erroneous solution, if the force balance in y-direction alone is consider-ed.

$$[\bar{P}_w] \ = \ 1 - \frac{\sin \pi s + \pi(1 - s)\cos \pi s}{\sin \pi s \cos \pi s + \pi(1 - s)} \qquad (C.22a)$$

Figure C.12 shows the bed separation as a function of the subglacial water pressure assuming that the force balance in y-direction over the cavity length is the same as without bed separation (a condition which holds for small cavities only). In contrast to the theories of Lliboutry (1968), Fowler (1986) and Kamb (1987), the critical pressure where the ice is practically fully separated from the bed is the crucial variable.

Neglecting the force balance in x-direction leads to a much smaller bed separation, indicated in Figure C.12 by a broken line. In that case, at the critical pressure the bed separation parameter is not s = 1 but s ≈ 0.6 and reaches s = 1 at the ice overburden pressure. This misunderstanding gives rise to an overrating of the effective pressure N which in our opinion should not appear in a realistic sliding law.

Friction between the basal ice and the bed can be introduced in Equation C.22, assuming that friction can be seen as a reduction of the driving shear stress. The effect on the bed separation is shown in Figure C.12 (line (b)) by an example where the friction coefficient is μ = 0.03, calculated by substituting τ in Equation C.22 with the effective basal shear stress $\tau_b = \tau - \tau_f$:

$$\tau - \tau_f \ = \ \pi r \ (P_o - P'_w) \ \frac{\sin \pi s \cos \pi s + \pi(1 - s)}{\sin \pi s + \pi(1 - s)\cos \pi s} \qquad (C.24)$$

Here it has been neglected that the friction slightly changes the stress distribution. Further details on friction follow in the next chapter.

C.3.4   Possible sliding law

        In the sliding law generally used (Eq.C.11), the
sliding velocity varies as the inverse effective pressure.
For constant shear stress the sliding velocity tends to in-
finity if the water pressure reaches the ice overburden pres-
sure. Most glaciers attain this state of accelerated motion
not at a well-defined value such as the ice overburden pres-
sure. Some never become instable, probably since the glacier
bed offers too much drag or a high water pressure cannot
build up. From the theoretical treatment of the sliding over
a sinusoidal bed it seems clear that one of the pertinent
variables to introduce in a sliding law is the critical pres-
sure, more exactly the difference between the acting water
pressure and the critical pressure. Also the separation pres-
sure as a point where the sliding velocity is increasing due
to cavity formation should appear in a realistic global bot-
tom boundary condition. Unfortunately it is not possible to
give a general relation for all possible values of the water
pressure, particulary for the sliding without bed separation
($P_w = 0$). The expression proposed below are intended to give
an idea how a possible sliding law could look

$$u_b \sim \tau_b^n \qquad \text{for} \quad P_w < P_s \ ,$$

and for sliding with bed separation

$$[u_b] \sim \left[\frac{\tau_b}{P_c - P_w}\right]^n \qquad \text{for} \quad P_w > P_s \ . \quad (C.25)$$

Such a functional relationship could describe the results of
the extended water pressure and surface velocity measurements
at Findelengletscher (Iken and Bindschadler, 1986), however
only in a qualitative sense.
From the calculation of the critical pressure for the case of
Findelengletscher follows a much too small value compared to
the measured water pressure values. The glacier should be at

the most in a state of unstable motion, what is actually not the case. Thus, with the above theory a too low value for the critical pressure results. Probably friction at the base between rock particles embedded in the ice and the rock bed gives rise to a higher value of the critical pressure. This aspect of the problem is examined more closely in Chapter D.

Chapter D

F R I C T I O N

D.1   Introduction

        A glacier does not slide frictionlessly over its bed
as assumed in most of the theoretical work (Weertman, 1957,
Lliboutry 1968, Nye 1969, 1970, Kamb 1970, Morland 1976a,
Fowler 1981). This fact is obvious and can be seen via erosi-
ve patterns such as grooves and striaes on ruck bumps in the
forefield of glaciers (Figure D.1).

        Basal ice generally contains debris in varying con-
centrations and sizes. When a glacier is sliding over a bed
of rigid or deformable substrata, there is some rock-to-rock
friction slowing down the sliding motion. The result of this
rubbing contact is abrasional wear with production of wear
debris. The most important factors for abrasion are the hard-
ness of both the rocks held in the ice and the bedrock, the
relative velocity between rock particle and bed (not a priori
equal to the sliding velocity) and the contact force by which
the clast is pressed against the bed (Drewry, 1986).

Figure D.1   Grooves on a rock bump near the front of
              Limmerngletscher (Glarnese Alps).

There have been several attempts to describe this phenomena
and there are quite different friction laws (Lliboutry 1979,
Morland 1976b, Reynaud 1973, Boulton 1974, Hallet 1979).
        A dynamic friction law connects a friction force al-
ways opposite to the direction of motion, to any characteris-
tic properties of the bodies involved. Thus there is a fun-
damental difference between sliding and friction laws. In
that sense the so-called solid friction law (Liboutry, 1968)
is a possible sliding law.
        Generally, the science of interacting surfaces in
relative motion is called tribology (Szeri, 1987); in a more
modern sense it can be defined as the study of friction, wear
and lubrication. Even early theories of friction were based
on the fact that practically all surfaces are rough on the
microscopic scale. The experimental "laws" governing fric-
tion, namely (1) friction is proportional to the normal load,
and (2) friction is independent of the apparent area of con-
tact, were first established by da Vinci, rediscovered by

Amontons and improved upon by Coulomb. Bowden and Tabor
(1964) developed the adhesion theory by which the above-men-
tioned laws of friction can easily be explained. They propos-
ed that friction is the force required to overcome welded
junctions formed between solids as a result of their molecul-
ar interactions.

There exists no uniform theory of friction. A lot of findings
seem to be preliminary and extremely dependent on the actual
circumstances in play. This makes it difficult to treat ques-
tions of friction without the know-how of an expert.

D.2   **Coulomb friction**

Coulomb friction is the most popular friction theo-
ry, including the above-mentioned experimental laws.

Coulomb friction is for the most part solid-solid friction.
In the case of a glacier, this would mean that ice is a rigid
body resting on a rigid rock bed. There is no motion at the
sliding interface except if the shear stress due to the
weight driving the sliding mass is great enough to overcome
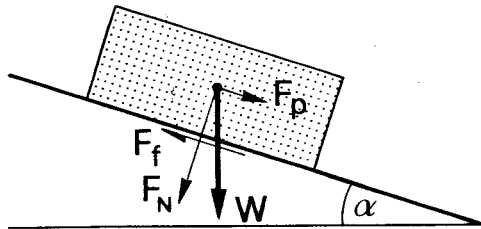the frictional drag (Figure D.2).

Figure D.2   Rigid body on a slope, first primitive model of
a glacier. F_p and F_N are components of the weight W
parallel and normal to the slope. F_f denotes sliding
or friction force.

To initiate the sliding motion a force at least as large as the friction force F_f, but of opposite direction

$$F_f = \mu_s F_N \qquad (D.1)$$

is required, where μ_s: coefficient of static friction and F_n: normal force, component of the weight W normal to the sliding interface.

Once sliding commences, the force to maintain the motion is a bit smaller than F_f because μ_s is replaced by μ_d: the coefficient of dynamic friction ($\mu_d < \mu_s$).

Regarding the glacier as a uniform slab on an inclined plane (angle α) the motion starts if:

$$\mu_s \leq \tan \alpha \quad .$$

In the following the friction coefficient is just called μ.

However, in the above case there is no deformation in the glacier considered to be an absolutly rigid material.
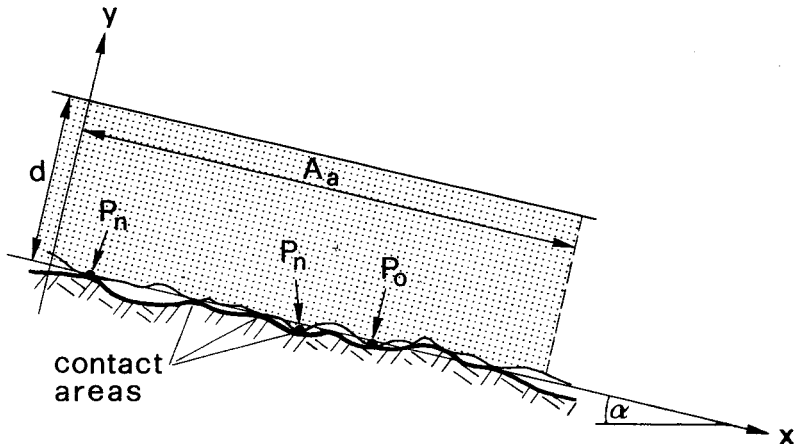

Figure D.3   Rigid body with rough sliding interface only in contact at a limited number of asperities.

A rigid body with a rough surface is not entirely in contact with the bed, but is so only at a limited number of asperities. The real contact area A_r is much smaller than the apparent area A_a of contact (Figure D.3).

At the asperities high stress concentrations will occur increasing with increasing load. This leads to deformation of the asperities until the contact areas are large enough to support the load. There seems to exist a typical size of contact area for a certain weight (Bowden and Tabor, 1964). Let P_n be the pressure the asperities can support and A_r the real contact area, that is the sum of the areas of individual asperity contacts, then

$$P_n \ = \ \frac{W}{A_r} \ = \ \frac{P_o A_a}{A_r} \ = \ \frac{P_o}{1-s} \qquad (D.2)$$

where $1-s$ is the proportion of real contact area on the total area defined as:

$$1 - s \ = \ \frac{A_r}{A_a}$$

and P_o is the pressure on the apparent area due to the weight of the body (in glaciology usually called ice overburden pressure) defined as

$$P_o = \frac{W}{A_a} \ .$$

In the case where there are water-filled cavities with water pressure P_w, the normal pressure at the contact areas gets smaller, because some of the weight of the body is balanced by the water pressure P_w expressed as height h_w of water column in a borehole. So

$$P_n \ = \ \frac{A_r \rho_i gh + (A_a - A_r)(\rho_i gh - \rho_w gh_w)}{A_r}$$

$$P_n \ = \ \frac{A_r P_o + (A_a - A_r)(P_o - P_w)}{A_r}$$

where ρ_i and ρ_w: density of ice and water respectively and with the effective pressure $N = P_o - P_w$ the normal pressure at the asperities is

$$P_n = \frac{P_o - P_w}{1 - s} + P_w = \frac{N}{1 - s} + P_w \quad . \quad (D.3)$$

If the real contact area is very small compared to the apparent contact area (i.d. $s \gg 0$) the water pressure P_w in (D.3) can be neglected:

$$P_n \approx \frac{N}{1 - s} \quad .$$

As long as the water pressure P_w is not equal to the ice overburden pressure P_o there are some small contact areas. A continuous water film exists only if the water pressure equals the overburden pressure. Then the ice mass considered as a rigid body is afloat and moving in an unstable way. As we know, in a real glacier this stage of accelerated motion is already reached at a lower water pressure than the ice overburden pressure, unless some stoss faces of the undulating bed are vertical.

Although there is no continuous water film, usually the true pressure P_n at the asperities is not considered but an average pressure $\bar{P}_n$ referring to the total area A_a:

$$\bar{P}_n = \frac{P_n A_r}{A_a} = (\frac{N}{1 - s} + P_w) \frac{A_r}{A_a}$$

$$= N + P_w \frac{A_r}{A_a}$$

$$\bar{P}_n = N + P_w (1 - s)$$

If the real contact area A_r is very small compared to the total area A_a, the second term can be neglected:

$$\bar{P}_n \approx N = (P_o - P_w)$$

and the friction law can simply be written as:

$$F_f \approx \mu N A_a.$$

(D.4)

Again there is only a sliding motion if the frictional force is smaller than the downhill component of the weight:

$$\mu N \leq \tau = \rho g h \sin\alpha \quad .$$

It follows assuming $\tau = P_o \tan\alpha$

$$\mu \leq \frac{P_o \tan\alpha}{N}$$

or

$$\mu \leq \frac{\tan\alpha}{1 - [P_w]}$$

where brackets denote a dimensionless value: $[P_o] = P_w/P_o$. Without a subglacial water pressure P_w one arrives at the usual balance condition

$$\mu \leq \tan \alpha \quad .$$

Figure D.4 shows that for an intermediate value of the friction coefficient ($\mu = 0.6$) and a mean bed slope of 5.7° ($\tan\alpha = 0.1$) a sliding motion is only possible if the water pressure is at least 80% of the ice overburden pressure. Considering a larger friction coefficient and a smaller basal shear stress (due to the friction from the valley walls) the sliding would be impossible under most conditions, except the very extraordinary case when the water pressure reaches the ice overburden pressure.

Yet in the above situation friction between rigid bodies is considered and thus there is no deformation in the basal ice. A glacier is certainly a sort of viscous body and therefore the Coulomb friction seems not to be appropriate.
Coulomb friction is usually not used in the strict sense of friction between rigid bodies as described above. In
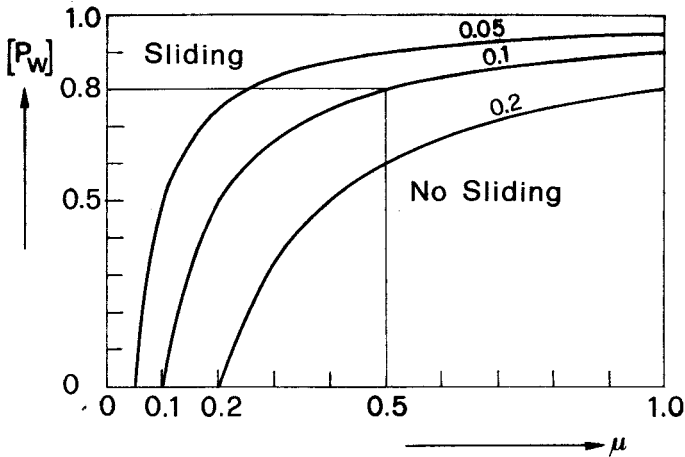
Figure D.4   Coulomb friction: Dependence of sliding on water
pressure $[P_w] = P_w/P_0$ and friction coefficient μ.
Three cases are considered with different mean bed
slopes: $\tan\alpha = 0.05, 0.1, 0.2$. Above a line, sliding
(for a given mean bed slope) is possible, since P_w
is large enough or μ is small enough.

some of the literature (e.g. Reynaud, 1973) it is just the
basal boundary condition in the sliding process which de-
scribes the interaction between the moving ice mass and the
glacier bed.

The reason for this complication is the nature of
the basal ice. Basal ice consists of two different materials:
rigid rocks and deformable ice. The choice of the friction
law should reasonably depend on the sort of ice-rock mixture.
The more rock debris there is in the ice, the stiffer the ba-
sal ice layer, which can be adequately described by a sort of
Coulomb friction law. On the other hand, if there are fewer
rock particles which are not in contact, a friction law such
as Hallet (1979) proposed seems appropriate. Accordingly, in
the following section a distinction is made between so-called
sandpaper friction and Hallet friction.

D.3   Sandpaper friction

D.3.1   Basic concepts

The concept that will be referred to as sandpaper friction is based on a two layer model consisting of a thin sediment layer poor in ice and a huge layer of more or less clean ice. In the sediment layer the rock particles are close together; the ice can no longer flow around them and is simply the glue holding the clasts together, yet due to the ice the basal layer is deformable. Between the rock particles in the layer and the rockbed there is Coulomb friction. Hence the basal layer rubs over the bedrock like a piece of sandpaper (Figure D.5). The difference between sandpaper and Coulomb friction is that the ice mass is really everywhere in contact with the bed, since the basal layer is deformable and adapts to the contours of the bed. The prinicipal difference will become visible and decisive if a subglacial water pressure is in operation. In that case Coulomb friction is simply proportional to the effective pressure N (eq. D.4) since the water pressure has access everywhere through the scratches
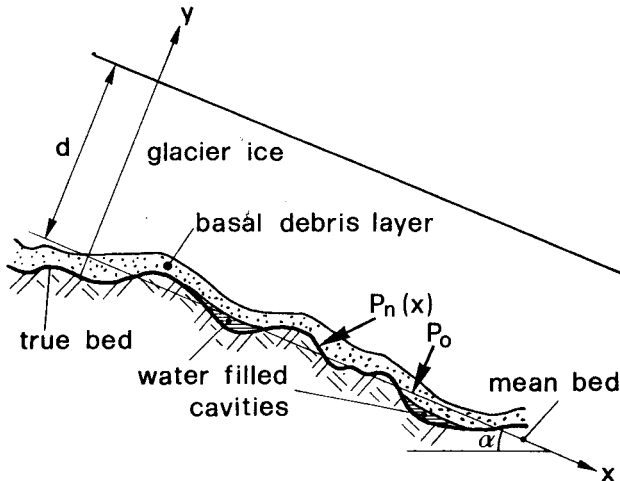

Figure D.5   **Sandpaper friction, two layer model**

between the two rigid bodies with rough surfaces. In contrast to the sandpaper friction, the water pressure can only act where the ice mass (including the basal layer) is separated from the bed.

D.3.2   Friction without bed separation

The force pressing the clast to the bed is the sum of the buoyant weight of the clast and the weight of the overlaying ice column (Boulton 1974). Disregarding the influence of the buoyant weight of the rock particles, the frictional force F_f is

$$F_f = \mu P_n A_a \tag{D.5}$$

where P_n is the normal force per square unit or the mean normal pressure. The normal stress $p_n(x)$ varies along the sliding interface (see Section C.3.3.1):

$$p_n(x) = P_0 + \Delta p(x) \tag{D.6}$$

where P_0 (= $\rho g d \cos\alpha$) is the ice overburden pressure, and if there is no bed separation the mean pressure is

$$P_n = \overline{p_n(x)} = P_0 \quad .$$

The frictional drag τ_f is, as in the case of Coulomb friction,

$$\tau_f = \mu P_0 \tag{D.6}$$

and the sliding velocity u_b (assuming a Weertman-type sliding law) (Weertman, 1957) is decreasing according to the reduction of the basal shear stress τ_b

$$u_b \sim \tau_b^3 \sim (\tau - \tau_f)^3, \tag{D.8}$$

assuming that a part of the driving shear stress τ is used to overcome the frictional drag τ_f.

D.3.3 Sandpaper friction with bed separation

D.3.3.1 **Frictional drag**

When cavities in the lee of bed undulations are for-ming, the contact area for friction gets smaller and there-fore the frictional drag is reduced. With regard to an arbi-trary bed geometry, let A_c be the area where cavities exist and s is the portion compared to the whole sliding interface A_a,

$$ s = \frac{A_c}{A_a} . $$

The remaining area A_r, the real contact area, where friction occurs is:

$$ A_r = A_a - A_c = (1 - s) A_a . $$

The frictional force F_f is:

$$ F_f = \mu \iint_{A_r} p_n(x) \, dA . \tag{D.9} $$

The above double integral is in the case of bed separation no longer equal to the product of the ice overburden pressure P_o and the glacier bed area A_a. The local normal pressure $p_n(x)$ is greater of amount ΔP on the upstream side of rock bumps where friction still is active than on the downstream side. The frictional force F_f is therefore not reduced proportion-ate to the decrease of the contact area A_r, but a bit less:

$$ F_f = \mu (P_o + \Delta P) A_r $$

$$= \mu \ (P_{0} + \Delta P) \ (1 - s) \ A_{a} \quad . \qquad (D.10)$$

From the balance condition (normal to the sliding interface):

$$P_{0} A_{a} = P_{w} A_{c} + (P_{0} + \Delta P) \ A_{r}$$

$$P_{0} A_{a} = P_{w} s A_{a} + (P_{0} + \Delta P)(1 - s) A_{a}$$

one gets

$$\Delta P = (P_{0} - P_{w}) \ \frac{s}{1-s} \qquad (D.11)$$

and therefore

$$F_{f} = \mu (P_{0} - s P_{w}) \ A_{a} \ , \qquad (D.12)$$

and the frictional drag, related to the whole glacier bed area, is

$$\tau_{f} = \mu (P_{0} - s P_{w}) \quad . \qquad (D.12a)$$

The frictional drag gets smaller if water pressure is in operation, but is not, as usually assumed, proportionate to the effective pressure N. The friction is not reduced as a consequence of a smaller effective pressure, but as a result of the smaller contact area. On the area without separation still in contact with the bed, the friction is about the same as before for small bed separation. Only in the case of extended separation do very large stress concentrations exist on the upstream side of a rock bump. For small values of s the reduced friction area is not compensated for by a surplus of the normal stress, and hence it follows

$$\tau_{f} = \mu (P_{0} - s P_{w}) > \mu N \quad .$$

Using the effective pressure N leads to an inadequate frictional drag. The friction is not linearly (proportionate to the effective pressure) reduced with increasing water pres-
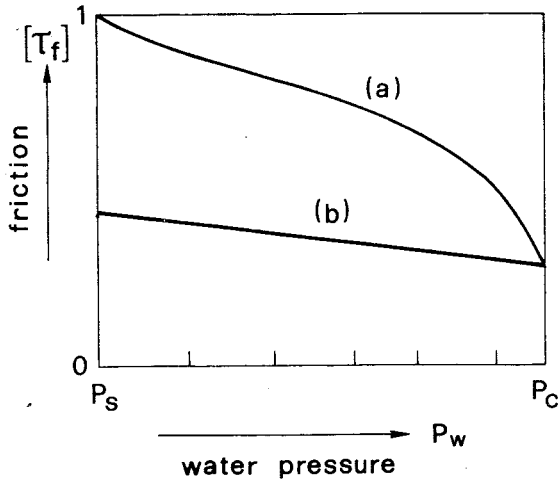
Figure D.6 Comparison of the dependence of Coulomb (a) and sandpaper (b) friction on the subglacial water pressure, normalized to $P_w = 0$ and $s = 0$ respectively. Only the interval between separation and critical pressure, in case of friction: P_s' and P_c', is shown.

sure, but more slowly. At the critical pressure the above drag terms for sandpaper and Coulomb friction respectively are identical (Figure D.6).

D.3.3.2 **Separation and critical pressure**

Friction along the sliding interface causes higher limiting values for both the separation and the critical pressure. In the special case of a sinusoidal bed, the separation and the critical pressure can be given as (Iken, 1981; see also Chapter C):

$$P_s = P_0 - \frac{\tau}{\pi r} \tag{D.13}$$

and

$$P_c = P_0 - \frac{\tau}{2\pi r} = P_0 - \frac{\tau}{\tan \beta} \tag{D.14}$$

respectively.

First of all, the influence of friction on the critical pressure will be studied. In the case of friction, an additional force is required to move the ice mass upward along the steepest tangent of the undulating glacier bed. In the following derivation a water pressure value near to the critical pressure is considered where the friction is restricted to a small area around the inflexion point. Until now the projection of the contact and the separation area on the mean slope was considered. This approximation is justified for small roughness. Yet near the critical pressure the difference between local bed slope (β) and mean slope (α) is largest. The real contact area, A_c, is therefore

$$A_c = \frac{(1-s)}{\cos \beta} \lambda \quad .$$

Now accordingly, the force balance parallel to the steepest tangent is considered

$$P_c' \lambda \sin\beta = P_c \lambda \sin\beta + \mu P_n' \frac{(1-s)}{\cos \beta} \lambda$$

and hence the critical pressure in case of friction is

$$P_c' = P_c + \mu P_n' \frac{(1-s)}{\cos\beta \sin\beta} \qquad (D.15)$$

where apostrophes denote values in the case of friction.
The pressure distribution at the bed is changed by the friction. P_n', the pressure the ice exerts on the bed, can be evaluated considering the force balance in y-direction

$$P_0 = s P_w' + P_n' \frac{1-s}{\cos \beta} \cos\beta - \mu P_n' (1-s) \frac{\sin\beta}{\cos\beta}$$

and hence

$$P_n' = \frac{P_0 - s P_w'}{(1-s) [1-\mu\tan\beta]} \qquad (D.16)$$

Inserting in Eq. (D.15) it follows that

$$P'_c = P_c + \frac{\mu \ (P_o - sP_w)}{\cos\beta \ \sin\beta \ [1-\mu\tan\beta]} \qquad .$$

Again for small roughness, we make the following assumptions for the trigonometric expressions: $\sin\beta \approx \tan\beta$ and $\cos\beta \approx 1$. The critical pressure in the case of friction can be given in simplified form as

$$P'_c = P_c + \frac{\mu}{\tan\beta} \ (P_o - sP_w) \qquad . \qquad (D.17)$$

Introducing the frictional drag $\tau_f = \mu(P_o - sP_w)$ (Eq. D.12), it becomes obvious that friction can be seen as a reduction of the driving shear stress

$$P'_c = P_c + \frac{\tau_f}{\tan\beta} = P_o - \frac{\tau - \tau_f}{\tan\beta} \qquad . \qquad (D.17a)$$

At the critical pressure $s = 1$ can be assumed, and for a sinusoidal bed $\tan\beta = 2\pi a/\lambda$, such that the critical pressure including the effect of friction can explicitly be expressed as

$$P'_c = \frac{P_c + \frac{\mu}{2\pi r} P_o}{1 + \frac{\mu}{2\pi r}} \qquad . \qquad (D.17b)$$

Assuming that the friction should have the same effect on the separation as on the critical pressure it follows that

$$P'_s = P_o - \frac{\tau - \tau_f}{\pi r} \qquad . \qquad (D.18)$$

Before the ice separates from the bed ($s = 0$) the frictional drag is $\tau_f = \mu P_o$ and hence

$$P'_s = P_s + \frac{\mu}{\pi \ r} P_o \qquad . \qquad (D.18a)$$

The derivation, based on an argument by analogy, of the separation pressure including the effect of friction, can be verified with the help of the formula for the bed separation, depending on the subglacial water pressure (Eq. C.24). Inserting the expression for the frictional drag and evaluating

the two extreme cases where s = 0 and s = 1 respectively, the Equations D.18a and D.17b result.

Figure D.7 contains a surprising result: since the frictional drag is reduced by increasing water pressure, the effect of friction on the separation pressure is much more pronounced than on the critical pressure. Thus the separation pressure exceeds the critical pressure for already small values of the friction coefficient. In the example considered (Figure D.7) of a sinusoidal bed with rather large roughness r = 0.16, this is the case for μ = 0.2 (for smaller roughness values e.g. r = 0.05, the separation pressure is equal to the critical pressure at a friction coefficient μ = 0.06). This means for larger values of the friction coefficient the sliding motion of an ice mass is constant (probably equal to zero), independent of the water pressure, unless the critical pressure is exceeded. In that case the glacier switches to the state of unstable motion (see Figure D.8, line (c)).
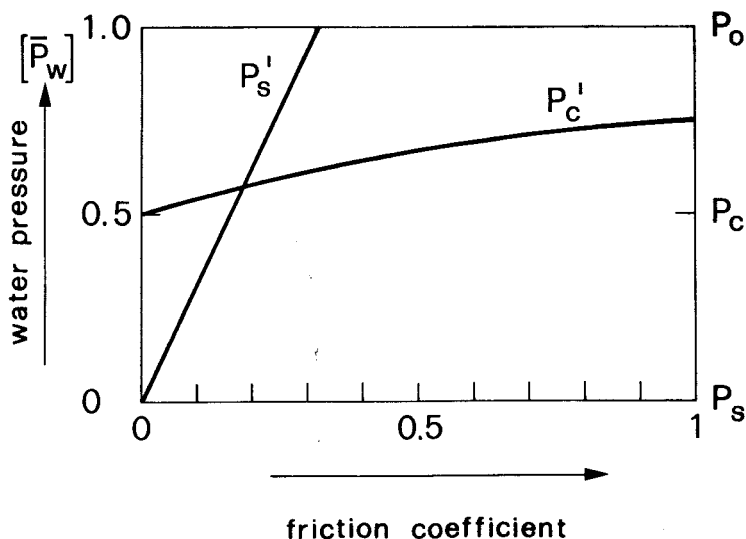

friction coefficient

Figure D.7   Dependence of separation [P'_s] and critical pressure [P'_c] on the friction coefficient μ in the case of sandpaper friction.

D.3.3.3 **Influence on the sliding motion**

We again assume that the friction leads to a reduction of the driving shear stress. The resultant effective shear stress is called basal shear stress $\tau_b' = \tau - \tau_f$. Accordingly the proposed functional relationship between subglacial water pressure and (dimensionless) sliding velocity (Eq. C.25) (for $P_w > P_s'$) is modified

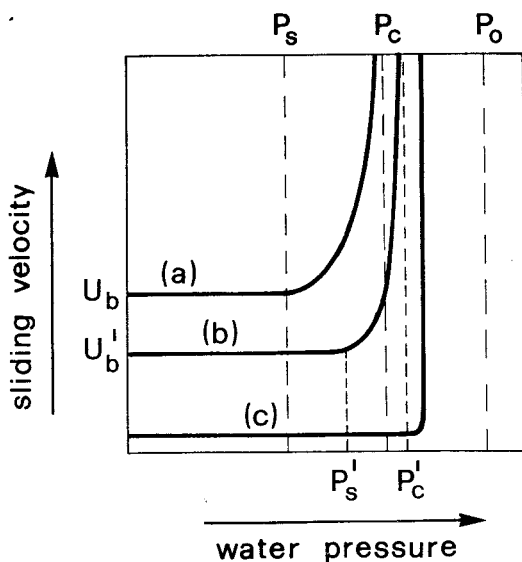$$[u_b'] \quad \sim \quad \left(\frac{\tau_b'}{P_c' - P_w}\right)^n \quad . \tag{D.24}$$

Figure D.8   Functional relationship between the water pressure and the sliding velocity without (a) and with sandpaper friction (b),(c) (values with apostrophes). Line (c) reflects the feature that for large friction the separation pressure can exceed the critical pressure. Thus as long as the water pressure is below the critical pressure the sliding motion is uniform. At the critical pressure the ice mass switches at once to the state of unstable motion.

Figure D.8 shows qualitatively the effect of sandpaper friction on the sliding motion. Line (a) gives the relation for debris-free ice; lines (b) and (c) indicate a possible relation between subglacial water pressure and sliding velocity for debris-rich basal ice. In case (b) the separation pressure is below the critical pressure. Line (c) illustrates the aforementioned "stick-slip" motion for large values of the friction coefficient.

D.4   Hallet friction

When the basal debris is rather sparse (< 15 % per volume) the contact force F pressing the rock particles to the bed no longer depends on the ice overburden pressure. According to Hallet (1979, 1981), the contact force F is proportional to the ice velocity v_n normal to the bed. Friction only occurs on surfaces along which ice converges with the bed, which correspond to positive values of v_n. On the lee side of bumps v_n is negative, and hence there is no friction.

If again it is assumed that the driving shear stress is partly used for deformational motion and partly for overcoming the frictional drag, the sliding velocity u_b is (according to a linear sliding law):

$$u_b = \bar{C} \, (\tau - \tau_f) \tag{D.25}$$

where u_b: basal sliding velocity
$\bar{C}$: constant describing bedrock roughness and ice viscosity
τ : average shear stress at the base (due to gravity)
τ_f: frictional drag

In Hallet's notation the above equation is written as follows:

$$u_b = \frac{1}{\xi\,\eta}\,(\tau - \mu\,c\,F)$$

where ξ : coefficient of bed geometry

η : ice viscosity

μ : coefficient of friction

c : aeral concentration of rock particles in contact with the bed

F : contact force between rock fragments and the bed (proportional to the ice velocity v_n normal to the bed)

A weak point in Hallet's theory is that he tacitly assumes that there are always enough rock particles on the upstream side of rock bumps. Shoemaker (1986) has shown, based on the fundamental work of Röthlisberger (1968), that a rock particle embedded in the basal ice is able only one time to contribute to friction and then is absorbed, if, as Hallet assumes, the melting rate is neglected. However, in large-scale straining areas (e.g. where the glacier is flowing over a step or a riegel) enough rock particles are transported to the bed, so that the Hallet friction concept applies.

Shoemaker (1988) adopts the linearized sliding law from Hallet (1981) (Eq. D.25) from a more global point of view. He does not look at a single bump as Hallet does, but is interested more in abrasional features on a large glacier bed area. His aim is to develop a basal friction drag term for a sliding law. Thus he rewrites Equation D.25

$$\tau = K_1\,u_b + K_2\,c\,u_b \ .$$

He furthermore argues that the contribution of basal melting to the vertical particle velocity u_p is not negligible. Indeed the particle velocity u_p, or more exactly the sliding velocity normal to the bed v_n, arises from three contributions: regelation sliding, uniform melting (due to geothermal heating and sliding friction) and vertical straining. However, it is difficult to determine which factor dominates, as it depends somewhat on the circumstances.

In the Hallet model of friction it is not so easy to determine the sliding velocity u_b, since the fricional term in the sliding law depends itself on the sliding velocity. Thus an iterative solution procedure is necessary.

What happens now when cavities in the lee of rock bumps are forming? Will the friction on the remaining smaller contact area intensify or not, and what is the influence on the separation and the critical pressure?

Iken (1985, unpublished) made an attempt in this direction and estimated the new critical pressure depending on particle concentration and size.

Starting again with the rectangular step model for the gla-cier sole she developed an expression for the critical pres-sure P_c' when friction according to the Hallet theory is in operation. An additional force is necessary to move the ice mass upwards (Figure D.9):

$$P_c' = P_c + \varepsilon \, \underline{b}/\underline{c} \, \mu \, c \, F \qquad\qquad (D.26)$$

where $\varepsilon\underline{b}$ is the contact area (areas $\underline{b}$ and $\underline{c}$ are shown in Fig-ure D.9). The contact force is (following Hallet)

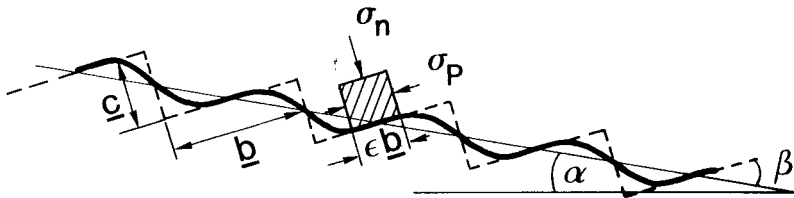$$F = \frac{R^3}{R_\star^2 + R^2} \, 4\pi \, f \, \eta \, v_n \qquad .$$

Figure D.9   At the critical water **pressure the glacier sole**
touches a sinusoidal bed at the contact area $\varepsilon\underline{b}$.
σ_n and σ_p are stress components normal respectively
parallel to the bed (from Iken, unpublished).

The normal stress σ_n on the contact area $\varepsilon \underline{b}$ follows from the force balance

$$\sigma_n = \frac{1}{\varepsilon} (P_0 + \tau \tan\beta - P_c) + P_c \quad .$$

Assuming that the stress component parallel to the bed is equal to the critical pressure ($\sigma_p = P_c$), the stress deviator σ_n' , the corresponding strain rate and finally the normal velocity v_n can be calculated. Actually, σ_p may be larger than P_c , thus the calculated v_n is probably an upper bound. The resulting critical pressure including the effect of Hallet friction, therefore also represents an upper boundary.

Considering a numerical example with a sinusoidal bed (wavelength $\lambda = 5$ m), other numerical values are:

$\tau = 1$ bar
$P_0 = 15.9$ bar
$R_* = 0.1$ m   (suggested by Hallet, 1981)
$f = 2.4$ ("   "   )
$\mu = 1.0$ ("   "   )
$R = 0.1$ m   (only one size of debris particle
                           will be considered)
$c = 2.5$ m^{-2} (corresponding to an areal concen-
                           tration of one-tenth of a close
                           packing of spherical particles)

Without friction due to debris a critical water pressure $P_c = 3.75$ bar is obtained. With debris containing basal ice: $P_c' \leq 10.3$ bar . For higher values of the critical pressure P_c' a larger debris content than $c = 2.5$ m^{-2} particles with radius $R = 0.1$ m per an area of 1 m^2 has to be assumed.

As in the case of sandpaper friction, friction of the Hallet type reduces the sliding velocity in the order of some ten percent and results in a higher critical water pressure. Yet the influence on the separation process can not be

estimated. The question of whether or not cavity formation will lead to stronger friction, cannot be answered, not even in a qualitative sense. As the normal velocity plays a decisive role in the Hallet friction model, a detailed study requires a numerical approach and an iterative procedure, since the flow pattern is changed by every change of the basal boundary condition.

Chapter E

N U M E R I C A L   A P P R O A C H

E.1   Introduction

In Chapter B the sliding problem was mathematically
formulated. It was mentioned that an analytic or closed form
solution for only very special conditions such as laminar
flow can be found. As soon as a more complicated and thus
more realistic glacier geometry is considered, a numerical
solution is an absolute necessity. Since the field equations
(the balance of mass and momentum and the constitutive rela-
tion for the stress [assuming that the thermal and mechanical
effects are decoupled]) are of elliptic form, the finite-ele-
ment method is appropriate.

However, the numerical treatment does not solve the
problems involved in glacier sliding. Crucial points such as
the formulation of the bottom boundary condition or the con-
stitutive relation are still present. Closed form solutions
are often crude, but still very usefull for discussing the
influence of different parameters, for detecting singular
points in the mathematical model and for checking the numeri-

cal computation. The latter one is quite essential and there-
fore the same simple model representing a complex natural
system should be used in numerical calculations as in analyt-
ical ones offering the possibilty to test the numerical solu-
tion for a particular case where a closed form solution ex-
ists. Thus in all simulations done in this work, the model is
the one described by the set of Equations B.1 to B.5. Except
in the case where the ice is separating from the bed (produc-
ing a mixed-boundary problem) the model was not modified in
any way. The boundary conditions and assumptions on which the
above model is based are in general the ones stated in Sec-
tion B.2.

The numerical simulations are only done for the case
of sliding over a sinusoidal bed. A more complex bed topog-
raphy was not considered to have a well-defined basal inter-
face and to strictly separate effects of bed topography and
different bottom boundary conditions. Principally the influ-
ence on the basal sliding velocity of bed topography, of con-
stitutive relation, of water pressure and of friction at the
ice/rock interface was studied. Varying one or more of the
above parameters the numerical simulations were generally a
sensitivity study for the basal sliding velocity.

E.2   Solution method

The finite-element method (FEM) is used to solve the
above set of partial differential equations being of the el-
liptic type. The FEM is one of the methods regularly used in
glacier and ice sheet modelling, but still has not the impor-
tance that one would, expect being a technique very popular
in fluid dynamics. Some of the applications of the FEM in
glaciology can be found in Iken (1977), Hooke et al. (1979),
Emery and Mirza (1980), Iken (1981), Sikonia (1982), Meysson-
nier (1983), Ott (1985), Schweizer (1985), Haeberli und
Schweizer (1988).

As it would be beyond the scope of this work, it is not the
authors's intention at this juncture to give a detailed in-
troduction to the FEM. There exist a number of fine textbooks
on the FEM (e.g. Zienkewicz [1977], Schwarz [1984]). In Zien-
kewicz (1977) the FEM is introduced by solving the flow prob-
lem of a viscous fluid. A few words on the principles of a
numerical approach are follow (Lliboutry, 1987c).

Solving a set of differential equations numerically
means to take the approach opposite to the one chosen in
mathematics in the 18th century: from the continuum back to
discrete points. All relevant functions of the coordinates
are computed at some points, called nodes. The set of partial
differential equations is therefore replaced by an approxima-
te set of ordinary equations, termed difference scheme. In
the FEM the studied domain is divided into a mosaic of ele-
ments (preferably triangles in the case of a plane problem)
with the nodes on the periphery of the elements. In each
element a set of functions, usually polynomials, is chosen
uniquely describing the problem in terms of its nodal values.
A polynomial has to fulfill going from one element to other
specific continuity requirements. Thus a nodal value must be
the same for all adjacent elements. This procedure to ensure
continuity is called assembling. Thus it is finally possible
to obtain an approximate value of, for example, the displace-
ment, at a certain discrete number of locactions for the dom-
ain studied. The accuracy of the computation and the resolu-
tion is merely a question of the chosen number of nodes and
elements. A general test of accuracy is, incidentally, to
double the number of elements which, if the numerical proce-
dure is appropriate, should lead to improved accuracy of the
computation.

Several different techniques exist, for instance the
initial strain or displacement formulation (DISP) or the ve-
locity-pressure formulation (V-P) within the FEM. The code
used in this study is based on a hybrid stress model for the
linear elasticity equations. It was developed for rock mecha-

nical problems at the Institut für Bauplanung und Baubetrieb
der ETH Zürich (IBETH) and is called RHEO-STAUB (Fritz 1981,
Fritz und Arn [1984]). Different rheologies can be studied by
the combination of rheological models consisting of springs,
dashpots and friction contacts arranged in parallel or in
series. Thus the available principal elements are the Hooke,
the Newton and the St.Venant elements, describing elastic,
viscous and plastic material behavior respectively. With ref-
erence to this one is quite free to model different rheologi-
es and a constitutive relation of the Glen type is well prac-
ticable. Although written for elastic problems in rock mecha-
nics, the perfect analogy between elasticity and viscosity
allows use of the program for the viscous, time dependent
flow (Zienkewicz [1977], pp.610-612). And although the code
is meant for the solution of two dimensional plane problems,
the excellent postprocessing and the fine documentation make
this program an easy-to-use and efficient tool for flow and
stability problems in glaciology.

E.3   General assumptions of the model

In this section there is special focus on parameters
involved in the sliding problem. Information will be given
concerning which parameters are chosen and which neglected,
and how this choice is made. It is important to note from the
start that ice will be considered as an isotropic, incompres-
sible fluid of constant density.
In the FE-program RHEO-STAUB the incompressibility is expres-
sed as Poisson's ration v (chosen value is $v = 0.499999$,
since $v = 0.5$ is not accepted). The assumption of constant
density is justified since the lowest meters of the ice mass
are considered. For simulation of high Alpine glacier flow
much influenced by a compressible firn layer, a model with
varying density and compressibility (increasing with depth)
has to be applied (Schweizer, 1988).

E.3.1   Temperature

        The temperature of an ice mass is fundamental for
the description of the deformational characteristics and the
basal boundary condition. Glaciers and ice sheets are not
isothermal, but in general polythermal, meaning that they
consist of two zones, cold and temperate, in which the ice is
below and at the melting point respectively (Haeberli, 1975).
The non-uniform temperature distribution leads to a coupling
between temperature and velocity field by the constitutive
relation.
Even in a numerical approach it does not seem possible to
maintain the thermo-mechanical coupling and to determine tem-
perature and velocity simultaneously. An iterative procedure
where the two unknown functions are sucessively computed to
serve each other as input for the next loop till convergence
is reached, is, on the other hand, conceivable.
In this study temperature and velocity field are not coupled,
thus the constitutive relation does not depend on the temper-
ature. The whole ice mass is at a constant temperature near
the melting point.
Although the glacier is sliding and the ice temperature
therefore should be at the melting point, a value for the
viscosity in the flow law is chosen corresponding to a tem-
perature value below the melting point, since no reliable
viscosity values at $0°C$ exist. Therefore the calculated
sliding velocities represent more likely a lower boundary.

E.3.2   Flow law

        Two sorts of constitutive relations are considered:
a Newtonian and a non-Newtonian called Glen's flow law
(Figure E.1). If written in terms of second deviatoric stress
and strain rate invariants, t'_{II} and $\dot{\varepsilon}_{II}$ the nonlinear
relation can be given as

$$\dot{\varepsilon}_{II} = A\, t'^{\,n}_{II}$$

where η is the viscosity. For the purpose of perfect analogy
to the elastic behaviour, the viscosity η' is introduced de-
fined as

$$\eta' = 2\eta \quad .$$

In this context the second invariant of the stress deviator
and the strain rate tensor are written as τ and $\dot{\varepsilon}$. The con-
stitutive relations used simplify to

$$\dot{\varepsilon} = A \tau^n$$

and

$$\dot{\varepsilon} = \frac{\tau}{\eta'} \quad .$$

From the compilation of different flow law parame-
ters by Paterson (1981) a value A for the computation

$$A = 3.5 \times 10^{-15} \text{ kPa}^{-3}\text{s}^{-1}$$
$$= 0.11 \text{ bar}^{-3}\text{a}^{-1}$$

is chosen. This value corresponds to a temperature about
1.6 °C below the melting point of ice at atmospheric pres-
sure.
For $n = 1$ and $\tau = 1.18$ bar $= 118$ kPa a value for the Newtoni-
an viscosity η' can be determined by

$$\eta' = \frac{1}{A\tau^2}$$

to

$$\eta' = 2.06 \times 10^{13} \text{ Pa s} \quad .$$

This viscosity value corresponds in the FE-program RHEO-STAUB
to an input value of the elasticity constant

$$E = 100 \text{ t/m}^2 \quad .$$

Of course the simulation of Glen's flow law is not
foreseen in the FE-program, but as mentioned above can be

approximated (Figure E.2). The Glen's flow law is simulated
by a series of bodies consisting of a Newton and a St.Venant
element parallely arranged. Thus ice is considered as a vis-
co-plastic material.
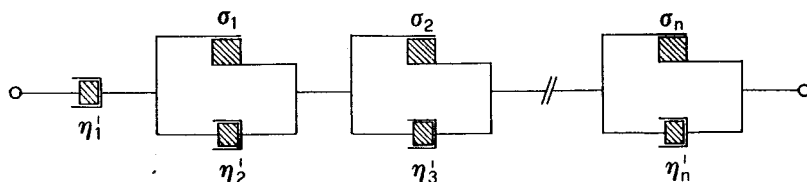

Figure E.2   Rheological model simulating the nonlinear vis-
              cous flow of ice by a series of bodies consisting of
              a Newton and a St.Venant element arranged in paral-
              lel.

The power law curve is stepwise linearized, i.e. for a cer-
tain stress range the deformation is linear viscous. So with
higher stress values the viscosity decreases, not continuous-
ly but stepwise due to the plastic elements describing the
feature of strain weakening or softening (Figure E.3). In
detail the procedure was the following: in a certain stress
interval the power law curve was approximated by a straight
line respecting the principle of least square deviation (Fig-
ure E.3). To obtain the best possible approximation the
stress interval should not be of identical length, but the
varying length of the power law curve in an interval should
be taken in account. Nevertheless, in this study the consid-
ered stress range was divided into 12 identical intervals
(due to a program limit) assuming that the error from the ap-
proximation is negligible.

       Much more relevant is the selection of the stress
range in which the power law should best be approximated. To
get an idea of the sort of effective stress values occurring
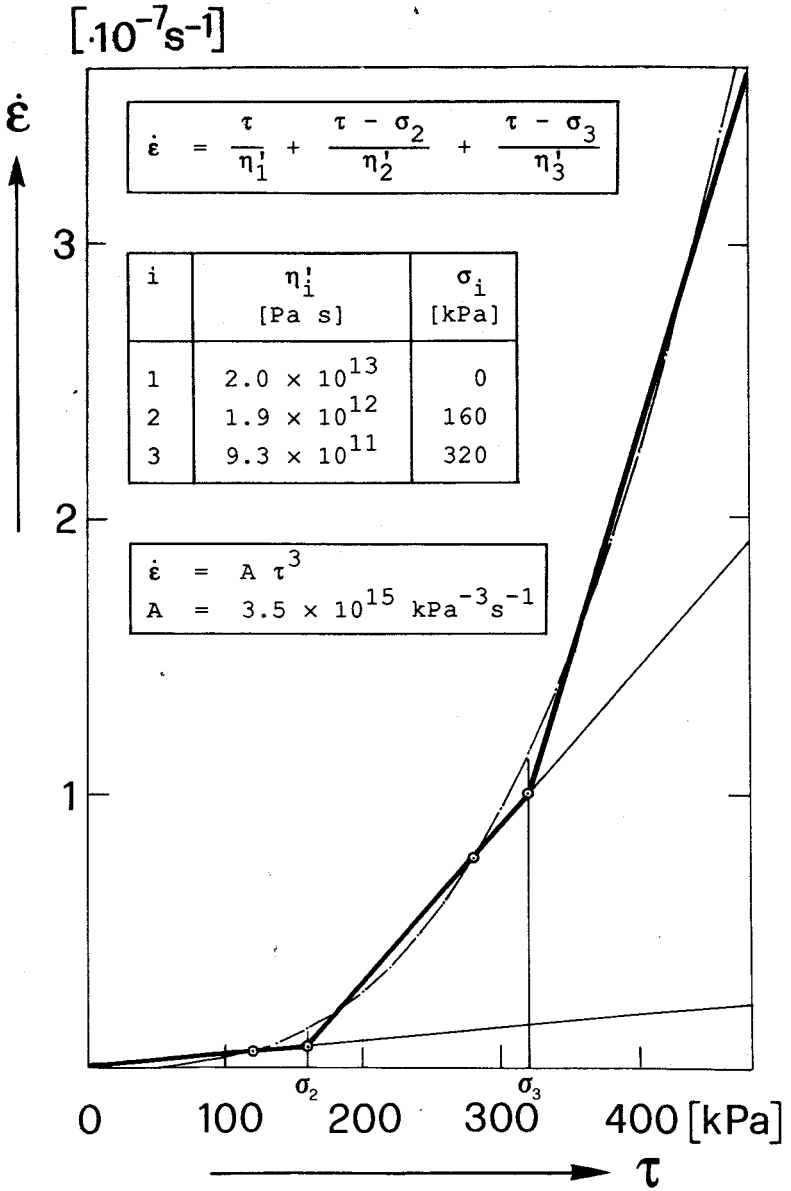the linear viscous case was analysed (Figure E.4).

$$\left[\cdot 10^{-7} s^{-1} \right]$$

$$\dot{\varepsilon} = \frac{\tau}{\eta_1'} + \frac{\tau - \sigma_2}{\eta_2'} + \frac{\tau - \sigma_3}{\eta_3'}$$

i	η_i' [Pa s]	σ_i [kPa]
1	2.0×10^{13}	0
2	1.9×10^{12}	160
3	9.3×10^{11}	320

$$\dot{\varepsilon} = A \tau^3$$
$$A = 3.5 \times 10^{15} \text{ kPa}^{-3} \text{s}^{-1}$$

Figure E.3 Stepwise linear approximation of Glen's flow law

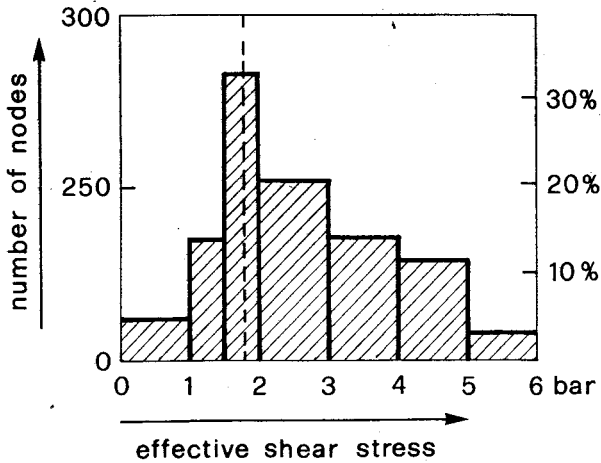**effective shear stress**

Figure E.4   Histogram showing the distribution of the
              effective shear stress in the lowest 25 m of a
              200 m thick glacier (linear rheology assumed).

A simple histogram representation shows that about 90% of the
effective stress values are between 100 and 500 kPa. Hence
the stress range of 0 to 480 kPa was divided in 12 identical
intervals. Figure E.3 shows the principle for the same stress
range, but only with 3 intervals of 160 kPa.

        The approximative stress-strain rate relation can be
expressed as (in simplified form)

$$\dot{\varepsilon} \; = \; \sum_{i=1}^{n} \left(\frac{\tau - \sigma_i}{\eta_i} \right)$$

where σ_i is the yield stress of the St.Venant element of the
i'th body. The yield stress of the first body σ_1 is zero.
(see Figure E.2).
A test of the above relation will be presented in a subse-
quent section.

        The approach starting with rheological models is not
very modern, but it is easy to perform. Another possibility

to overcome the nonlinearity of' the constitutive relation is an iterative procedure computing the effective shear stress and the accordingly effective viscosity with a linear flow law, adjusting the viscosity locally and restarting the com- putation (Iken, 1981). The disadvantage of this method is that one has to interact permanently with the computer, as the method is not implemented in the program.

The FE-program RHEO-STAUB was primarily developed to analyse the elastic deformation of rocks and therefore a viscous problem has to be transformed to an elastic one. In our case the Glen's flow law is simulated by a series of visco-plastic bodies and has to be transformed to a series of elasto-plastic bodies. To do so, one uses the rheological time dependent version of the program offering the facility to combine rheological models. However there is the restric- tion that in a rheological model all three bodies (Hooke, Newton and St.Venant) have to appear. So it is impossible to just substitute the viscosity with corresponding elasticity values. The rheological body has to consist of a viscosity value. As Dashpot and spring are arranged in parallel, into a so-called Kelvin or Voight body, it follows that the elastic deformation or the strain occurs not instantaneously, but is reached gradually (Jaeger, 1969):

$$\varepsilon = \frac{\tau}{E} \; (\; 1 - e^{-\frac{E \; t}{\eta}}) .$$

The larger the viscosity value the sooner the strain will reach its yield value: τ/E.

In summary one can say that first the Glen's flow is approximated by a stepwise linear viscous relation and the according viscosity values were transformed to elasticity values. The stress intervals of the stepwise linearization define the plasticity values and the viscosity values, pre- ferably very large ones, are arbitrarily chosen. These three values determine the flow charateristics of a rheological

body. Table 1 gives the input values of the twelve rheologi-
cal bodies arranged in series which have been used in all
models with Glen's flow law.

Table E.1   Input values of the rheology simulating Glen's
flow law. E is elasticity, ETA viscosity and C plas-
ticity value in t/m^2. (1 t/m^2 = 9.81 kPa). To illus-
trate the original viscosity values (now transformed
to elasticity ones) are given in Pa s. n is the num-
ber of body. 12 bodies arranged in series, each body
consisting of a Newton (ETA), a Hooke (E) and a
St.Venant (C) element arranged in parallel are used.

n	E	ETA	C	η'
1	1151	–	–	2.37×10^{14}
2	111.4	148500	4.1	2.30×10^{13}
3	53.88	71840	8.2	1.11×10^{13}
4	36.13	48170	12.2	7.45×10^{12}
5	27.06	36080	16.3	5.58×10^{12}
6	21.65	28870	20.4	4.46×10^{12}
7	18.05	24060	24.5	3.72×10^{12}
8	15.47	20620	28.6	3.19×10^{12}
9	13.53	18040	32.6	2.79×10^{12}
10	12.03	16040	36.7	2.48×10^{12}
11	10.83	14440	40.8	2.23×10^{12}
12	9.84	13120	44.9	2.03×10^{12}

E.3.3. Summary

In this study no improvement concerning the ice pro-
perties were made compared to similar modelling studies. The
state of knowledge for instance on the creep behaviour does
not allow to leave the old tracks. Temperature effects on the
other hand, may be important but were neglected, leading to
an untractable form of the model. The purpose of all simpli-
fications is to gain a consistent, well-posed problem as the
basis for our study on the bottom boundary condition.

E.4   **Geometry**

E.4.1.   Shape of the modeled area

The glacier sliding problem over an undulating wavy bed is studied in a longitudinal section along the flow direction. This can be achieved by considering the ice mass to be infinitely wide, presenting us with a plane problem. The glacier is in a steady state, i.e. it does not change its shape. Compressing or extending flow is compensated only by accumulation and ablation. Climatic changes prevent a real glacier from reaching this ideal state, at least for a long time. As the present study is not modelling the response of a glacier to climatic changes, the steady state assumption is well justified. Our focus is on the bottom boundary condition and therefore on the lowest meters of a glacier or ice sheet. Hence only a section of 25 × 60 m is chosen for simulation of the flow (Figure E.5) and not the whole ice mass. Of course, the same conditions have to be fulfilled in the small section, just as if the whole glacier were being modelled. This means on the upper border of the section the boundary condition has to be such that the weight of the overlaying, not modelled ice is included. Since the FE-program RHEO-STAUB makes it possible in each node to specify certain boundary conditions the desired effect can easily be achieved.

The whole glacier is assumed to be 200 m thick and the average slope is 0.1, corresponding to an angle of 5.7°. In the section of 25 × 60 m the distance from node to node, or the mesh-size is about 1 m, varying between 70 cm at the bottom and nearly 4 m at the top (Figure E.6). The grid in Figure E.6 is used for all computations. The number of nodes is 1271 and there are 2400 triangle elements.

The height of the modelled section is 25 m, since it is assumed that about one wavelength above the mean bed the velocity variations due to the undulating bed are of minor importance. The length of 60 m for the undulating bed was chosen to include three wavelengths of 20 m. It is necessary
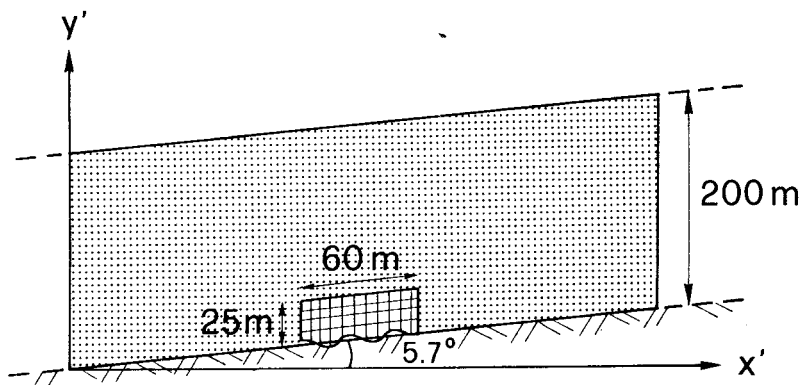
Figure E.5   Modeled section at the bottom of the ice mass.

to consider more than one wavelength to be able to adjust the boundary condition at the front and the back end such that the modelled section is in equilibrium, i.e. there exists no longitudinal stress accelerating or slowing down the ice mass. A wavelength of 20 m guarantees that the sliding is only due to the process of enhanced deformation and not of regelation. On the other hand, as 20 m is rather at the limit for small-scale bed topography, the length of the section, 60 m, makes it easy to study the flow over a sinusoidal bed with a smaller wavelength than 6, 10 or 12 m. Even smaller ones are of course possible, but need a greater number of nodes, i.e. a finer mesh has to be developed. In addition to the wavelength the roughness (= amplitude/wavelength) is varied. Typical roughness values are 0.02, 0.05, 0.10.

E.4.2.   Real bed topography

In order to obtain an idea of the roughness and wavelength of a real undulating rock bed, the forefield of Findelengletscher was studied. In 1980 Iken (personal commu-
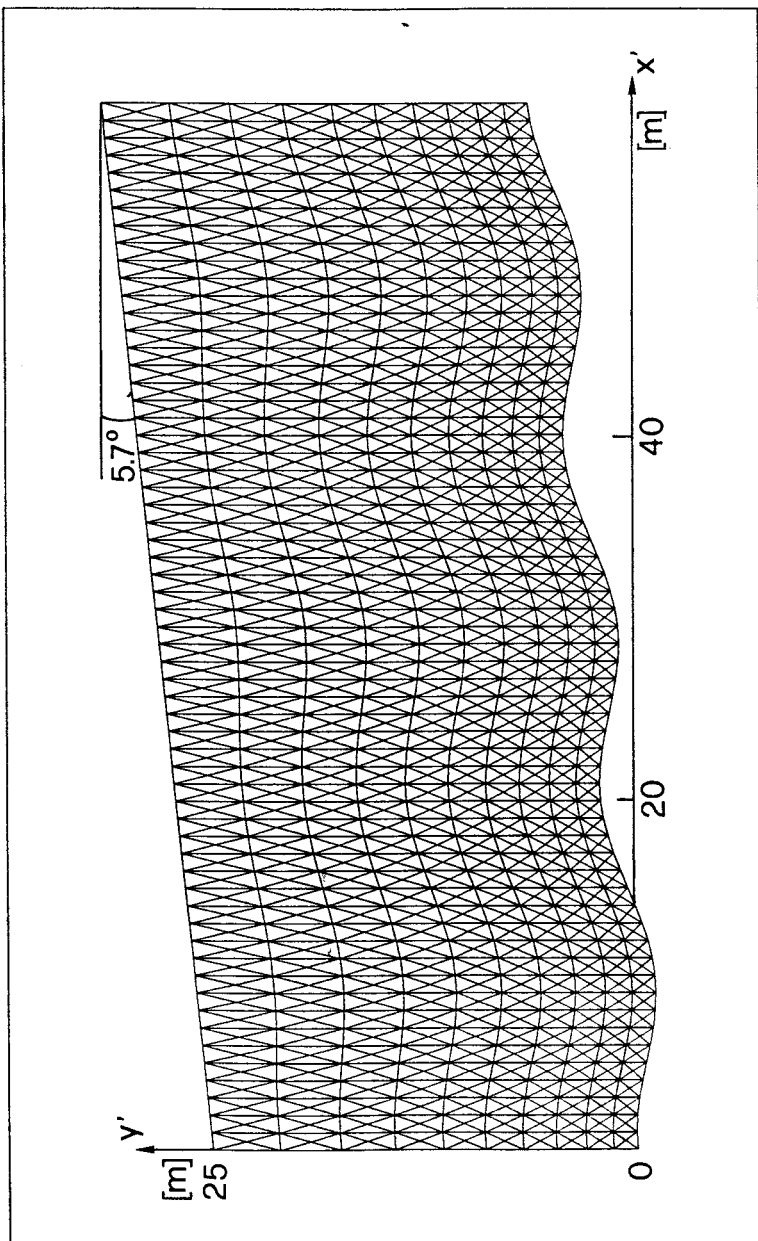
Figure E.6   Finite element grid

nication) surveyed two profiles in front of the advancing
snout, currently overrun by the glacier. In 1987 a few more
profiles in the flow direction indicated by striaes were sur-
veyed (Figure E.7). For the situation see Figure E.8.

When seen for the first time all profiles (Figure
E.9) look very smooth. If one examines the general downhill
trend, i.e. the large scale bed topography, in Profiles 1 and
2 (indicated in Figure E.9 by a broken line) a wavelength of

Figure E.7   Surveying of the former glacier bed of Finde-
              lengletscher in 1987: Hermann Bösch operating the
              distance measurement instrument.

about 30 m and an amplitude of 50 cm is found. Thus the
roughness would be about 0.02. In Profile 3 the wavelength is
even longer. Profile 5 which is on the left side of the
stream where the topography seems to be more small scaled
confirms the first impression. The wavelength is about 20 m.
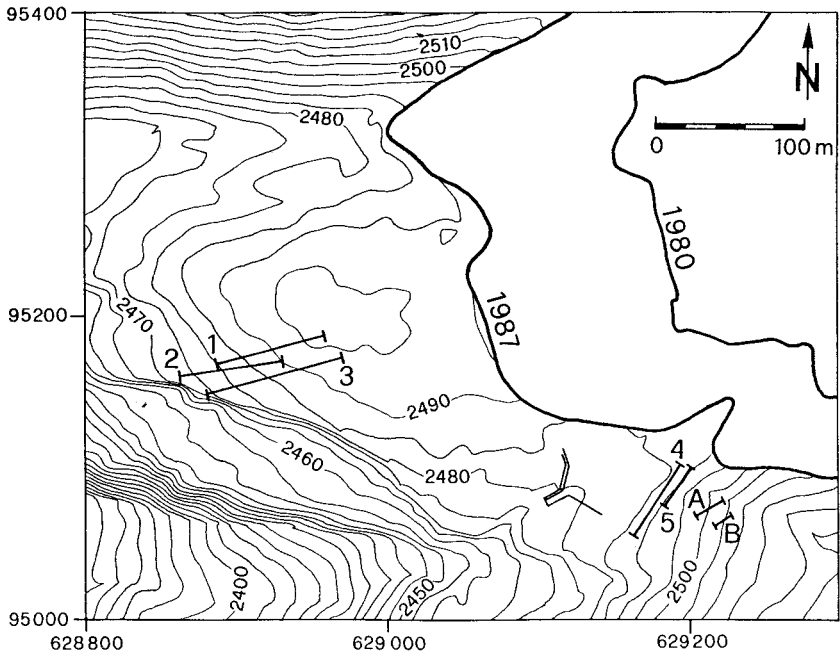
Figure E.8   Map of the area in front of Findelengletscher.
             Profiles surveyed in 1980: A and B, and in 1987:
             1 to 5.
             Contour interval is 5 m. Numbers are Swiss national
             survey coordinates.

        It is obvious that in this sort of investigation
there is a danger of locating the survey at the place where
one expects to find the results desired. In other words, it
can not be proved that the measured profiles are representa-
tive, especially not for a general glacier bed. Nevertheless,
the aim of the small study of the forefield was to show that
the assumptions that our model is based on may be considered
realistic. In actual fact a rather large wavelength and a
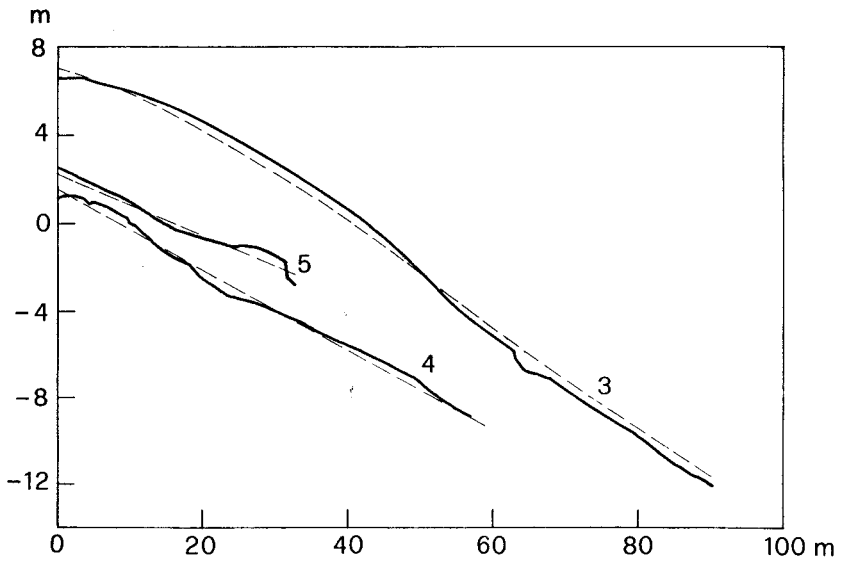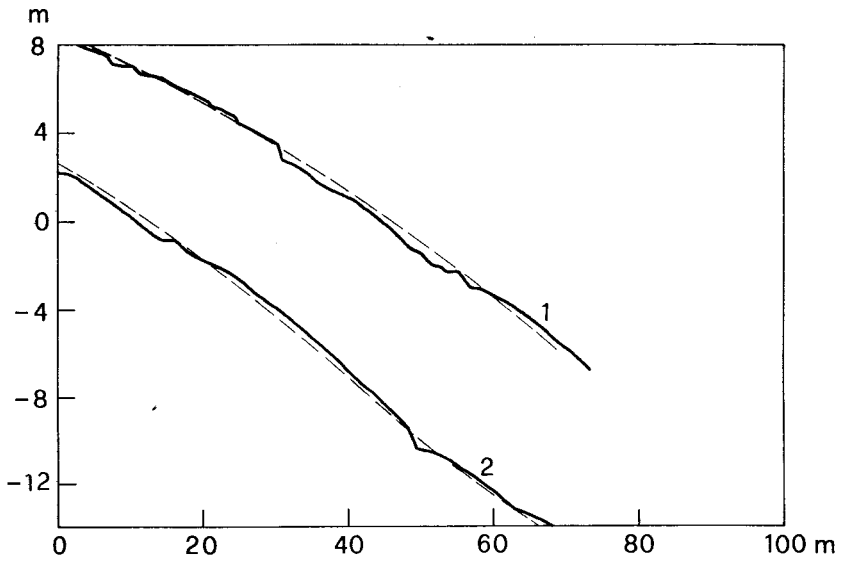small bed roughness were found.

Figure E.9   Some bed profiles on former glacier bed of Fin-
            delengletscher. Profile numbers refer to the map
            (Figure E.8).

E.5 **Boundary conditions**

In this section the detailed boundary conditions around the modelled section, the lowest 25 m of a glacier or ice sheet, are described.

E.5.1   Top, front and back side

At the top of the modeled section the weight of the overlying ice (a column of h = 175 m) has to be introduced by accordingly prescribed nodal forces. As the surface of the ice mass is free of stress, no other conditions must be considered. The distance between adjacent nodes at the top is 1.0 m and correspondingly, the area on which the ice overburden pressure is acting is $A = 1.00 \text{ m}^2$. The nodal forces in x- and y-direction are:

$$F_x = \rho gh \sin \alpha \, A$$

$$F_y = \rho gh \cos \alpha \, A$$

In the x'- y'-system used in the numerical computations the following input values result ($\rho = 900 \text{ kg/m}^3$, $g = 9.81 \text{ m/s}^2$, h = 175 m, $\alpha = 5.71°$):

$$F_{x'} = \rho gh \cos\alpha \sin\alpha \, A = -15.594 \text{ t/m}^2$$

$$F_{y'} = \rho gh \cos^2\alpha \, A = -155.94 \text{ t/m}^2$$

At the front and the back side of the 25 × 60 m section the boundary conditions have to be chosen such that no accelerating force exists. It is the same sort of problem as in simulating the flow of an infinitely wide, parallel sided slab (laminar flow), but as the bed is undulating and the ice mass is sliding, the nodal forces cannot simply be determined with the help of the analytic solution of laminar flow. An iterative procedure has to be applied in order to achieve a steady

state. This complication could be overcome by introducing a periodic boundary condition requiring the velocity on the front and back side to be identical (Raymond, 1978). This very tricky procedure is not applicable since it is not implemented in our FE-program. Instead, the trial and error method must be chosen: taking the inner stress values of the previous computation as new boundary conditions at the front and the back side, again and again, until the velocity difference between the front and back side is negligible. When initially carried out, this procedure was not very effective. Convergence is achieved faster if one adopts the nodal forces according to the deviation from the mean of front and back side velocity values. This means for instance, if the front velocity is 2 % larger than the average velocity the nodal forces at the front are chosen 2 % larger than the computation before. By repeating this procedure 3 to 6 times a stable and hence not accelerated ice mass, is arrived at.

A change in the basal boundary condition as varying roughness or debris concentration affecting the friction influences the boundary conditions at the front and back end. Thus the adjustment of the nodal forces is a nearly permanent and rather troublesome requirement.

E.5.2   Bottom boundary condition

Three cases are generally considered: no slip, perfect slip and sliding with friction.
It is always assumed that the ice mass is lying on an impermeable and undeformable bed: a classic hard bed (Paterson, 1985). This assumption is controversial, since a great number of glaciologists (e.g. Boulton, Clarke) argue that the hard bed would be a very exotic case and that most glaciers and ice sheets are lying on sediments: on a soft bed. We do not want to revive this sophisticated dispute. It is quite probable that both camps are right. In fact, soft and hard beds do exist. However, in a numerical computation one needs a certain distinct interface. It would be altogether possible

to introduce a sediment layer between ice and bed-rock and a part of the deformation could be within the sediment. The hard bed is certainly not the only possibility, but it is a realistic case and an attractive interface for modelling.

E.5.2.1 No slip

In this case there is no sliding; the ice mass adheres to its bed. This sort of bottom boundary condition is chosen only for test computations or, for instance to determine the portion of deformation on the whole motion. It merely prescribes that in each node along the bottom the velocity components are equal to zero.

E.5.2.2 Perfect slip

This is the usual bottom boundary condition: the ice mass is sliding frictionless (due to a thin water layer between rock and ice) over the undulating glacier bed. The roughness prevents the glacier from slipping away. The frictionless sliding is simulated by prescribing that the velocity vector have the direction of the local bed. The ice is forced to move along the bed profile. Most of the computations were performed with this classic basal boundary condition.

To move in the direction of the bed means to determine in each node a slope. At first it was not clear which slope should be chosen: the slope to the preceding node or the slope to the succeeding one, or the average of both. (Figure E.10) After a series of tests with different examples the best results were obtained for the slope of the tangent to the real sinusoidal curve at the point of the node. This is of course theoretically the right solution, but the ice is now in the numerical model no longer flowing along the ice rock interface, since the sinusoidal bed is approximated by straight lines from node to node.
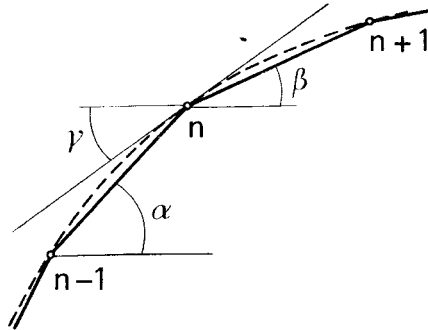
Figure E.10   Section of the glacier bed in the numerical
              model. n-1, n, n+1 are three nodes connected by
              straight lines, approximating the sinusoidal bed
              (dashed line). For the "perfect-slip" condition
              the direction of the tangent at the sinusoidal curve
              is chosen as the prescribed flow direction.

E.5.2.3 Sliding with friction

As outlined in Chapter D, friction between the rock
bed and particles embedded in the basal ice plays an impor-
tant role in the sliding process. In the numerical modelling
a friction of the Hallet type was introduced, appropriate in
the case of sparse debris. In general the dimension and con-
centration of the rock particles and the sliding velocity
normal to the bed are the pertinent variables.
The frictional drag is (Hallet [1981], for $R_* \approx R$, see Section
D.5):

$$\tau_f = \mu \, c \, F \approx 2 \, \pi \, \tilde{f} \, \mu \, c \, \eta \, R \, v_n$$

where μ : coefficient of friction
        c : aeral concentration of rock fragments in
               contact with the bed
        F : contact force
        $\tilde{f}$: factor of the viscous drag of sphere near
               the bed

η : viscosity of ice

R : radius of rock particle

v_n: sliding velocity normal to the bed

The velocity v_n normal to the bed will be determined by the computation. The other variables are constants for a particular case in the numerical simulation. The following values are chosen:

$$\mu = 1.0$$
$$c = 2.5\ m^{-2} \ldots\ 7.5\ m^{-2}$$
$$\tilde{f} = 2.4$$
$$R = 0.1\ m$$

Discussion of numerical values:

(a)   **Friction coefficient** μ

$\mu = 1.0$ suggested by Hallet is of course an upper limit. Under most rock-rock contact conditions μ is likely to be in the order of 0.5 to 0.7 (Drewry, 1986).

(b)   **Debris concentration** c

$c = 2.5\ m^{-2}$ corresponds to an aeral concentration of one-tenth of a close packing of spherical particles, i.e. in an area of $1m^2$ 2.5 particles of 10 cm radius are in contact with the bed and hence contribute to friction. Hallet defines a debris concentration P^*:

$$P^* = 4\ R^2 c\ ,$$

where P^* is the portion of the bed effectively covered by debris. The maximum possible concentration is $P^* = 1$, representing a close cube packing of spherical particles all in contact with the bed. The model Hallet developed is applicable for debris concentrations smaller than about 30%.

The principle for considering a single striating rock inclusion is introduced for modelling purposes. Many

glaciers possess a dirty basal layer in which the concentration of debris may rise to 50-60% by volume (Drewry,1986).

In the ice tunnel (dug in fall 1985) at the snout of Findelengletscher it was possible to study the basal ice in detail (for situation see Figure E.8). At the end of the tunnel the glacier bed was present as a well-polished rock bed. The ice was separated from the bed, probably due to a large-scale longitudinal compression (in 1985 the glacier was at the end of a 200 m advance). The lowest 10 - 30 cm a dirty, stratified layer consisting of ice and debris of very different size (10^{-6}m to 10^{-1}m) was observed. On the larger particles on the bottom side, striaes from rock to rock contact were visible. Some parts were broken out of the basal layer for closer examination in the cold laboratory of the VAW.

Three things were chiefly of interest: (1) Is the ice in the debris layer regelation or glacier ice? (2) What is the debris concentration? (3) How large is the contact area?

(1) The first question could be answered by an analysis of grain size. Attempts were made, but due to a lack of equipment (no multi-stage available) and experience the investigation was not successful. In principal, Souchez and Lorrain (1987) studied the basal ice layer from the chemical point of view. They found that ice accretion may be a frequent phenomenon at the glacier sole.

(2) The debris concentration was determined simply by weighing, melting and reweighing the sample. The mean concentration from 5 samples is 72% by weight. Smallest concentration is 64%, largest 83%. With a density of rock (ρ_r = 2.7 g/cm^3) and of ice (ρ_i = 0.9 g/cm^3) the average debris concentration (by volume) is 46%. However the determination of the debris concentration is only a rough estimation, due to the small number of probes and the inhomogenity of the basal layer. But at least it seems clear that a basal layer with a high (let say 50%) debris concentration at the specific location of the tunnel does exist.

(3) The third question is difficult to answer, especially since only small parts of the bottom of the ice were visible. Figure E.11 shows the bottom of a piece broken out of the basal debris layer. One means of determining the areal concentration is to count out the contact area with the help of a frame. Each visible rock fragment (larger than 0.5 cm in diameter) is marked with a square. The contact area is compared to the total area of the bottom. In our particular case about 22 % were covered with rock fragments (Figure E.12). Again it must be said that only a single piece was studied and that the result may be accidental.

In summary one can say that the basal ice layer was dirty and stratified. It seems to be developed by ice and debris accretion and it plays an important role controlling partly both erosion and sliding.
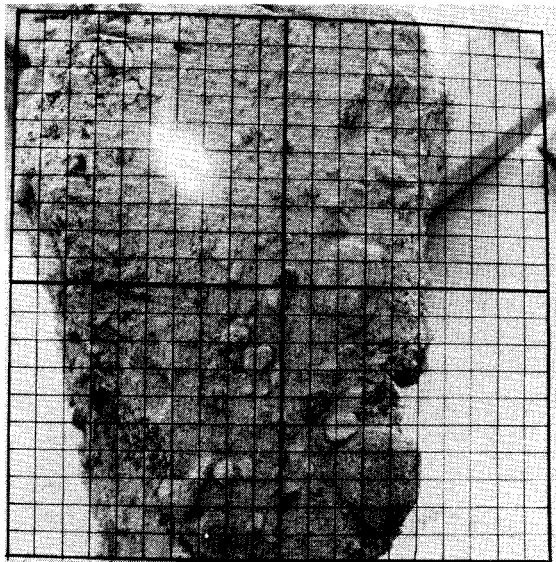

Figure E.11   Bottom side of a piece broken out of the basal ice layer accessible in the ice tunnel at the snout of Findelengletscher. Grid distance is 1 cm.
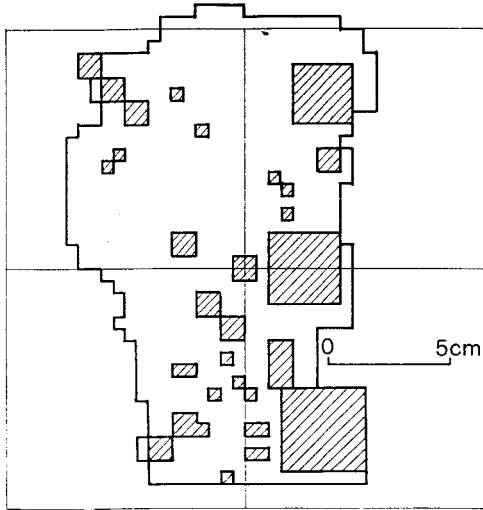
Figure E.12   Primitively digitized bottom of a rock fragment
             with rock contact areas (dashed squares).
             See Figure above.

(c)   **Factor $\tilde{f}$**

$\tilde{f} = 2.4$ is suggested by Hallet primarily based on
an unpublished study by Watts. $\tilde{f}$ takes into account the vis-
cous drag of a sphere contacting the glacier bed.

(d)   **Particle radius R**

         It is assumed that the debris fragments are spheres
with a radius R = 10 cm, a value suggested by Hallet. Smaller
and larger sizes can easily be introduced. However, for
smaller fragments a finer FE-grid has to be developed. A mesh
size equal to the particle size would be ideal. The model
could definitely be improved by considering different parti-
cle sizes.

(e)   **Normal velocity v_n**

         The normal velocity is mainly responsible for the
value of the contact force. The particle size influences the
sliding velocity normal to the bed. As the fragments contri-

buting to the friction have to be in contact with the bed, v_n is determined at the centre of the spherical particle. Thus one has to calculate the sliding velocity normal to the bed at a distance from the bed equal to the particle radius. As the FE-mesh is not fine enough, the velocity 10 cm above the bed is interpolated from the velocity value in the first node above the bed (about 60 cm above). At the bed the normal velocity is of course zero, since the ice slides along the bed.

v_n is partly positive (on the upstream side of rock bumps where the ice flows towards the bed), about zero (at the top of the bumps) and partly negative (on the leeward side where the ice flows away from the bed). A typical value 1 m above the bed is 50 cm/a. It is assumed that the normal velocity decreases linearly with depth. Thus at the centre of
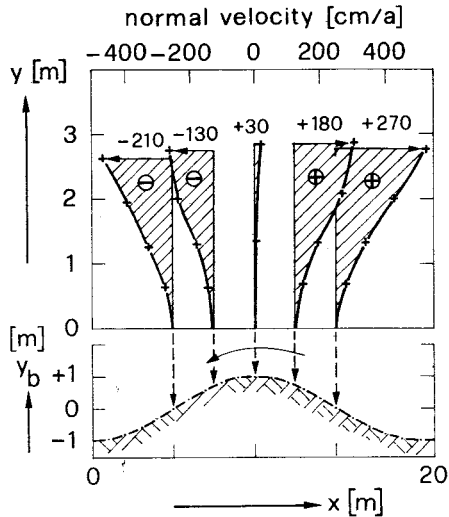

Figure E.13   Distribution of the sliding velocity normal to the bed some meters above a rock bump. Flow direction from right to left. "+" sign denotes positive values of the normal velocity (which means the ice flows towards the bed), "-" sign denotes negative values, respectively.

the spherical rock particles (R = 10 cm) the normal velocity is about 5 cm/a. Figure E.12 shows some velocity values normal to the bed above a bump.

For varying the amount of friction different values of the concentration c are selected. In principal, the particle radius R or the friction coefficient μ could also be changed with a similar effect. The friction varies as the friction coefficient and as the square of the particle radius. A change of the debris concentration, for instance, from c = 2.5 m^{-2} to c = 10.0 m^{-2} corresponds to a doubling of the particle radius. In other words, in a sensitivity study on the friction it does not really matter which of the variables, debris concentration, particle size or friction coefficient, are changed; the effect on the friction can be identical.

E.5.2.4 **Bed separation**

Bed separation occurs if the subglacial water pressure is larger than the minimal normal stress the ice exerts on the glacier bed. The effect of the water pressure is simulated by introducing a force normal to the local bed slope. The force corresponding to a certain given water pressure is principally acting in all nodes where the normal stress is smaller than the water pressure. However, the separation area is larger than the area where the normal stress is smaller than the water pressure. This fact is known (e.g. Iken, 1981) and a relationship between water pressure and cavity length was given in Section C.3.3.3. For the numerical computation this means that in each wavelength, at least in the two adjacent nodes, where the normal stress is already larger than the water pressure, the normal force is also introduced. Figure E.14 indicates the nodes in which water pressure is acting. Generally, the amount of bed separation is chosen to ensure the largest possible basal sliding velocity. This means that it was at times necessary to perform a series of numerical computations to determine the separation area.
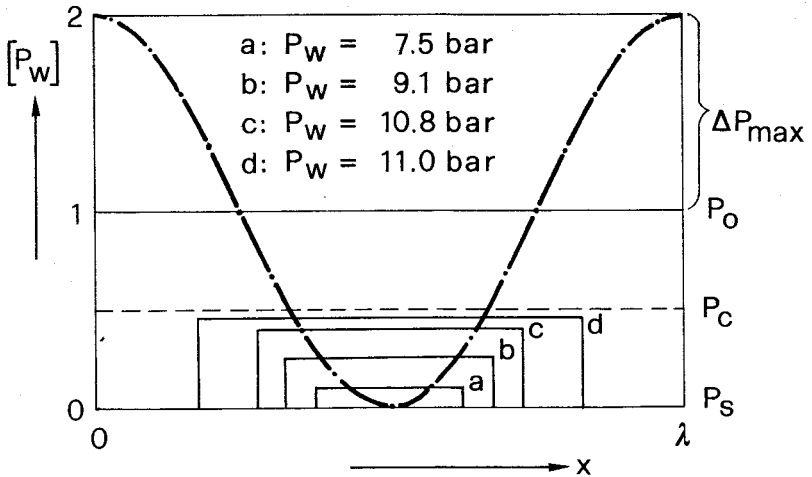
Figure F.14   Distribution of the normal stress and area of
              bed separation along a wavelength for different
              water pressure values.

E.5.2.5 Summary

        To give an overview on the basal boundary conditions
used an example with friction and acting water pressure is
considered. This means three different boundary conditions
apply: (1) perfect slip, (2) bed separation and (3) friction
(see Figure E.15). Perfect slip means that a node at the bed
is forced to move in a certain direction (parallel to the lo-
cal slope). Bed separation is performed such that at a node a
force according to the given water pressure is acting upward
normal to the local slope. The friction condition is similar
but the force is directed parallel to the local slope but
against the direction of motion. The ice mass is then deform-
ing due to its own weight respecting prescribed forces and
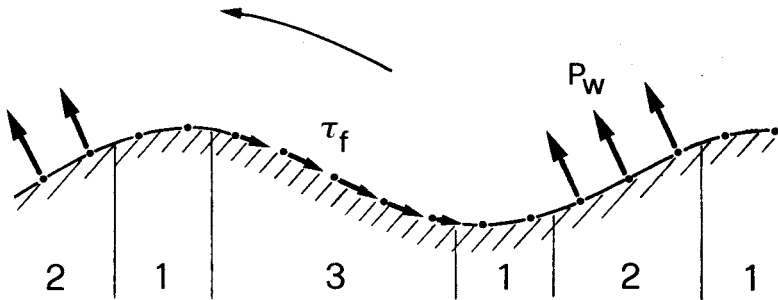directions of motion.

Figure E.15 Overview of the different boundary conditions at
the base: (1) perfect slip, (2) water pressure lead-
ing to bed separation and (3) frictional force.

E.6   **Test computation**

It is an absolute necessity to compare the results
of a numerical computation with a closed form solution. In
glacier motion problems the relevant test case is the laminar
glacier flow. For a Newtonian fluid this was done by Schwei-
zer (1985) and again independently by Wagner (1988). The FE-
program RHEO-STAUB proved to be an excellent tool for the
solution of two-dimensional, linear viscous flow problems.

The above-mentioned tests showed that the error of
the numerically calculated velocity vectors and stress com-
ponents was less than about 1% and 5% respectively. The ac-
curacy of the stress values is generally poorer. Deviations
from the analytical solution, for instance, for the shear
stress at the base of 12% , did exist. Principally, the ac-
curacy is fine inside the studied domain. The fact that the
nodal values are mean values leads to inaccuracy at the edg-
es, at the surface and at the bottom.

However, this lack of accuracy can be eliminated by an improvement in the FE-mesh. The smaller the stress differences between adjacent nodes, the smaller the error at the edges due to averaging. If the number of nodes in an ice column is doubled twice, when modelling the linear viscous flow of an ice mass 200 m thick, the result is a remarkable improvement in accuracy (Figure E.16). The error of the basal
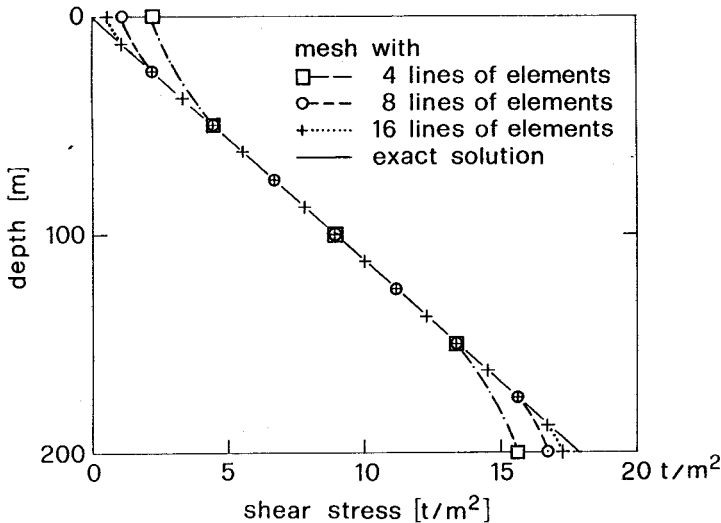

Figure E.16   Shear stress τ_{xy} in a 200 m thick ice mass (inclination 5.71°) for three models with different FE-mesh sizes. In an ice column there are 5, 9 and 17 nodes respectively. The improvement of the FE-mesh leads to a much better accuracy at the bottom and at the surface. Errors at the bottom are 12.5%, 6.25% and 3.14% respectively.

shear stress is 12.5%, 6.25% and 3.14% respectively for the three cases. In the third one with the finest mesh the velocity values were exact within 0.2%.

It remains to be shown here that with the rheological form of the FE-program the non-Newtonian flow can be simulated.

E.6.1 Geometry and material properties

The problem of plane laminar flow is considered for testing purposes. In a 200 m deep glacier a section of 200 × 500 m is chosen. The ice is considered as a non-Newtonian, incompressible fluid of constant density adhering at the glacier bed. In detail the following values are used:

length: $l = 500$ m
slope: $\alpha = 5.71^{\circ}$
depth: $D = 200$ m $\cos\alpha = 199$ m
flow law parameters: $A = 3.5 \times 10^{-24}$ Pa^{-3} s^{-1}
                     $n = 3$
density: $\rho = 900$ kg/m^3
grav. acceleration: $g = 9.81$ m/s^2

E.6.2 Analytical solution

The analytical solution follows from the Equations B.5 to B.8. The ice overburden pressure, the basal shear stress and the surface velocity correspond to the numerical values above:

$$\sigma_x = \sigma_y = 17.5 \text{ bar}$$
$$\tau_{xy} = 1.75 \text{ bar}$$
$$u_s = 58.7 \text{ m/a} \quad .$$

A velocity profile is given in Table E.2 and in Figure E.17.

E.6.3 Numerical solution

Some results of the calculation of the velocity field are given in Table E.2 and Figure E.17. Stress values at the bottom are

$$\sigma_x = 17.05 \text{ bar}$$
$$\sigma_y = 17.10 \text{ bar}$$
$$\tau_{xy} = 1.70 \text{ bar} \quad .$$

The above values are already transformed such that they can
be directly compared with the above values of the closed form
solution. The velocity at the surface is

$$U_s = 53.5 \text{ m/a} .$$

Table E.2   Comparison of some velocity values of the analyt-
           ical (u) and the numerical (U) solution in case of a
           non-linear flow law. Subscript s denotes surface ve-
           locity.

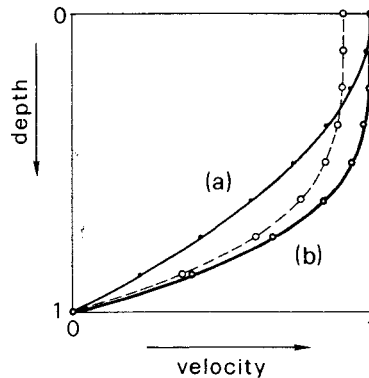| y [m]	u [m/a]	u/u_s	U [m/a]	U/U_s
200	58.7	1.000	53.5	1.000
175	58.7	1.000	53.4	0.999
150	58.5	0.996	53.2	0.995
125	57.5	0.980	52.2	0.975
100	55.0	0.938	49.9	0.933
75	49.7	0.847	44.9	0.839
50	40.1	0.684	36.2	0.677
25	24.3	0.414	21.7	0.408
0	0.	0.	0.	0.

Figure E.17   Velocity profile for linear (a) and nonlinear
           (b) viscous flow law. Comparison between analytical
           solution (curve) and numerical solution (dots).
           Dashed line shows numerical solution normalized to
           the analytical one.

E.6.4   Discussion

        The surface velocity of the numerical solution is
definitely too small. However, the difference between it and
the analytical solution can be explained by the too small ba-
sal shear stress. As the velocity at the surface varies as
the third power of the shear stress at the bottom, a shear
stress of only 97% should lead to a surface velocity of only
91% : 53.5 m/a. That is in fact the case. The inaccuracy of
the velocity values is mainly due to inexact stress values
resulting from averaging in the numerical solution method.
Therefore it seems clear that one could reach the exact solu-
tion by a continuous improvement of the FE-mesh. It is prob-
able and shown in fact for the case of linear viscous flow
(Figure E.14) that the numerical solution approximates the
analytical one. In other words, the rheological model (Table
E.1) used in all nonlinear computations is able to simulate
nonlinear viscous, so-called Glen's flow.
The confidence in the rheological version of the program is
supported by the coincidence of the velocity profiles. The
typical bulging profile of Glen's flow can be reproduced
sucessfully.

Chapter F

N U M E R I C A L   S I M U L A T I O N   O F
G L A C I E R   S L I D I N G :   R E S U L T S

This chapter contains the results of the numerical computations of the sliding of an ice mass over a rigid sinusoidal bed. The influence of bed geometry, rock-to-rock friction and subglacial water pressure on the sliding velocity is studied. The basal boundary condition is varied essentially.

The results support the fundamental statement that the properties of the basal ice, especially the debris concentration, are relevant variables in the sliding process. Starting with a perfectly lubricated bed the friction can affect the sliding velocity as much as the subglacial water pressure, however with an inverse sign.

Most of the numerical calculations are done for both the linear viscous and the nonlinear viscous ice rheology. The reason that all computations do not consistently include the nonlinear flow law is based on the tremendous time supply. A typical calculation time (CPU-time) on a CDC Cyber 180-855 is ten hours, whereas the calculations using a linear viscous flow law normally run in less than one minute.

F.1   **Sliding without bed separation**

The sliding over a rigid perfectly lubricated sinus-
oidal bed is, in the case of a linear viscous flow law, the
only instance where a comparison with a closed form solution
is practicable (Nye, 1969).

F.1.1   Linear viscous sliding

The results of simulations of the sliding with a
linear viscous flow law (in the following simply called "lin-
ear viscous sliding") are compared with the solution of Nye
(1969). Nye's solution which considers a bed geometry with
only one wavelength substantially larger than the transition
wavelength (thus regelation can be neglected), can be given
as (see Section C.2, Eq. C.3a)

$$u_b = \frac{\lambda \; \tau_b}{8 \; \pi^3 \; \eta \; r^2} \quad .$$

With the values of our model (in the following called princi-
pal model: $\lambda = 20m$, $\tau = 1.75bar$, $r = 0.05$, $\eta = 1 \times 10^{13}$ Pa s;
for details see Chapter E) one gets a sliding velocity

$$u_b = 17.24 \; m/a \quad .$$

The numerically calculated velocity is

$$U_b = 17.25 \; m/a \quad .$$

Accordingly the error is smaller than 0.1 %. This test com-
parison shows that the assessment of the boundary condition
at the bottom and the top of the modelled section is appro-
priate. In detail the perfect slip condition at the ice-rock
interface is well simulated.
The velocity value U_b of the numerical calculation is the

mean of the nodal values along the bed, but only of the middle of the three wavelength.

At the top of the modelled section the velocity is

$$U_t = 28.40 \text{ m/a} \quad ,$$

thus the deformational part of the motion is

$$U_d = 11.56 \text{ m/a} \quad .$$

Starting with Eq. B.7 one would expect

$$u_d = 12.47 \text{ m/a}$$

as deformation in the lowest 25 m of a 200 m thick ice mass. The difference cannot only be due to too small shear stress values, but the deformation seems to be in fact smaller if the bed is undulating. When modelling the whole 200 m thick ice mass (frozen to its bed), the deformation in the lowest 25 m is 12.08 m/a. In comparison, the deformational velocity is 4.3 % smaller in the case of the undulating bed.

The properties of ice as an incompressible, linear viscous fluid are reflected in the feature of the flow or velocity field (Figure F.1). Where the flow is confined to a narrow band the ice is flowing and sliding faster, and correspondingly slower where it is wide. This characteristic is also visible in Figure F.1 via the contour lines of constant velocity. The sliding velocity is largest on the crest of the rock bumps and smallest down in the valley. However, looking closely, the velocity minimum does not occur at the bed, but about 2 m above it. One reason may be that the flow line is shorter there than at the bed and hence, in order to fulfill the continuity requirement, the velocity has to be a bit smaller than it is directly at the bed.
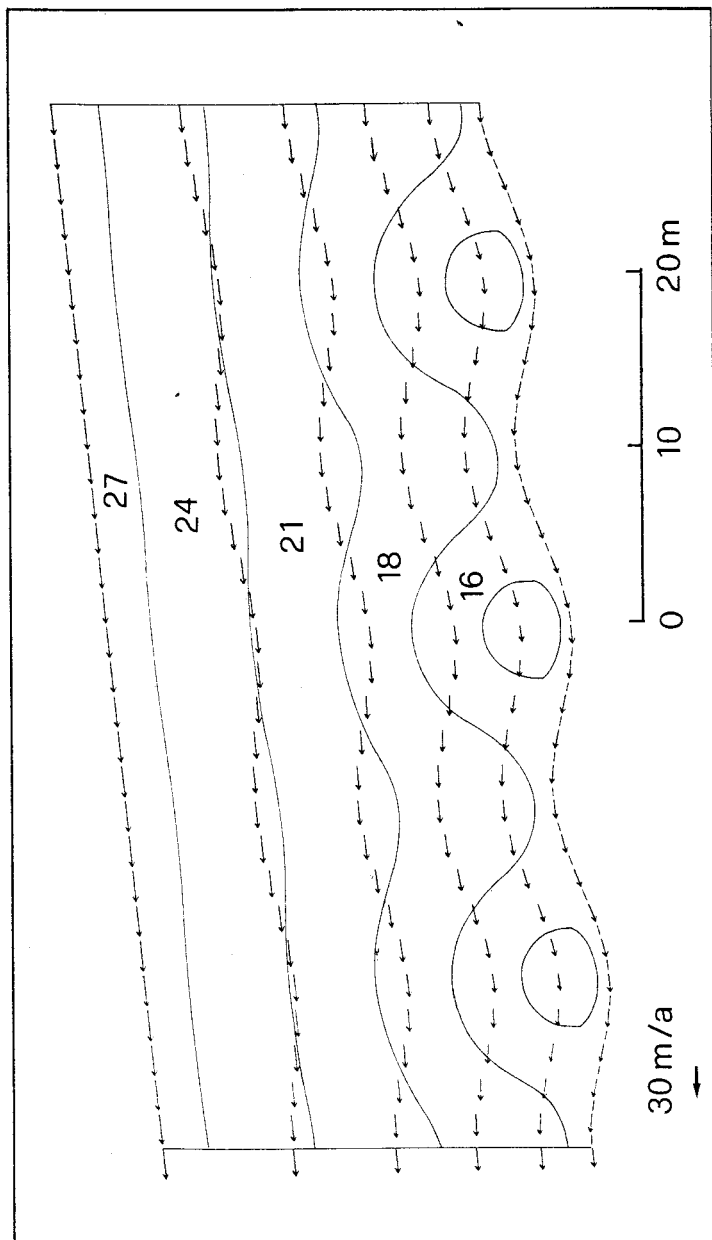
Figure F.1 Velocity field of the principal model, representing the motion (includ-
ing sliding) in the lowest 25 m of a 200 m thick ice mass. Thin lines are
contour lines of constant velocity. Numbers are velocity values in m/a.
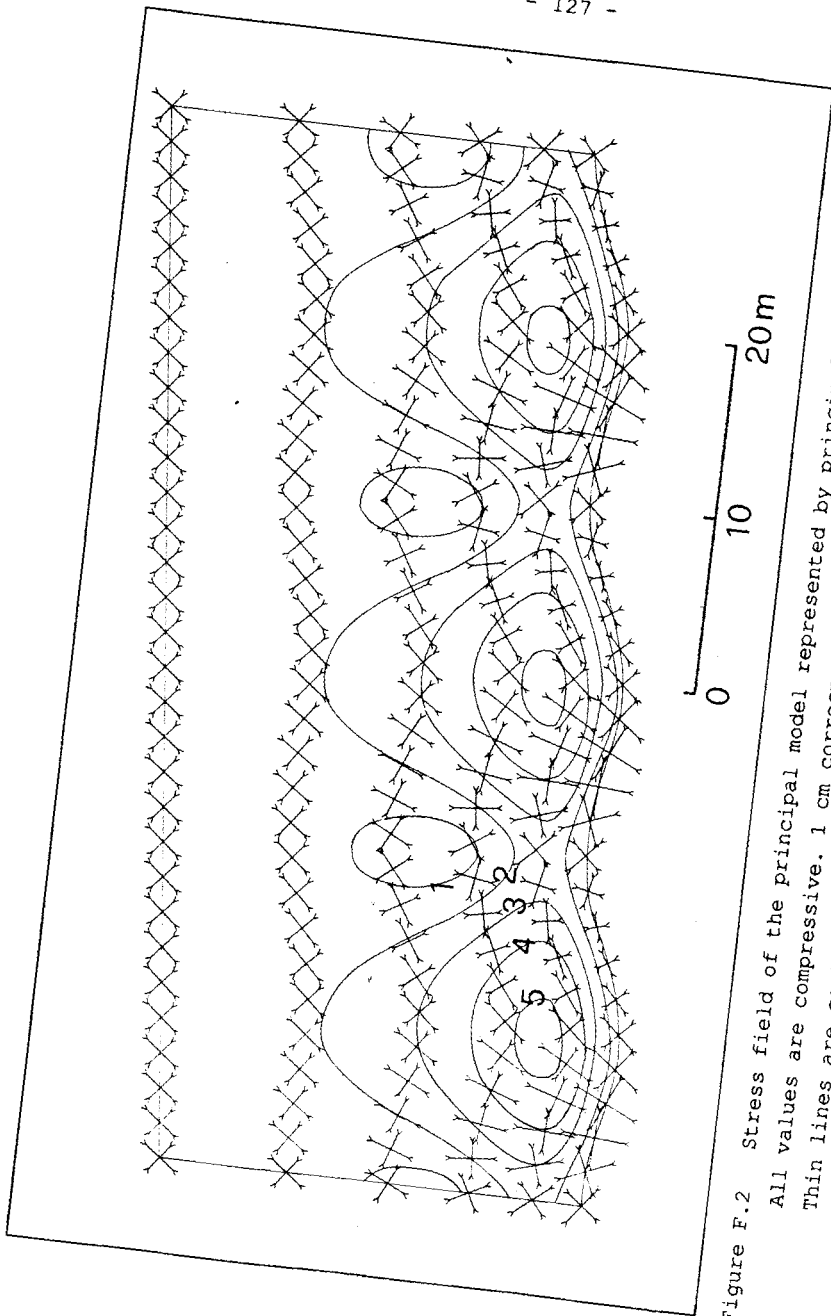
Figure F.2 Stress field of the principal model represented by principal stresses.
All values are compressive. 1 cm corresponds to a stress value of 20 bar.
Thin lines are contour lines of constant effective stress ($\tau_{eff} = \frac{1}{2}|\sigma_1 - \sigma_2|$).
Numbers indicate effective stress values in tenth of bars.

Figure F.2 shows the stress field represented by principal stresses. On first view it can be easily seen that the modelled section is well balanced, that at the top more or less laminar flow conditions are valid and that on the uphill side of the bumps large compressive stresses exist. In a subsequent section the stress distribution at the bed will be discussed in detail.

In the following some pertinent variables along the ice-rock interface are particulary studied.

(a)   **Sliding velocity U_b**
As previously mentioned, the numerically calculated sliding velocity indicated above is an average value. The velocity is larger on the crest and smaller on the base of a rock bump (Figure F.3): a typical flow pattern of a fluid. The sliding velocity varies between 16.85 m/a and 17.68 m/a.

(b)   **Velocity normal to the bed V_n**
The normal velocity directly at the bed is identical to zero. Values as for instance in Figure F.3, are always given at a certain distance (mostly 10 cm or 1 m) above the bed, calculated from the first node line above the bed (see Section E.5.2.3). In contrast to the normal stress or the sliding velocity, the normal velocity is not a single harmonic function. We don't see any plausible explanation for this feature. It could be an effect of not quite accurate inclination values. To calculate the normal velocity, the direction of the velocity vector is compared with the bed inclination and a certain deviation is expressed as normal velocity. As was aforementioned, the normal velocity is calculated from velocity values 1 m above the bed. The error and therefore the second harmonic could well be due to this discrepancy between the place from where the inclination angles are taken and the place where the velocity is calculated.
Maximum and minimum values of the normal velocity occur where one would expect them to: on the uphill and downhill side respectively, but not at the inflexion points.

A typical value 1 m above the bed is 50 cm/a. Near the bed the ice flows a few centimeters per year against the rock.
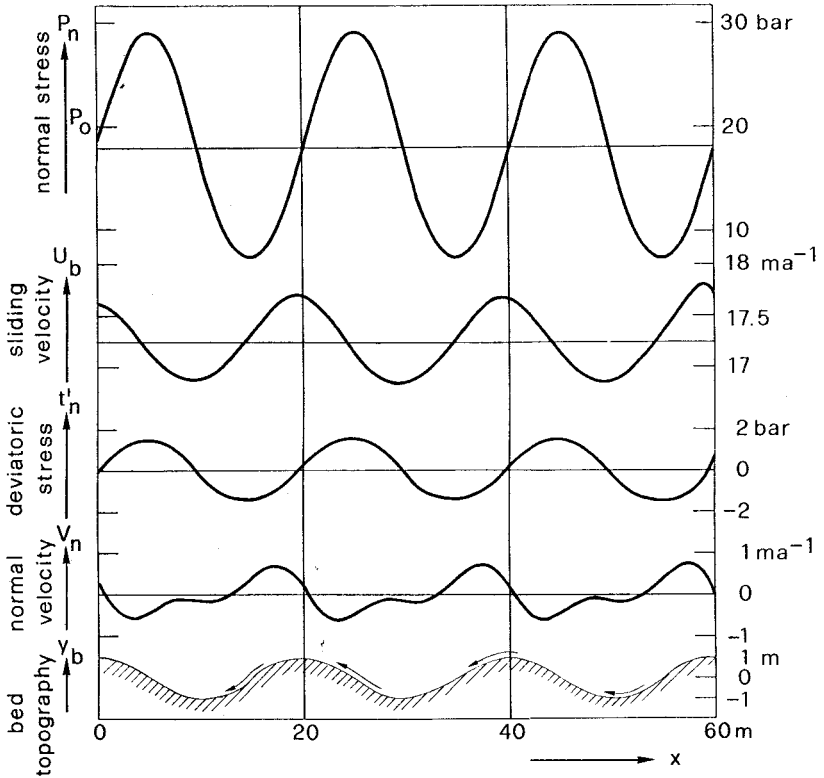

Figure F.3 Numerically calculated values along the sliding interface of normal stress P_n, normal component of stress deviator t_n', normal velocity V_n, sliding velocity U_b and bed topography y_b.

(c)   **Normal stress** P_n

The pressure the ice exerts on the bed is oscillat-
ing, as shown in Section C.14

$$p_n(x) = P_0 + \Delta p_{max} \cos\left(\frac{2\pi x}{\lambda}\right) \quad .$$

In the considered case of the principal model there is

$$P_0 = 17.5 \text{ bar}$$

and

$$\Delta p_{max} = 11.1 \text{ bar} \quad .$$

Thus the normal stress p_n varies between 6.35 bar and 28.6
bar. Figure F.3 depicts the result of the numerical solution
generally reproducing the analytical one within 1 %.
However, there is a large deviation in the lee of the bed un-
dulations where the pressure is minimal: 7.11 bar instead of
6.35 bar, an error of 12 %. In Figure F.3 the three fine
straight lines indicate the theoretical values of the average
normal pressure and the two extreme ones between which the
pressure is oscillating.

(d)   **Normal stress deviator** t_n'

The stress deviator component normal to the bed rep-
resents the local stress distribution without the influence
of the hydrostatic pressure. It could be a pertinent variable
for simulating sliding with friction. On areas where the nor-
mal stress deviator is positive (meaning compressive) the
friction would be active. Figure F.3 supports this idea. The
normal stress oscillates in accordance with the bed topogra-
phy, simply shifted by a quarter of a wavelength. Positive
values contributing to friction are on the uphill side, and
negative ones on the downhill side of rock bumps. However,
the results of the nonlinear viscous sliding (in a subsequent
section) suggest that one should reject the idea outlined
above of involving the normal component of the stress devia-
tor to simulate sliding with friction.

A series of different models are computed for the purpose of studying the effect of varying geometry and for again testing the solution of Nye (1969). Nye suggests that the basal sliding velocity varies as the wavelength and as the inverse of the second power of the roughness. This dependence and also the velocity values could be reproduced by the numerical computations. Table F.1 provides an overview. The numerically calculated values generally coincide well with the analytically computed ones. Larger variations exist if the velocity is significantly different from the one of the principal model ($\lambda = 20$ m, $r = 0.05$). This is due to boundary conditions which are not sufficiently adapted to the new conditions. A continuous improvement of the boundary conditions at the front and the back side could probably guarantee a coincidence within more than 99 % accuracy.

Table F.1   Compilation of numerically calculated velocity values (in m/a) compared to exact values from the Nye solution. To each pair of roughness and wavelength two values are given: the upper one originates from the closed form solution of Nye and the lower one is numerically computed.

λ \ r	0.02	0.04	0.05	0.06	0.08	0.10
6 m	32.33	8.08	5.17	3.59	2.02	1.29
			5.28			
10 m	53.89	13.47	8.62	5.99	3.37	2.16
	53.52	**13.11**	**8.76**	**5.79**	**3.27**	**2.10**
20 m	107.77	26.94	17.24	11.97	6.74	4.31
	112.56	**27.09**	**17.25**	**11.69**	**6.43**	**4.06**
30 m	302.36	75.59	48.38	33.59	18.90	12.09
			46.36			

To summarize, the sliding of an ice mass along a distinct undulating interface considering linear viscous ice rheology can be simulated. In so far as the numerically calculated results can be compared with an analytical solution and therefore the accuracy can be estimated, it is justified to say that the simulation is done well and the model produces satisfactory results.

F.1.2   Nonlinear viscous sliding

The results of the simulations of the sliding of an ice mass over a undulating bed considering nonlinear viscous ice rheology (in the following simply called: "nonlinear viscous sliding") can be compared with the treatment of Kamb (1970). However, Kamb's solution is an approximate one. In case of large deviations between two different, both not exact approaches, it is hard to say which one is more appropriate. The detailed tests outlined above mainly justify confidence in the results of the numerical computations.
In the following section the results of the simulation of the nonlinear viscous sliding are compared with the results of the simulation of the linear viscous sliding.

Considering again the principal model ($\lambda = 20$ m and $r = 0.05$) one gets a numerically calculated sliding velocity

$$U_b = 47.44 \text{ m/a} \quad .$$

Kamb's solution for a wavelength of the bed undulation much larger than the transition wavelength (Eq. C.5a) predicts a more than 5 times larger sliding velocity

$$u_b = 246 \text{ m/a} \quad .$$

This discrepancy cannot be explained by shear stress values that are possibly too small due to averaging in the FE-pro-

gram. One reason could be that Kamb's solution being an approximate one is not appropriate to the characteristics of our model. This means that the wavelength could be too large (λ = 20 m). However, the numerically computed value seems to be quite realistic. Together with the velocity due to internal deformation a surface velocity of 106 m/a seems to be reasonable for a 200 m thick glacier.

At the top of the modelled section (25 m above the bed) the total motion in one year is

$$U_t = 86.23 \text{ m/a} \quad .$$

Hence the creep velocity is

$$U_d = 38.80 \text{ m/a} \quad .$$

Without sliding, thus frozen to the bottom, but still with a wavy bed the velocity due to deformation is only 20.51 m/a. Theoretically the creep velocity in the lowest 25 m of a 200 m thick ice mass should be (see Section E.6.3)

$$u_d = 24.29 \text{ m/a} \quad .$$

In the numerical simulation of the whole 200 m thick ice mass frozen to its bed only 21.69 m/a results. Again, as in the case of linear viscous sliding, the deformation is smaller if the bed is undulating.

But on the other hand, now the deformational part of the motion is larger in the case of sliding than in the case of none. This additional contribution: 18.29 m/a is an effect of the strain softening. If the ice is sliding, the larger stress concentrations around the bumps lead to enhanced creep.

The **velocity field** in Figure F.4 is strikingly similar to the linear viscous sliding field in Figure F.1. Corresponding to the much larger deformational motion, the rela-

tive difference between the velocity at the bottom and at the top of the modelled section is about 20% larger. In contrast to the linear viscous case the minimal velocity value is directly at the bed. The bed undulations become apparent higher up. Even at the top of the section the velocity vectors can clearly be seen to submerge and emerge. The y-component varies ±25% around the average value which represents laminar flow. In the linear viscous case the variation is only 0.5% . One would in fact rather expect the opposite, namely that the effect of the bed undulations is concentrated more closely near the bed, because the ice is more deformable than in the case where it is considered a linear viscous fluid. It is possible that the much larger (by a factor of 3) sliding velocity turns it the other way round.

   The **stress field** (Figure F.5) is quite different as compared to the linear viscous case (Figure F.2). In contrast to the velocity field there are some differences visible on the first view, especially at the top and at the bottom of the modelled section. Again all stresses are compressive.
In the uppermost node line there is a very strange orientation of some principal axes of stress, a feature not at all existent in the adjacent node line below. At the bottom one can recognize larger stress values and also larger differences between the two principal stresses, hence the stress deviator values will be larger, too. Furthermore, it is obvious that it is not possible to balance the ice mass exactly such that the stress values at the edges (left and right) are the same as the corresponding ones in the middle.
All together one gets the impression that the stress field does look somehow suspicious. The more detailed discussion below will show that a certain pattern is also emerging in the stress field. And on the other hand, the velocity field does not give rise to any doubt.

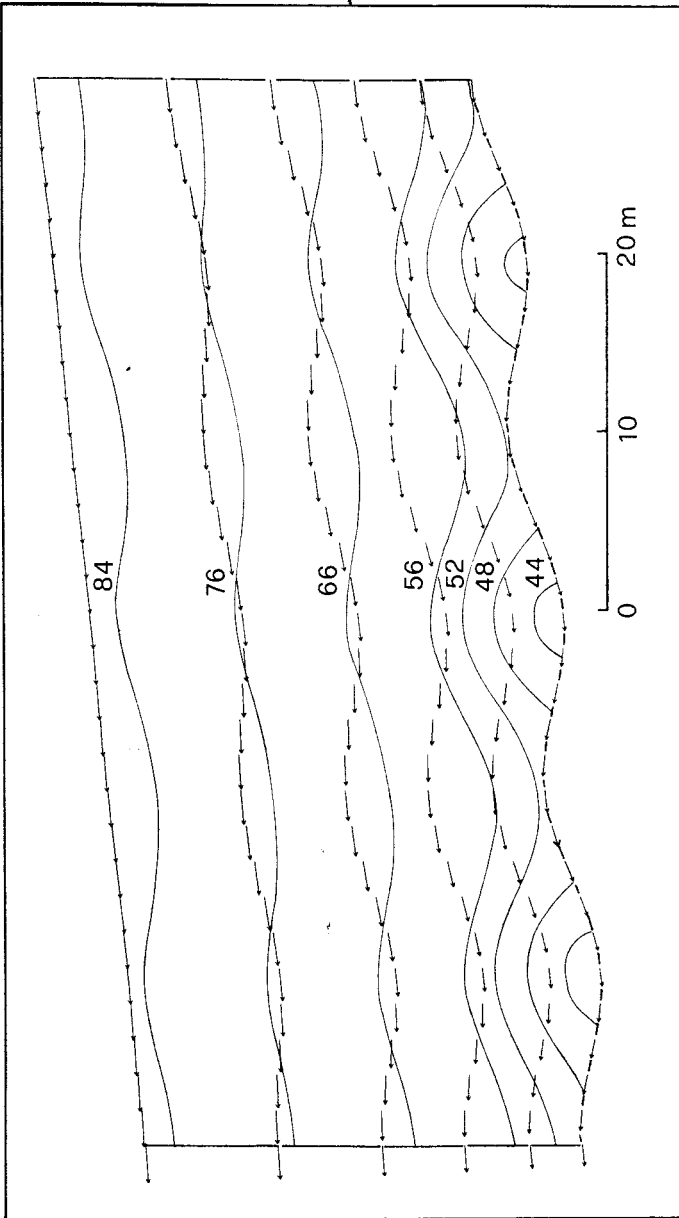   Again some variables along the sliding interface are more fully discussed.

Figure F.4 Velocity field of the principal model, representing the motion (includ-
ing sliding) in the lowest 25 m of a 200 m thick ice mass considered as a
nonlinear viscous fluid. Thin lines are contour lines of constant velocity.
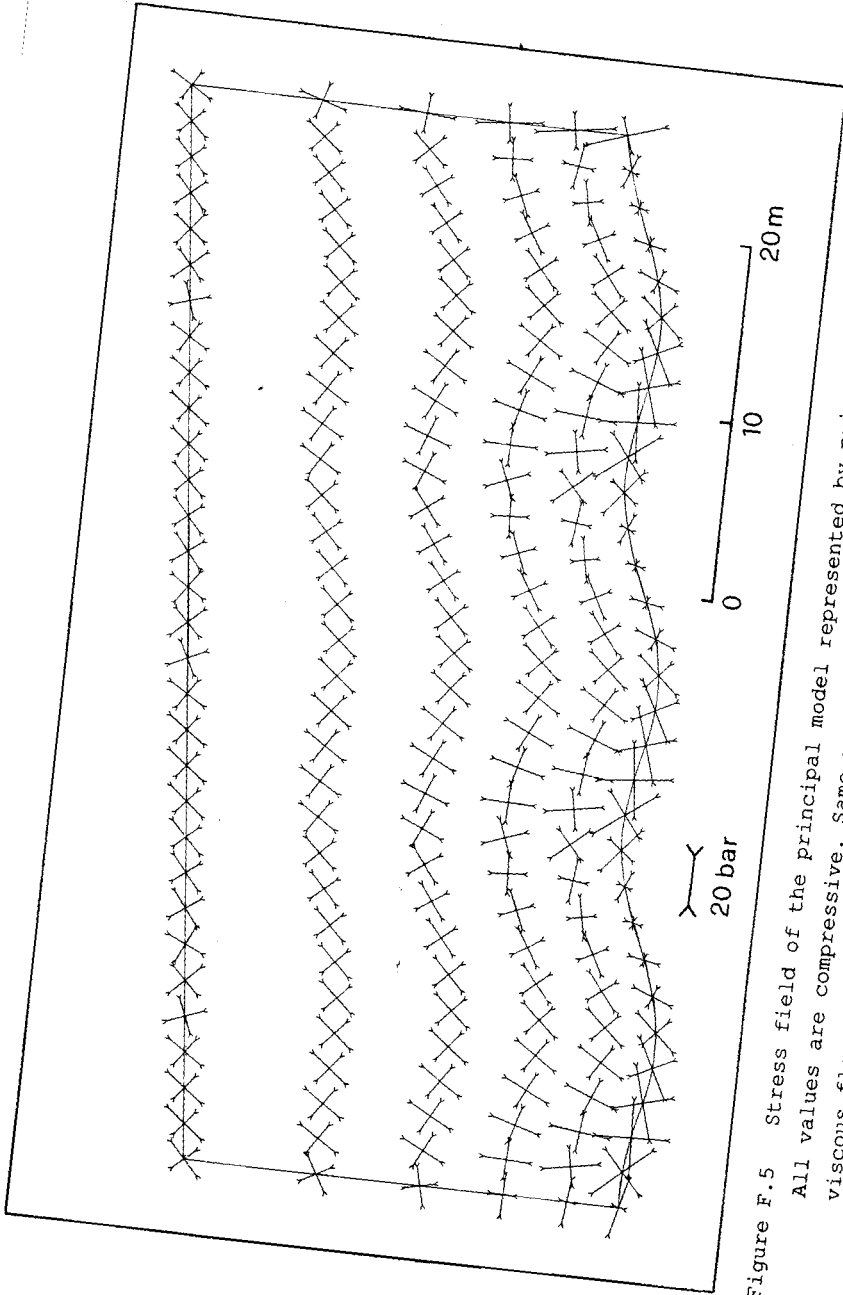Numbers indicated velocity values in m/a.

Figure F.5   Stress field of the principal model represented by principal stresses.
All values are compressive. Same representation as in the case of a linear
viscous flow law.

(a)   **Sliding velocity, U_b**

The sliding velocity at the bed varies much more ($\pm 9.1\%$) (Figure F.6) than in the case of linear viscous sliding ($\pm 2.4\%$) (Figure F.3). This is an effect of the strain softening leading to correspondingly larger velocity values where there are stress concentrations.

(b)   **Velocity normal to the bed V_n**

The normal velocity is larger than in the linear viscous case. A typical value is 2 m/a (1 m above the bed). This increase is not only due to the larger sliding. There is an effective increase of about 20%. This difference will be important for modelling the friction. In contrast to the linear viscous case there is only one minimum and one maximum within one wavelength. However, the normal velocity is again not a single harmonic function. The extreme values are not at the inflexion points but shifted more to the crest of a rock bump.

(c)   **Normal stress P_n**

As for the normal velocity, the curve of the normal stress (Figure F.6) is asymmetrical. The extreme values are about 10% larger and shifted towards the crest of a rock bump. It follows that the stress concentrations and differences are larger around a bump. The normal stress function resembles a saw-blade.

(d)   **Normal stress deviator t_n'**

The component of the stress deviator normal to the bed (loosely referred to as "normal stress deviator") (Figure F.6) is calculated as follows

$$t_n'(x) = P_n(x) - \frac{1}{2}(\sigma_1 + \sigma_2)$$

where σ_1 and σ_2 are the principal stresses. The asymmetrical characteristic of the normal stress P_n gives rise to a rather strange course of the local stresses at the bed, for instance negative, thus tensile on the uphill side of rock bumps.
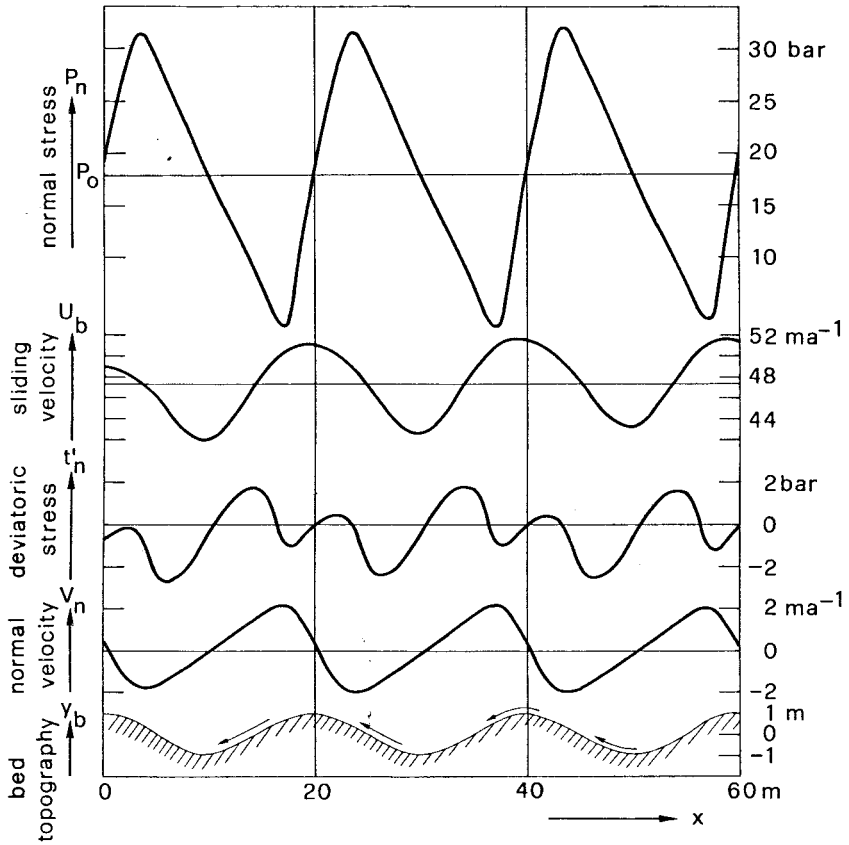
Figure F.6   Some variables along the sliding interface of
            the principal model simulating the motion of an ice
            mass over a wavy bed considering ice as a nonlinear
            viscous fluid.

From the definition above it is clear that in the case of an
asymmetrical distribution of the normal stress such features
will appear. The idea of choosing the stress deviator compo-
nent normal to the bed as a pertinent variable for simulating
sliding with friction is abandoned.

Again, as in the case of the sliding with a linear
viscous flow law, some models with different wavelength and
roughness are computed. Table F.3 provides an overview.
The sliding velocity does not, as Kamb (1970) proposed, vary
as the wavelength and as the inverse of the fourth power of
the roughness (in fact, the roughness appears also in the nu-
merator but with less effect compared to the fourth power in
the denominator). Taking the example with wavelength λ = 20 m
and roughness r = 0.08 the sliding velocity should, following
Kamb, increase by a factor of about 12 from (taking our nu-
merically computed value) 13.8 m/a to 168 m/a, if the rough-
ness is halved to r = 0.04. Table F.2 shows in our case only
an increase by a factor 6.3, still more than in the case of a
linear viscous flow law where for constant wavelength a halv-
ing of the roughness leads to a four times larger sliding ve-
locity. Thus the dependence on the roughness is stronger than
in the linear viscous case but not as strong as Kamb proposed
(Figure F.7).

r λ	0.04	0.05	0.06	0.08	0.10
10 m	26.3	16.2	9.9	5.0	3.0
20 m	86.8	47.4	29.2	13.8	7.9

Table F.2   Numerically calculated sliding velocity (non-
            linear viscous ice rheology) in m/a for varying
            roughness r and wavelength λ.
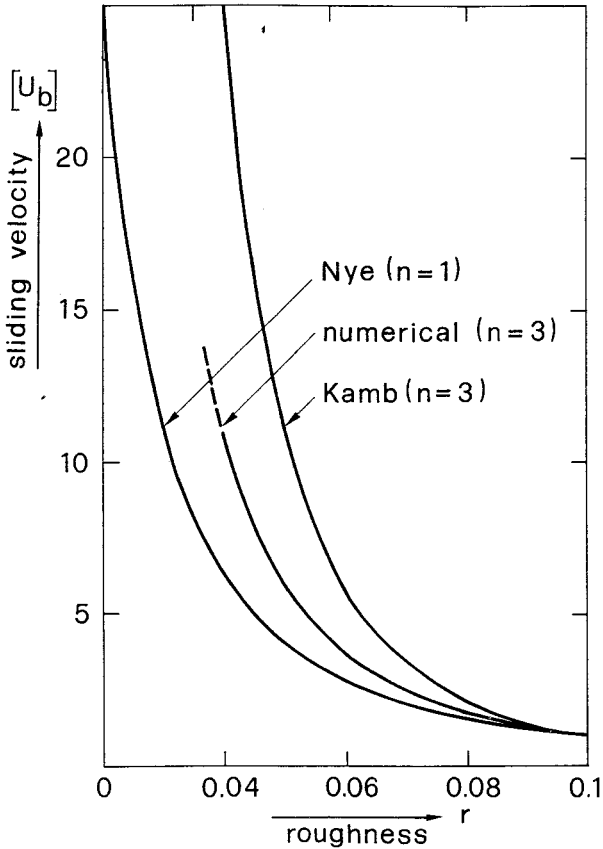
Figure F.7   Dependence of sliding velocity on roughness
            according to sliding theories by Nye (1969) and Kamb
            (1970) and derived by finite-element solution.

        In Section C.2 another approach, a numerical one by
Raymond (1978), was presented. This author introduced into
the sliding law a constant K to be determined by numerical
computation to damp down the strong dependence on the rough-
ness. The K-value for the different models in the above table
can be determined (Table F.3). Raymond calculated two K-val-
ues (n = 3) also with a finite-element program for roughness
0.005 and 0.10 and got 0.44 and 0.6 respectively.

λ \ r	0.04	0.05	0.06	0.08	0.10
10 m	0.24	0.28	0.30	0.35	0.39
20 m	0.29	0.31	0.34	0.39	0.43

Table F.3   Values of the constant K in the sliding law
(Eq. C.5c) (Raymond, 1978) deduced by finite-element
solution (see Table F.2) for different roughness r
and wavelength λ.
Values taken are: τ_b = 1.748 bar, $\bar{N}$ = 1.042 bar $a^{1/3}$

Considering that the velocity values generally tend to be a
bit too small, the K-values (Table F.3) are likely to be lar-
ger, and thus the values given are lower bounds. For in-
stance, a 50% larger sliding velocity would lead to a 14%
larger constant K. However, definitely smaller sliding veloc-
ities result from this, as opposed to Kamb's derivation. To
get for instance the velocity given by Kamb (246 m/a), a val-
ue of K = 0.54 would be necessary (we proposed K = 0.31).

It was mentioned earlier that the deformational part
of the overall motion is in the case of a nonlinear viscous
flow law much larger due to strain softening. For the above
presented models with different roughness values and wave-
length λ = 20 m, the effect of enhanced creep is studied. It
is obvious (Table F.4) that an increasing roughness is caus-
ing a larger portion of deformation due to strain softening.
The larger the roughness, the higher the stress concentra-
tions, and creep is enforced accordingly. In the last column
of Table F.4 the contribution of the strain softening is com-
pared to the sliding velocity supporting the above statement.

r	U_t	U_b	$U_d + U_{ss}$	U_{ss}	U_{ss}/U_b
0.04	135.0	86.8	48.2	26.5	0.31
0.05	86.2	47.4	38.8	17.1	0.36
0.06	62.5	29.2	33.3	11.6	0.40
0.08	41.6	13.8	27.7	6.0	0.44
0.10	33.1	7.9	25.2	3.5	0.45

Table F.4   Sliding and deformational part of the motion (in
m/a) for varying roughness (wavelength λ = 20 m).
There are:

U_t :   velocity at the top of the modelled section

U_b :   velocity at the bed

U_d :   velocity due to deformation

U_{ss}: velocity due to strain softening

It follows: $U_t = U_b + U_d + U_{ss}$

U_d is taken from the results of the model simulating
the flow of the whole ice mass: U_d = 21.7 m/a .

C.F. Raymond (personal communication) proposes to define the
sliding velocity as sum of the velocity at the interface (U_b)
and of the velocity due to strain softening (U_{ss}). This would
lead to a 30-45% larger sliding velocity.

F.1.3   Sliding with friction

The next step in simulating the sliding of an ice
mass over a wavy, rigid bed is to introduce a friction at the
sliding interface due to a dirty, debris-rich basal ice lay-
er. Thus the sliding interface is no longer perfectly lubri-
cated, but there is a frictional force parallel to the bed
rock slowing down the motion. Rock particles embedded in the
basal ice and pressed against the bed give rise to friction.
Principally the influence of a varying debris concentration

in the basal ice on the sliding velocity is studied. The
friction model of Hallet (1981) is adopted to the finite-
element computation (for details see Section E.5.2.3). It
must be pointed out that in Hallet's model the debris concen-
tration does not correspond to the conventional definition,
but refers to the number of rock particles in contact with
the bed per unit area (called by Hallet "aeral concentration
of rock particle in contact with the bed"). This sort of de-
finiton is appropriate in simulating the frictional effect of
rock particles in the basal layer, but it is difficult to ap-
ply for determining by field measurements (Shoemaker, 1988).

First of all, for three different geometries the ef-
fect of increasing debris concentration on the sliding velo-
city is studied. The three models are: the so-called "princi-
pal model" (λ = 20 m, r = 0.05; called "2005"), one with lar-
ger roughness (λ = 20 m, r = 0.10; called "2010") and one
with a smaller wavelength (λ = 10m, r = 0.05; called "1005").
The simulations are done using a linear viscous flow law.
Table F.5 is a compilation of the results, illustrated in
Figures F.8a,b. For all three geometries the reduction of the

c	0.	1.25	2.5	3.75	5.0	6.25	7.5
λ=10m r=0.05	8.76	7.70 87.9%	6.64 75.8%	5.58 63.7%	4.53 51.7%	3.46 39.6%	2.41 27.5%
λ=20m r=0.05	17.25	15.30 88.7%	13.53 78.4%	11.76 68.2%	9.99 57.9%	8.23 47.7%	6.46 37.4%
λ=20m r=0.1	4.31	4.01 92.9%	3.70 85.9%	3.40 78.8%	3.09 71.8%	2.79 64.7%	2.48 57.6%

Table F.5   Effect of areal concentration of rock particles
(c in m^{-2}) on the sliding velocity (in m/a) for
varying wavelength and roughness. Reduced sliding
velocity is given as percentage.

sliding velocity is linear to the debris concentration. The
model known as "1005" is slowed down the most, while "2010"
with the smallest sliding velocity is slowed down the least.
However, with only three models it is almost pure speculation
to say that the reduction of the slding velocity varies as
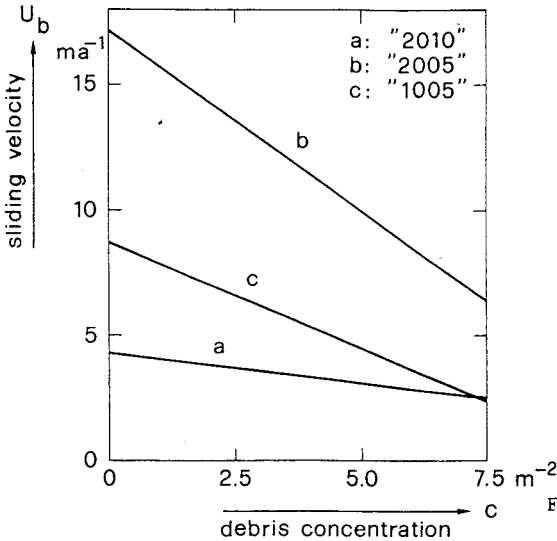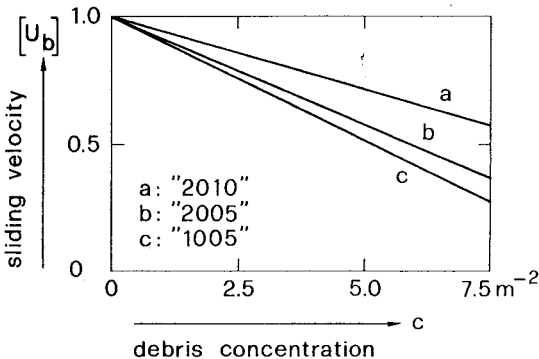the inverse of both the roughness and the wavelength.

Figure F.8a,b
Dependence of slid-
ing veloctiy on de-
bris concentration
for three models
with different
geometries. Above
(a) in absolute
values, below (b)
normalized to the
sliding velocity
for the case of no
friction (so-called
reduced sliding
velocity).

The above results can be used only in a qualitative
sense, since the sliding velocities are much too small. This
follows simply from the fact that the frictional force is
proportional to the normal velocity calculated from the model
without friction. Thus to get an appropriate result one is
forced to use an iterative procedure. The numerically comput-
ed normal velocity of the previous run is used to calculate
the fricitonal force as input for the subsequent run. Conver-
gence within three digits is reached after about ten steps.
The iterations are done for the principal model for two dif-
ferent debris concentrations: $c = 3.75 \text{ m}^{-2}$ and $c = 6.25 \text{ m}^{-2}$.
An aeral concentration of $c = 3.75 \text{ m}^{-2}$ means that 15% of the

c	3.75	6.75
U_{bf}	13.5	11.8
U_{bf}/U_b	0.78	0.67

Table F.6   Sliding velocity (U_{bf} in m/a) of the principal
model (iterative solution) for two different values
of the debris concentration (c in m^{-2}). The quotient
U_{bf}/U_b denotes the reduced sliding velocity.
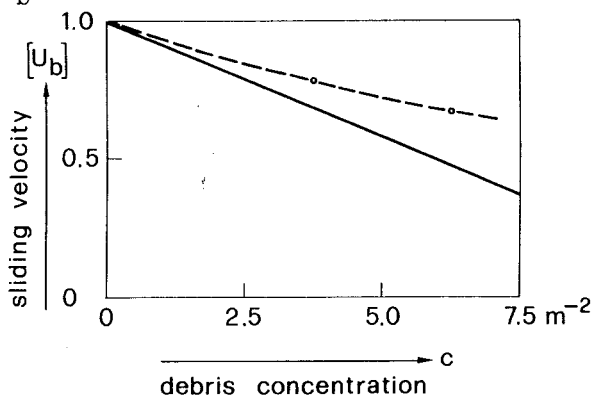U_b: sliding velocity for debris-free ice.

Figure F.9   Dependence of reduced sliding velocity on the
debris concentration. Upper points and dashed line
show iterative solution.

sliding interface is covered with rock particles of 10 cm ra-
dius contributing to friction. Table F.6 contains the re-
sults.

It is surprising that the two cited above reduced sliding ve-
locities and the one without friction are not located on a
straight line (Figure F.9). Thus the reduced sliding velocity
does not vary linearly as the inverse of the debris concen-
tration.

    We are now looking more closely at the principal mo-
del with a debris concentration of $c = 3.75 \ m^{-2}$. The sliding
velocity is as mentioned

$$U_{bf} = 13.5 \ m/a \quad .$$

At the top of the modeled section the velocity is

$$U_{tf} = 24.6 \ m/a \quad .$$

Thus the difference obtained is the velocity due to deforma-
tion

$$U_{df} = 11.1 \ m/a \quad ,$$

a value slightly smaller (3.5%) than in the case of no fric-
tion.

The **velocity field** (Figure F.10) is not remarkable in any
way. It is very similar to the one without friction (Figure
F.1), altough the velocity vectors are smaller. The scale in
Figures F.1 and F.10 is the same, so the velocities can be
directly compared.

The **stress field** (Figure F.11) distinctly shows the two dif-
ferent boundary conditions at the glacier bed. On the up-
stream side of the rock bumps the orientation of the axis of
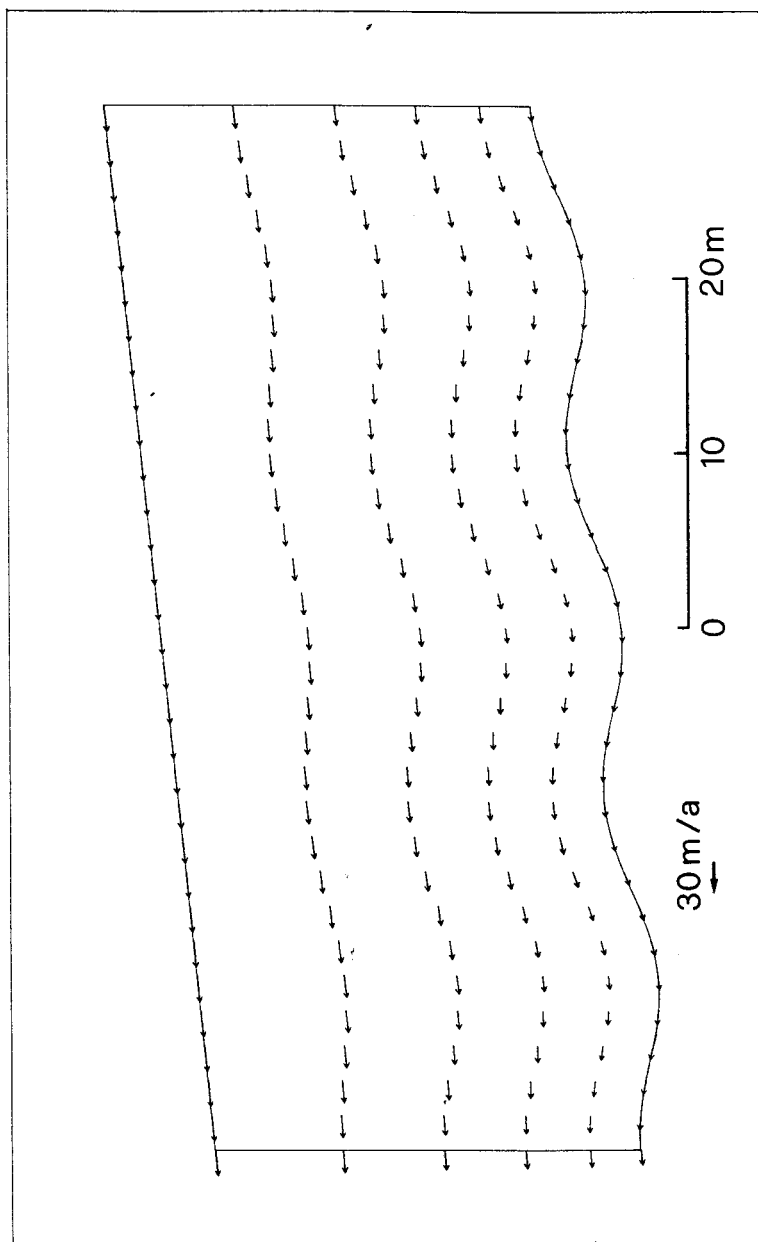principal stress is about 45° inclined to the interface, the

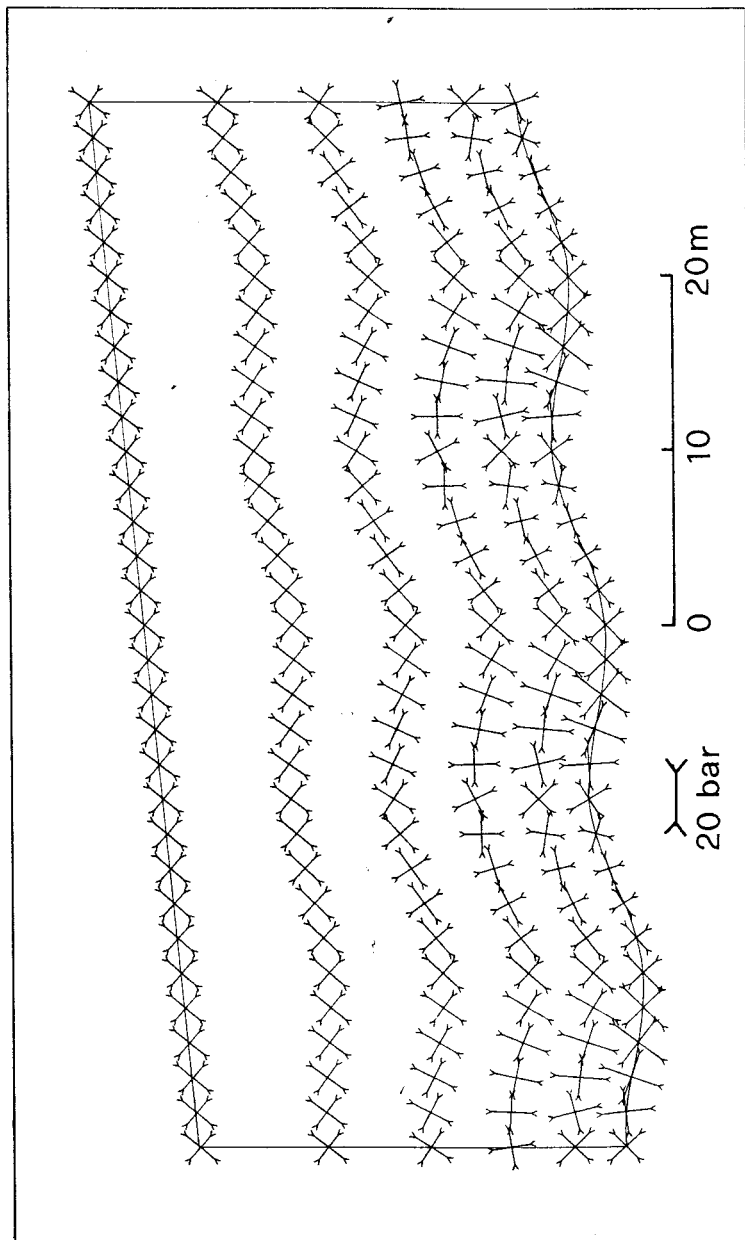Figure F.10 Velocity field of the principal model with a debris concentration of
c = 3.75 m^{-2}.

Figure F.11   Stress field of the principal model with a debris concentration of
$c = 3.75 \ m^{-2}$.

effect of a large shear stress due to friction. On the lee
side where no friction is existent and the bed is perfectly
lubricated, one of the axes of principal stress is nearly
parallel to the sliding interface.

Figure F.12 unites some variables along the sliding
interface, subsequently discussed in detail.

(a)   **Sliding velocity U_{bf}**
The sliding velocity varies between 13.0 m/a and
14.0 m/a (Figure F.12). The variation is a bit larger (±3.7%)
than in the case of no friction (±2.4%), probably an effect
of the varying boundary condition. The curve of the sliding
velocity is no longer in phase with the bed undulation, but
shifted downhill about one-tenth of a wavelength. At the top
of rock bump is the last node where a frictional force slows
down the motion, thus the largest velocity is a bit later
just after the top, in the lee where the bed is again per-
fectly lubricated.

(b)   **Velocity normal to the bed V_n**
The velocity component normal to the sliding inter-
face is calculated from the velocity values in the node line
1 m above the bed. Although the sliding velocity is in case
of friction generally smaller, the component normal to the
bed is it not, but is increasing relatively about 15-20% com-
pared to the case of no friction. This means that the normal
velocity is generally reduced less than the sliding velocity.
In addition the curve (Figure F.12) is very similar to the
one without friction.

(d)   **Normal stress P_n**
The normal stress (Figure F.12) is substantially
less oscillating than in the case of no friction, however, it
still has a mean pressure of about 17.4 bar. Varying between
26.5 bar and 9.1 bar the amplitude of the stress oscillations
is only

$$\Delta p_{max} = 8.66 \text{ bar}$$

instead of 11.1 bar as one could expect from the theory.

The result is important for the case where subgla-
cial water pressure is acting. Key values such as the separa-
tion pressure depend on the minimal normal stress. In the
considered case of friction the minimum normal stress is in-
creased from 6.4 bar to 9.1 bar, an increase of more than
40%. The amplitude of stress oscillation is defined as (Eq.
C.15)

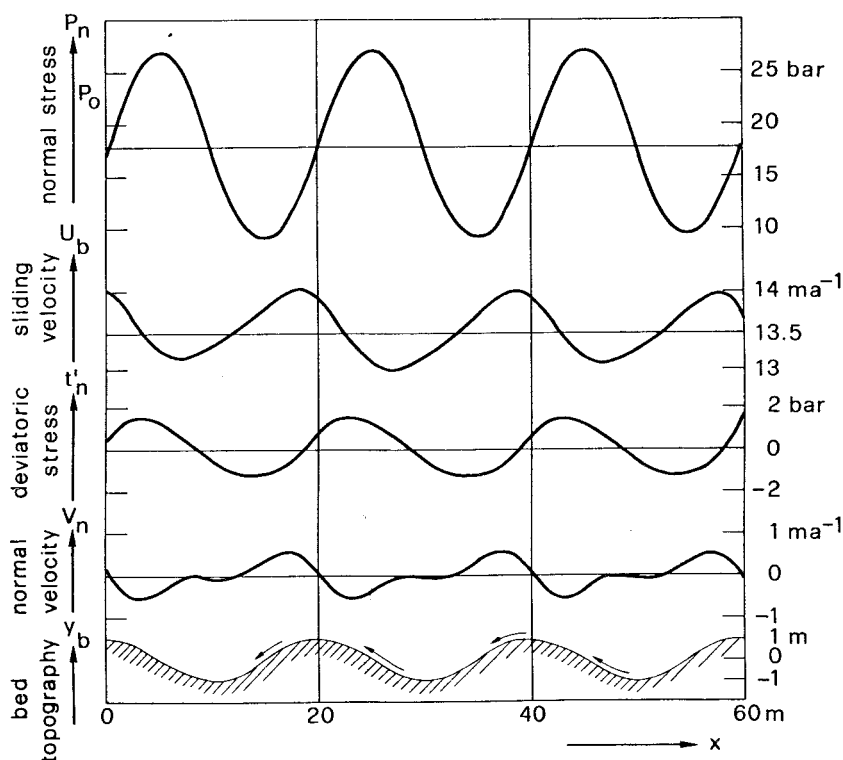$$\Delta p_{max} = \frac{\lambda \, \tau_b}{\pi \, a} \quad .$$

Figure F.12   Some typical values along the sliding interface
of the principal model for sliding with friction
(aeral basal debris concentration c = 3.75 m^{-2},
iterative solution).

As wavelength and amplitude of bed undulation are constant, the smaller amplitude of the normal stress must be due to a smaller driving shear stress. In the case of solid friction between ice and rock, a part of the shear stress due to gravity is used to overcome the friction, thus less is left for driving the ice mass downhill. A basal shear stress

$$\tau_b = 1.36 \text{ bar}$$

results, only 78% of the shear stress due to gravity

$$\tau = \rho g h \sin\alpha = 1.75 \text{ bar}.$$

The reduction of the shear stress is in perfect agreement with the reduction of the sliding velocity. The shear stress used to overcome the friction is

$$\tau - \tau_b = \tau_f = 0.387 \text{ bar} \quad .$$

(d)   **Normal stress deviator t_n'**

The curve of the stress deviator component normal to the bed (Figure F.12) is, as the curve of the sliding velocity, shifted downhill. Maximum and minimum values do not coincide with the inflexion points of the undulating bed. Absolute values are about the same as in the case of no friction: 1.5 bar.

There are some computations done for the case of a nonlinear viscous flow law of ice to detect the general trend. The idea was to take the principal model and to numerically calculate the sliding velocity for the same increasing values of the debris concentration. The normal velocity values of the principal model without friction are used to determine the frictional nodal forces. But already a debris concentration of $c = 3.75 \text{ m}^{-2}$ leads to an uphill motion at the base of about 5 m/a (Table F.7, Figure F.13).

c	1.25	1.875	2.5	3.75
U_{bf}	25.52	17.38	10.52	-5.35
U_{bf}/U_b	0.538	0.366	0.222	

Table F.7   Sliding velocity (U_{bf} in m/a) of the principal
            model for different values of the debris concentra-
            tion (c in m^{-2}) using a nonlinear viscous flow law.
            U_{bf}/U_b is the reduced sliding velocity.
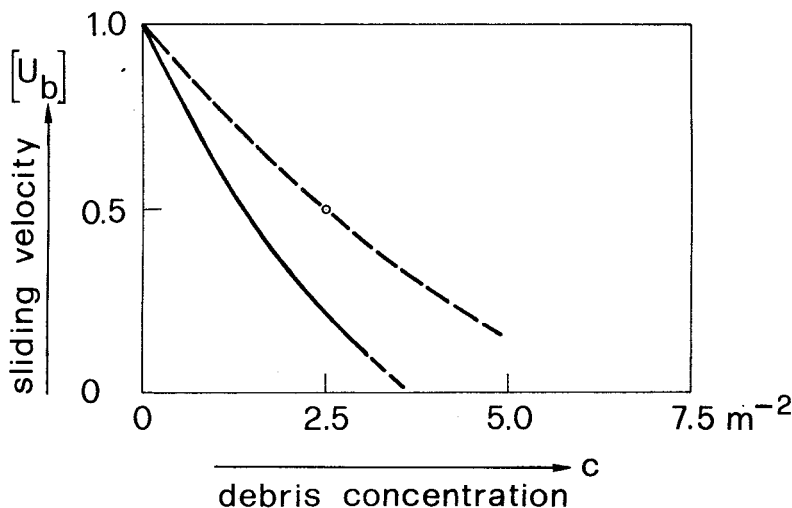

Figure F.13   Dependence of nonlinear viscous sliding veloc-
              ity U_{bf} on the debris concentration c. Dashed line
              indicates probable curve of iterative solution.

It is obvious that if the iterative procedure to determine
the frictional force were applied, the reduction of the slid-
ing velocity would not be so tremendous. It was shown above
that the reduction of the sliding velocity corresponds to a
reduction of the driving shear stress τ_b. Using a nonlinear
viscous flow law such as Glen's law with exponent n = 3 it
can be assumed that the decrease in the sliding velocity is
correspondingly   larger.   For   a   debris   concentration   of
c = 3.75 m^{-2} one gets a reduced sliding velocity of 0.78 when

a linear viscous flow law is applied. It is supposed that with nonlinear ice rheology the reduction is $(0.78)^3 = 0.48$, which means that if about 15% of the glacier bed is covered with rock particles embedded in the basal ice contributing to friction, the sliding velocity is halved compared to the case of clean ice on a perfectly lubricated bed (Figure F.13).

F.2   Sliding with bed separation

Sliding with bed separation as an effect of sub-lacial water pressure was studied in detail by Iken (1981) using an earlier version of the finite element code RHEO-STAUB. In particular the transient stages of growing and shrinking water-filled cavities at the ice-bedrock interface were analysed. The introduction of a frictional drag at the sliding interface is the innovation of the present study. In this context the effect on the separation and the critical pressure is of main interest. The present work does not extend to the point where the cavities reach a steady state shape. Except for one, all computations are done using a linear-viscous flow law. The effect of subglacial water pressure on the sliding velocity without any friction is considered first, as the basis for this study, and the friction is added afterwards.

F.2.1   Frictionless sliding with bed separation

According to the theory, bed separation and hence the onset of cavity formation starts when the subglacial water pressure reaches the minimal normal stress. This limiting value is known as separation pressure. In the case of the principal model (λ = 20 m, r = 0.05) the separation pressure

is given as

$$P_s \; = \; 6.35 \text{ bar}$$

(for details see Section C.3.3.2). At a subgacial water pressure

$$P_w \; > \; 11.91 \text{ bar} \; = \; P_c$$

(called critical pressure) the glacier motion becomes accelerated, i.e. unstable. For studying the effect of the subglacial water pressure on the sliding velocity, eight different models with increasing water pressure values between 6.35 bar and 11.64 bar are chosen.

Table F.8 and Figure F.14 contain the results of the numerical computations of the corresponding sliding velocities.

P_w	$[\bar{P}_w]$	U_{bw}	U_{bw}/U_b
7.46	0.1	17.06	0.99
8.58	0.2	17.61	1.02
9.13	0.25	18.42	1.07
9.69	0.3	19.58	1.14
10.25	0.35	22.44	1.30
10.80	0.4	25.32	1.47
11.36	0.45	37.26	2.20
11.91	0.475	45.01	2.66

Table F.8 Numerically calculated sliding velocity U_{bw} (in m/a) for different values of the subglacial water pressure P_w (in bar). U_{bw}/U_b represents the relative increase compared to the sliding velocity without bed separation (U_b = 17.25 m/a). The normalized dimensionless water pressure $[\bar{P}_w]$ expresses the relation to the separation pressure (P_s: $[\bar{P}_w]$ = 0), the critical pressure (P_c: $[P_w]$ = 0.5) and the mean ice overburden pressure (P_o : $[P_w]$ = 1.0).

Figure F.14 shows the very typical relationship be-
tween the sliding velocity and the subglacial water pressure:
For a given geometry the sliding velocity is a constant, as
long as the water pressure is below the separation pressure
(determined, neglecting friction, only by the geometry). Then
the velocity is progressively increasing with increasing wa-
ter pressure. However, if the water pressure exceeds the
critical pressure the ice mass accelerates and becomes unsta-
ble and the velocity theoretically tends to infinity. The
above is true only for the very special case of an ice mass
sliding without friction over a rigid, sinusoidal rock bed.
No effects of friction nor any changes in the subglacial
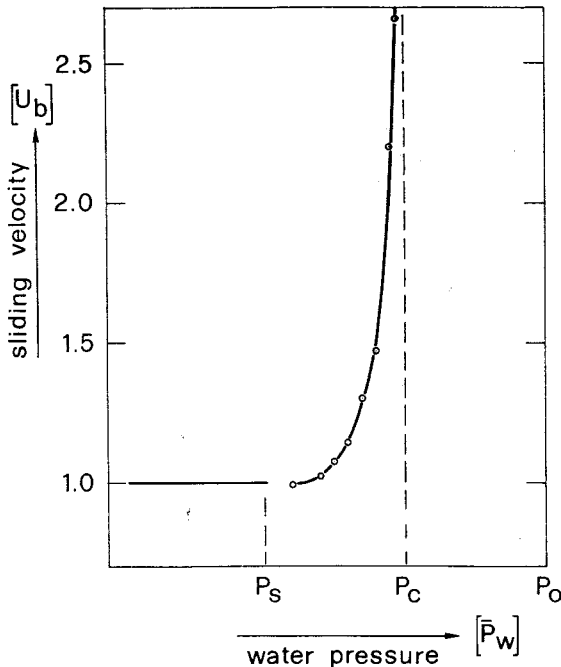hydraulic system are considered.

Figure F.14   Dependence of sliding velocity on the subgla-
cial water pressure. Normalized representation:
$[U_b] = U_{bw}/U_b$ and $[P_w] = P_w/P_o$; $U_b = 17.25$ m/a,
$P_o = 17.48$ bar.

A few words on the details of the numerical computation: For a given water pressure the sliding velocity depends strongly on the area where the water pressure is acting. As discussed in Chapter E, stable cavities cover a larger area than one would expect from the distribution of the normal stress. For the numerical computation considering transient cavities, the area of acting water pressure was chosen with the help of the theoretical relationship for the bed separation (see Section C.3.3.3). However, since only certain discrete values for the area can be chosen taking three, five, seven etc. nodes, the curve (Figure F.14) describing the relation between subgacial water pressure and sliding velocity grows not continuously but stepwise. This deficiency could only be removed by increasing the number of nodes directly at the sliding interface. For a given cavity size, the sliding velocity varies with the water pressure. Only when the area where the water pressure can attack is enlarged by including another two nodes, does the slope become steeper and finally the typical progressively increasing curve results.

Again a characteristic velocity (Figure F.15) and stress (Figure F.16) field of the principal model are shown for a water pressure value of 11.6 bar (near to the critical pressure of 11.9 bar). Some features are worth pointing out: Clearly visible is the flow away from the bed in the lee of the rock bumps (producing cavities) and the upward motion at the top of the modelled section. This means the subglacial water pressure is lifting the whole ice mass a little bit. Remarkable in the stress field are the principal stresses in the lee of the bed undulation, representing exactly the prescribed boundary condition, and the large stress values on the upstream side being important with regard to simulating friction.

There is only a single numerical computation performed for the case of a nonlinear flow law. The sliding velocity is calculated at a water pressure $P_w = 10.8$ bar
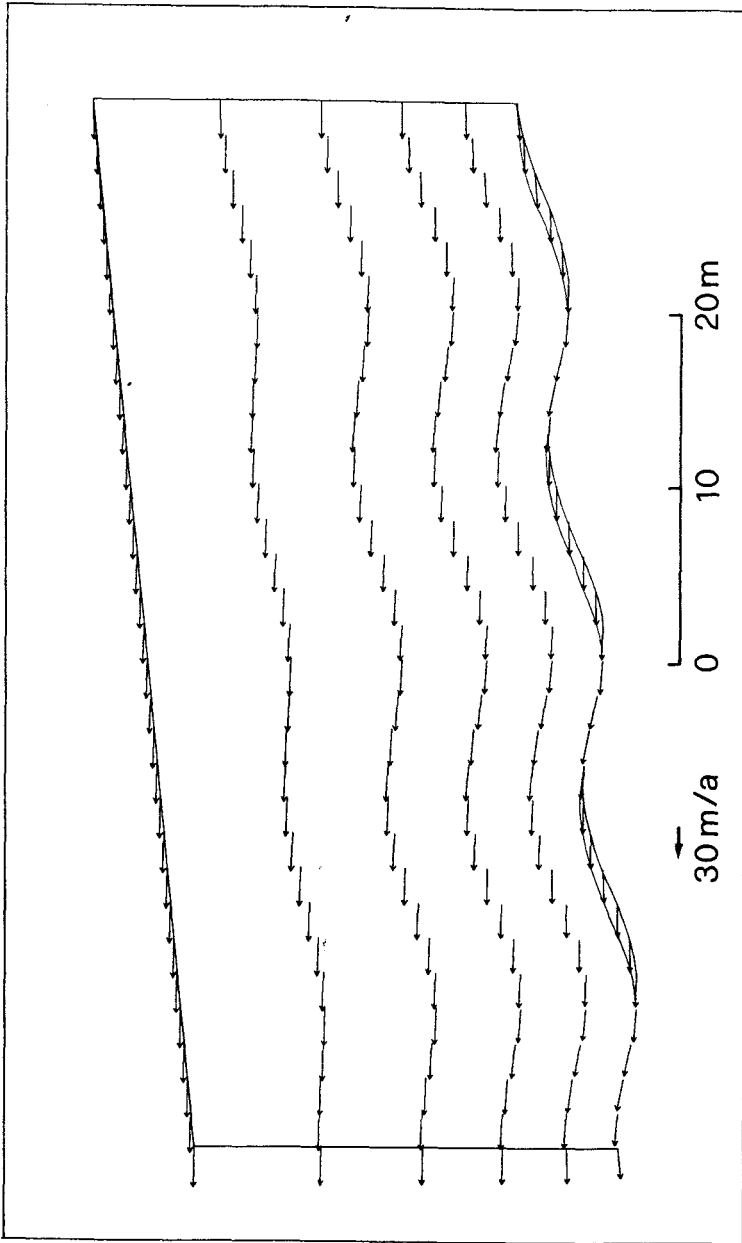
Figure F.15   Velocity field of the principal model for subglacial water pressure of $P_w = 11.6$ bar.
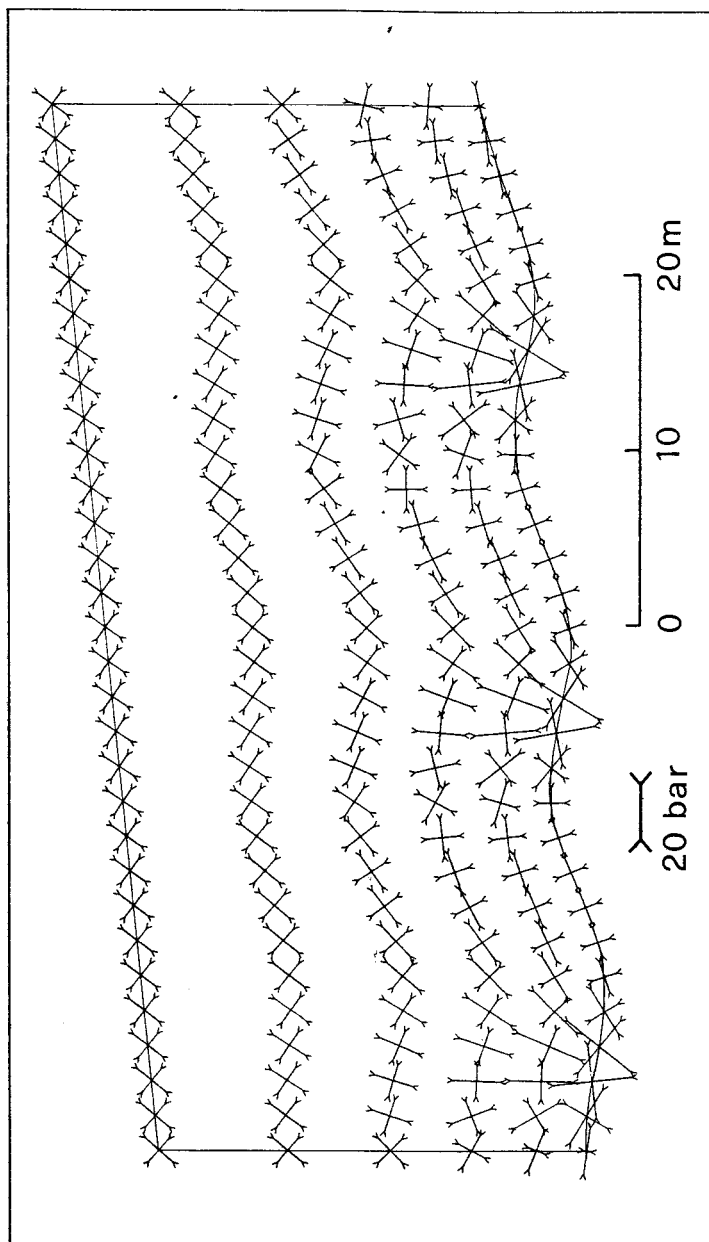
Figure F.16 Stress field of the principal model represented by principal stresses. There is no friction, but a subglacial water pressure of $P_W = 11.6$ bar is acting.

$$U_{bw} = 67.78 \text{ m/a}$$

a comparably small value, since the sliding velocity where no water pressure is acting is

$$U_b = 47.44 \text{ m/a} \quad .$$

The quotient U_{bw}/U_b expressing the increase of the sliding velocity in the case of bed separation is even a little smaller than the one obtained using a linear viscous flow law (1.43 compared to 1.47). Therefore one can say that the sort of flow law used seems not to be important for the amount of the velocity increase in the case of bed separation, at least in the case studied where the bed separation is rather small (s = 0.35).

F.2.2   Sliding with friction in presence of bed separation

Up to this point the two effects of bed separation and of friction due to debris in the basal ice were studied separately. Combining the two important variables, subglacial water pressure and aeral basal debris concentration will show, for instance, whether the friction is enforced if the ice is separating from the rock bed.

As pointed out in the previous section, a crucial variable is the area of bed separation varying with the debris concentration. It is therefore critical to compare cases with different debris concentrations. For the sake of clarity, the amount of bed separation s is given in most results of the numerical computations (for the definition of s see Section C.3.3.3). The parameter s is determined only approximately by simply comparing the number of nodes where the water pressure is acting with the number of all nodes (=20) in one single wavelength.

c	U_{bwf}	U_{bwf}/U_{bw}
0.	25.32	1.0
1.25	21.00	0.84
2.5	17.19	0.68
3.75	13.38	0.53
5.0	9.61	0.37
6.25	5.90	0.22
7.5	2.45	0.07

Table F.9 Numerically calculated sliding velocity values
(U_{bwf} in m/a) for increasing debris concentration
(c in m^{-2}) at a constant water pressure P_w= 10.8bar.
U_{bw}: sliding velocity of debris-free ice

The dependence of the sliding velocity on the debris concen-
tration in the case of bed separation was studied with a con-
stant value of the subglacial water pressure P_w= 10.8 bar and
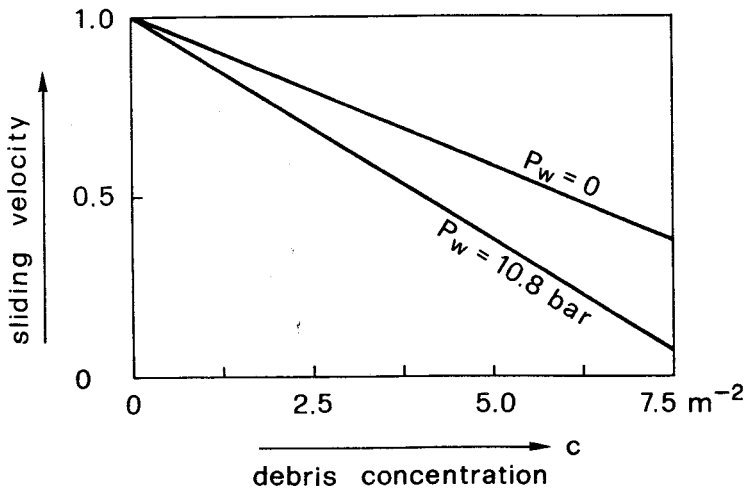

Figure F.17 Dependence of sliding velocity on the debris
concentration in basal ice for a water pressure of
10.8 bar and a bed separation parameter of s = 0.35.
Upper line gives the relation in the case of no bed
separation.

a constant bed separation parameter s = 0.35 (a rather unrealistic assumption). The results can be found in Table F.9 and in Figure F.17 where the reduction of the sliding velocity is also given for the case of no bed separation (see Table F.5). The water pressure P_w = 10.8 bar has to be seen in relation to the separation and the critical pressure. In the case of clean basal ice (c = 0) the water pressure P_w is near the critical pressure, and on the other hand, for dirty basal ice (c = 5.0) the chosen water pressure is about in the middle between the two limiting pressures (as will be shown below). In other words it is not easy to give precise quantitative values for the increase of friction in the case of bed separation. However, an increase is explicitly proven and a

P_w	s	U_{bwf}	U_{bwf}/U_b
8.58	0.15	13.19	0.76
9.69	0.25	13.40	0.78
10.80	0.35	15.01	0.87
11.36	0.45	17.68	1.03
11.64	0.45	19.12	1.11
11.91	0.45	20.56	1.19
12.47	0.55	30.11	1.75

P_w	s	U_{bwf}	U_{bwf}/U_b
10.80	0.15	9.68	0.56
11.36	0.15	9.79	0.57
11.64	0.35	16.75	0.97
11.91	0.35	17.33	1.01
13.03	0.45	26.36	1.53
13.47	0.55	42.57	2.47

Table F.10a,b   Dependence of the basal sliding velocity U_{bwf}
(in m/a) on the subglacial water pressure P_w (in
bar) in the case of friction for two values of the
debris concentration: above (a) for c = 2.5 m^{-2} and
below (b) for c = 5.0 m^{-2}. The amount of bed separa-
tion is expressed by the parameter s. Without bed
separation and without friction the sliding velocity
is U_b = 17.25 m/a.

rough estimation is 50%. Without considering the effect of
the smaller sliding velocity in the case of friction (leading
to smaller frictional forces) the reduction of the sliding
velocity varies linearly as the debris concentration for a
certain constant water pressure. No iterations are made to
take into account the reduction of friction due to the reduc-
ed sliding velocity.

How the sliding velocity in the case of friction is
dependent on the water pressure is studied for two different
debris concentrations: $c = 2.5 \text{ m}^{-2}$ and $c = 5.0 \text{ m}^{-2}$ (Tables
F.10a and F.10b). Hence, in contrast to the computation
above, the amount of friction is constant but the separation
area increases with increasing water pressure. However, the
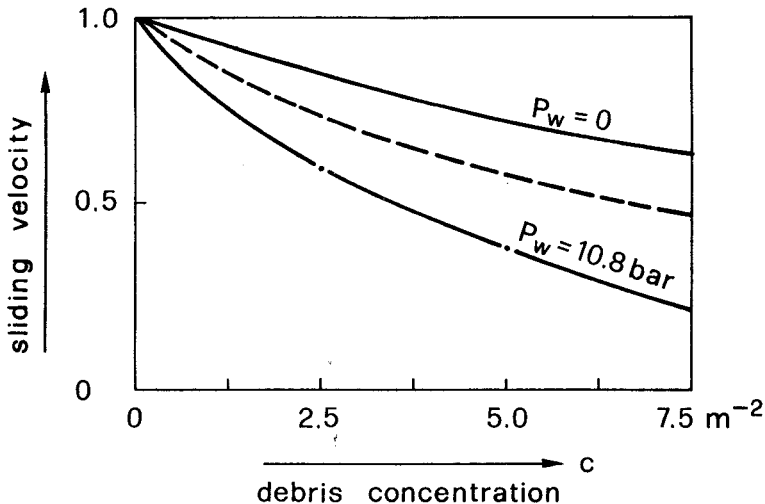separation process is different for the two debris concentra-

Figure F.18   Dependence of basal sliding velocity on the de-
         bris concentration in basal ice in the case of no
         bed separation ($P_w = 0$, iterative solution, see Fig-
         ure F.9) and in the case of bed separation for a wa-
         ter pressure of $P_w = 10.8$ bar. Dashed line shows es-
         timated iterative solution for the case of bed sepa-
         ration. Linear viscous flow law is used.

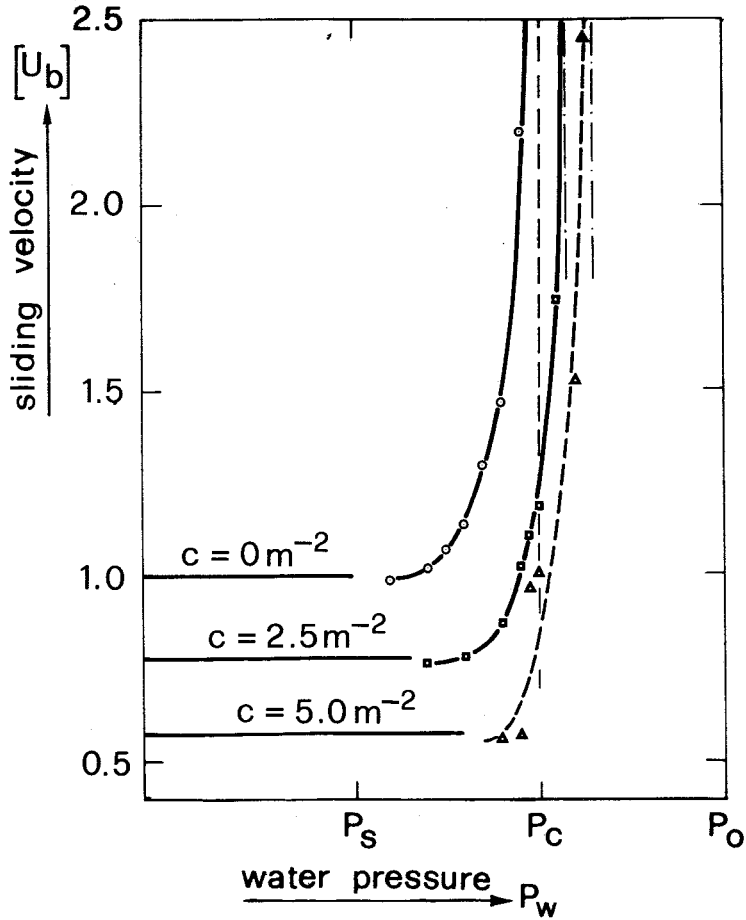Figure F.19   Dependence of the basal sliding velocity U_b on
both the subglacial water pressure P_w and the basal
debris concentration c. The sliding velocities are
normalized to the velocity which was calculated
without friction and without bed separation. Two
cases with c = 2.5 m^{-2} and c = 5.0 m^{-2} are consider-
ed. Horizontal lines at left side represent the
state before bed separation starts. Dashed vertical
lines (asymptotes) give the critical pressure, ris-
ing with increasing debris concentration.

tions. The larger the friction the later starts the separa-
tion. For instance, at a water pressure of P_w = 10.8 bar the
bed separation parameter is s = 0.35 and s = 0.15 respective-
ly for the debris concentrations studied. In Figure F.18 this
effect is taken into account and it is tried to give an over-
view including an estimation of an iterative solution in the
case of friction. In contrast to Figure F.17 in which the
variation of the bed separation is neglected, the sliding ve-
locity varies not linearly as the debris concentration.

Figure F.19 shows the results of the numerical com-
putations of sliding with friction in the case of bed separa-
tion for both, varying debris concentration and varying water
pressure. The typical relationship between sliding velocity
and subglacial water pressure remains valid, also in the case
of friction. However, the curves are shifted to the right, to
larger water pressure values. This simply means separation
and critical pressure are larger in the case of friction.

The critical and the separation pressure depend on
the normal stress amplitude Δp_{max} which is as shown in Sec-
tion F.1.3 smaller in the case of friction than without.
Based on the calculation of the normal stress amplitude for a
debris concentration of c = 3.75 m^{-2} (see Section F.1.3), the
stress amplitude for the debris concentrations c = 2.5 m^{-2}
and c = 5.0 m^{-2} can be determined by a linear interpolation
to 9.48 bar and 7.84 bar respectively. This values of the
normal stress amplitude can be used to calculate (Eq. C.16
and C.17) the separation and the critical pressure in the
case of friction. The smaller oscillation of the normal
stress leads to smaller values of the separation and the
critical pressure. Table F.11 is a compilation of calculated
values of the separation and the critical pressure based on
the numerical computation of the normal stress amplitude in
Section F.1.3.

Figure F.18 shows clearly that the pressure values
calculated in the way described above coincide with the val-
ues which can be drawn from the figure. This fact is a fur-

c	0.	2.5	5.0
P_s	6.35	7.99	9.64
P_c	11.91	12.74	13.56

Table F.11   Separation (P_s) and critical pressure (P_c) (in bar) of the principal model for different debris concentrations (c in m^{-2}); P_o = 17.5 bar.

ther indication that the assumption that friction can be seen as a reduction of the driving shear stress may be true.

In contrast to the theoretical considerations on Coulomb friction in section D.3.3.2, the assumption (from sliding without friction) that the critical pressure is half-way between the separation and the ice overburden pressure holds true. It seems obvious that for larger debris concentrations the critical pressure at which the unstable sliding motion starts can well be near the ice overburden pressure. However, the separation pressure is increasing accordingly. From the field work on the Findelengletscher (Iken and Bindschadler, 1986) a stronger effect on the critical pressure than on the separation pressure was expected. This observation could not be reproduced by the numerical calculations.

Chapter G

CONCLUSIONS

G.1 Summary

The results from the field work on the Findelenglet-
scher (Iken and Bindschadler, 1986)   formed the starting
point of this report. The glacier advanced about 185 m bet-
ween 1979 and 1982. Theoretical studies of glacier sliding
should help to understand the mechanics involved, in particu-
lar in the presence of friction. However, the reader is not
provided with a complete state-of-the-art account of sliding,
since the problem is much too complex.

Long-term combined velocity and water pressure mea-
surements on Findelengletscher gave rise to the key question:
What causes the Findelengletscher to move stably at water
pressure values near the ice overburden pressure?
From the theoretical point of view there are no ar-
guments to refute the existence of a critical pressure caus-
ing unstable sliding well below the ice overburden pressure.
The probable explanation is that friction at the base leads
to the observed feature. Thus the aim of the study was to

clarify the influence of friction on the sliding behaviour of
a glacier with special regard to the critical pressure.

Based on the well-known theory on frictionless slid-
ing over a sinusoidal bed (Nye, 1969) a relation was develop-
ed between the subglacial water pressure and the bed separa-
tion in which the critical pressure is a pertinent variable.
If the water pressure exceeds the critical pressure the ice
is fully separated and the water pressure has access to the
whole glacier bed area: the motion becomes unstable.

The classic basal boundary condition is the perfect
slip condition where a thin water film prevents all friction.
This assumption is doubtful, as striaes on rock bumps demon-
strate. Friction is mainly due to the interaction between
rock particles in the basal ice layer and the glacier bed.
Relevant to the sort of process is the debris concentration
in the basal ice layer. We distinguish between sandpaper
friction and Hallet friction. Sandpaper friction applies for
large debris concentrations (>50% per volume) with particles
being in close contact and is a sort of Coulomb friction. Be-
cause Coulomb friction is basically reserved for the friction
between rigid bodies (ice is a viscous one), the term sandpa-
per friction was invented based on the image of the ice mass
rubbing like a piece of sandpaper over the undulating bed.
Hallet friction is based on the abrasion model by Hallet
(1981) and is appropriate for small debris concentration,
where the rock particles are no longer in contact with each
other and the ice can accordingly flow around them. Hence the
force pressing the particles to the bed depends in this case
not on the ice overburden or effective pressure, but on the
local flow pattern.

To evaluate the effect of friction of the Hallet
type on the sliding velocity in the presence of subglacial
cavity formation a numerical approach is necessary. Consider-
ing ice as an incompressible, viscous fluid the resulting set
of differential equations describing the glacier flow was
numerically solved by the finite-element method using a well-
established code (RHEO-STAUB).

Frictionless sliding was simulated as a test of the solution method. Nye's (1969) solution for linear viscous flow law could be reproduced. Yet, using a nonlinear flow law, the results were different from those obtained by Kamb (1970). His approximative solution seems to depend too strongly on the roughness.

The numerical simulations of sliding with friction showed clearly that in the case of a nonlinear viscous flow law, a debris concentration of about 10% per volume slows down the sliding motion to 50% of the value calculated with debris-free ice. Thus friction is an important factor in the sliding process. When the ice separates from the bed the Hallet friction does not vary much, but to start the bed separation a larger water pressure must operate: 25% larger in the case where the debris concentration is about 10%. With or without friction the sliding velocity increases strongly when the water pressure approaches a certain value: the critical pressure. Friction gives rise to an increase of the critical pressure, closer to the ice overburden pressure. Thus the assumption remains that the critical pressure is halfway between the separation and the ice overburden pressure. This result is compiled in Figure F.19.

The sandpaper friction has a similar effect on the sliding motion, providing the sliding starts at all. It can easily prevent any sliding to occur. For instance, for a mean bed slope of 5.7° and an intermediate value of the friction coefficient (μ = 0.5), a sliding motion is only possible if the water pressure is at least 80% of the ice overburden pressure. If the ice separates from the bed the frictional drag is decreasing, not proportional to the decreasing effective pressure, but more slowly. The bed separation is affected by the frictional drag and as in the case of Hallet friction, both separation and critical pressure are shifted to larger water pressure values. It is possible that the separation pressure is theoretically larger than the critical pressure.

G.2   Conclusions

        Friction between a dirty basal layer and the glacier
bed is a relevant process. One of the basic working assump-
tions proved to be reasonable: friction can be seen as a re-
duction of the driving shear stress. This viewpoint provides
a very useful basis for including the frictional drag into
existing sliding laws which should in our opinion contain the
critical pressure as an important variable. We propose a re-
lation such as Equation D.24, since with and without friction
the numerical computations simulating the sliding of an ice
mass over a sinusoidal bed with bed separation verified the
existence of the critical pressure.

        One of the principal differences between sandpaper
and Hallet friction is the influence of the water pressure in
case of bed separation. The effect on separation and critical
pressure is quite different. The frictional drag is in the
case of Hallet friction nearly independent of the water pres-
sure. And hence critical and separation pressure increase si-
multaneously. Therefore, in the case of Hallet friction the
critical pressure is halfway between the separation pressure
and the ice overburden pressure. In the case of sandpaper
friction the frictional drag is reduced with increasing water
pressure. This gives rise to an interesting result: the sepa-
ration pressure is larger than the critical pressure for al-
ready small values of the friction coefficient. This leads to
stick-slip motion. Yet both types of friction cannot explain
the observation at Findelengletscher, where the critical
pressure was much more affected than the separation pressure.
Extensive permanent sliding motion (≥50% of the whole move-
ment) seems only to be possible if the friction is of the
Hallet type. Therefore, if the sliding velocity and some wa-
ter pressure values of a glacier are known one can then es-
timate the type of friction and furthermore the basal debris
concentration. Two typical examples seem to be: Findelenglet-
scher and Unteraargletscher. The first one is sliding all the
time and a small debris concentration will cause friction of
the Hallet type. Unteraargletscher, on the other hand, is

rather slow-moving and debris-covered in the lower part. Cal-
culation of the surface velocity, based on internal ice de-
formation, suggests that the sliding velocity is negligible,
except during the melt season. The basal debris concentration
seems to be high and hence sandpaper friction is acting.

G.3   Open questions and outlook

A distinct classification of a larger number of gla-
ciers is not yet possible, partly due a lack of field data,
partly due to the more qualitative results of the study. This
work was primarily conceived as a sensitivity study on slid-
ing. Realistic, but not actually measured values were chosen
for the numerical simulation describing a very idealized sit-
uation. A glacier is of course not two-dimensional and the
bed is not sinusoidal.

A weak point in Hallet's theory is that he tacitly
assumes that there are always rock particles in contact with
the bed. Actually the rock fragments tend to move away from
the bedrock by the action of the strain field. It is not
clear whether the production of new rock fragments by erosion
will balance the first effect. These physical processes at
the base, including abrasion and erosion, remain to be inves-
tigated.

The next step should be to become even more specific
and try to model the dynamic movement of certain real gla-
ciers for which abundant data is available. Detailed informa-
tion of the geometry (three-dimensional), the surface veloci-
ty, the internal deformation and the mass balance is neces-
sary. A relatively large amount of information exists for
Findelengletscher. Investigations on former glacier beds
could perhaps improve the knowledge on actual glacier beds.
More attention should be paid to the question of sediment
("soft") beds, as they are widespread.

Because sliding can be a dominant process in the
motion of glaciers, it would be worthwhile to seek a general
sliding law (a rather far-off aim at present).

References

Aellen, M. and Iken, A., (1979): Variationen der Gletscherbe-wegung. VAW-Mitteilung No.37, p.111-125.

Bentley, Ch.R., (1987): Antarctic ice streams: a review. Journal of Geophysical Research, Vol.92, No.B9, p.8843-8858, Aug.10, 1987.

Berner, W., Stauffer, B. and Oeschger, H. (1978): Dynamic glacier flow model and the production of internal meltwater. Zeitschrift für Gletscherkunde und Gla-zialgeologie, Bd. 13, p.209-217.

Bindschadler, R. (1983): The importance of pressurized sub-glacial water in separation and sliding at the gla-cier bed. Journal of Glaciology, Vol.29, No.101, p.3-19.

Boulton, G.S. (1974): Processes and patterns of glacial ero-sion. (In Coates (Ed.) Glacial geomorpholoy Bingham-ton, NY, p.41-87.

Bowden, F.P. and Tabor, D. (1964): The friction and lubrica-tion of solids, Part 1 and 2, Clarendon Press, Oxford, 544 pp.

Budd et al. (1979): Empirical studies of ice sliding. Journal of Glaciology, Vol.23, p.157-180.

Clarke, G.K.C. (1987): A short history of scientific inves-tigations on glaciers. Journal of Glaciology. Special Issue 1987, p.4-24.

Dahl-Jensen, D. (1985): Determination of the flow properties at Dye 3, South Greenland, by bore-hole tilting meas-urements and pertubation modelling. Journal of Gla-ciology, Vol.31, No.108, p.92-98

Drewry, D. (1986): Glacial Geologic Processes. Edward Arnold Ltd., London, 276 pp.

Echelmeyer, K. and Zhongxiang, W. (1987): Direct observation of basal sliding and deformation of basal drift at sub-freezing temperatures. Journal of Glaciology, Vol.33, No.113, p.83-98.

Emery, J.J. and Mirza, F.A. (1980): Finite Element Method Simulation of Large Ice Mass Flow Behaviour. In Tryde, P. (Ed.), Physics and Mechanics of Ice, IUTAM Symposium Copenhagen 1979, Springer Verlag, p.82-92.

Engelhardt, H.F, W.D. Harrison and B. Kamb (1978): Basal sliding and conditions at the glacier bed as revealed by borehole photography. Journal of Glaciology, No. 84, p.469-508.

Fowler, A.C. (1981): A theoretical treatment of the sliding of glaciers in the absence of cavitation. Ph.Trans.of Roy.Soc.Ser.A, Vol.298, No.1445, p.637-685.

Fowler, A.C. (1986): A sliding law for glaciers of constant viscosity in the presence of subglacial cavitation. Proc.R.Soc.London A 407, p.147-170.

Fowler, A.C. (1987): Sliding with cavity formation. Journal of Glaciology, Vol.33, No. 115, p.255-267.

Fritz, P. (1981): Numerische Erfassung rheologischer Probleme in der Felsmechanik. ETH-Diss Nr.6848, 102 pp.

Fritz, P. and Arn, Th. (1983): Benutzeranleitung "RHEO-STAUB". Inst.f.Strassen-, Eisenbahn-, und Felsbau, ETH Zürich.

Gilbert, G.K. (1910): Harriman Alaska series, Vol.3., Glaciers and glaciation. Washington DC, Smithsonian Institution.

Haeberli, W. (1976): Eistemperaturen in den Alpen. Zeitschrift für Gletscherkunde und Glazialgeologie, Bd. XI, 2, p.203-220

Haeberli, W. (1986): Factors influencing the distribution of rocky and sedimentary glacier beds. In Vischer, D. (Ed.), Hydraulic effects at the glaicer bed and related phenomena, International Workshop at Interlaken, Switzerland, VAW-Mitteilung No.90, p.48-49.

Haeberli, W. und Schweizer, J. (1988): Rhonegletscher 1850: Eismechanische Ueberlegungen zu einem historischen Gletscherstand. In Vischer, D. (Ed.), Schnee, Eis und Wasser alpiner Gletscher, VAW-Mittlg. No.94, p.59-70.

Hallet, B. (1979): A theoretical model of glacier abrasion. Journal of Glaciology No. 89, p.39-50.

Hallet, B. (1981): Glacial Abrasion and Sliding: their dependence on the debris concentration in basal ice. Annals of Glaciology No. 2, p.23-28 .

Hooke, R.L., C.F.Raymond, R.L.Hotchkiss and R.J.Gustafson (1979): Calculations of velocity and temperature in a polar glacier using the finite-element method. Journal of Glaciology, Vol.24, p.131-146.

Hutter, K. (1982): A mathematical model of polythermal glaciers and ice sheets. Geophys. Astrophys. Fluid Dynamics, Vol. 21, p.201-224.

Hutter, K. (1983): Theoretical Glaciology. D.Reidel Publishing Company, Dordrecht, Holland, 510 pp.

Iken, A. (1977): Movement of a large ice mass before breaking off. Journal of Glaciology, Vol.19, No.81, p.595-605.

Iken, A. (1978): Variations of surface velocities of some Alpine glaciers méasured at intervals of a few hours. Comparison with Arctic glaciers. Zeitschrift für Gletscherkunde und Glazialgeologie, Band 13, p.23-35.

Iken, A. (1981): The effect of the subglacial water pressure on the sliding velocity of a glacier in an idealized numerical model. Journal of Glaciology, Vol.27, No.97, p.407-421.

Iken, A., Röthlisberger, H., Flotron, A. and Haeberli, W. (1983): The uplift of Unteraargletscher at the beginning of the melt season - a consequence of water storage at the bed? Journal of Glaciology, Vol.29, No.101, p.28-47.

Iken, A. and Bindschadler, R.A. (1986): Combined measurements of subglacial water pressure and surface velocity of Findelengletscher, Switzerland: Conclusions about Drainage System and Sliding mechanism. Journal of Glaciology, Vol.32, No.110, p.101-119.

Jaeger, J.C. (1969): Elasticity, fracture and flow. 3rd ed., Chapman and Hall, London, 268 pp.

Kamb, B. (1970): Sliding Motion of Glaciers: Theory and Observation. Review of Geophysics and Space Physics, Vol.8, No.4, p.673-728.

Kamb, B. et al (1985): Glacier Surge Mechanism: 1982-1983 Surge of Variegated Glacier, Alaska. Science, 1 February 1985, Vol.227, No.4686, p.469-479.

Kamb, B. (1987): Glacier Surge Mechanism based on Linked-Cavity Configuration of the Basal Water Conduit System. Journal of Geophysical Research, No.B9, Vol.92. p.9083-9100.

Lliboutry, L. (1958): Contribution à la théorie du frottement du glacier sur son lit. Comptes Rendus Hebdomadaires des Séances de l'Académie des Sciences (Paris), Tom.247, No.3, p.318-320.

Lliboutry, L. (1968): General theory of subglacial cavitation and sliding of temperate glaciers. Journal of Glaciology, Vol.7, No.49, p.21-58.

Lliboutry, L. (1975): Loi de glissement d'un glacier sans cavitation. Annales de Geophysique, t.31, fasc.2, 1975, p.207-255.

Lliboutry, L. (1979): Local friction laws for glaciers: a critical review and new openings. Journal of Glaciology Vol.23, No.89, p.67-95.

Lliboutry, L. (1987a): Realistic, yet single bottom boundary conditions for Glaciers and Ice sheets. Journal of

Geophys.Res., Vol.92, No.B9, August 10, 1987, p.9101-9109.

Lliboutry, L. (1987b): Sliding of cold ice sheets. IAHS Publ., No.170, p.131-143.

Lliboutry, L.A. (1987c): Very slow flows of solids. Martinus Nijhoff Publishers, Dordrecht, 510 pp.

Lliboutry, L. and Duval, P. (1985): Various isotropic and anisotropic ices found in glaciers and polar ice caps on their corresponding rheologics. Ann.Geophys., 3, 2, p.207-224.

Meyssonnier, J. (1983): Ecoulement de la glace sur un lit de forme simple: expérience, modelisation, parametrisation du frottement. Diss., Publication no.438 du Laboratoire de Glaciologie, l'Universite scientifique et medicale de Grenoble, 358 pp.

Morland, L.W. (1976a): Glaciers sliding down an inclined wavy bed. Journal of Glaciology, Vol.17, No.77, p.447-462.

Morland, L.W. (1976b): Glacier sliding down an inclined wavy bed with friction. Journal of Glaciology, Vol.17, No.77, p.463-477.

Nye, J.F. (1959): The motion of ice sheets and glaciers. Journal of Glaciology, Vol.3, No.26, p.493-507.

Nye, J.F. (1965): The flow of glacier in a channel of rectangular, elliptic or parabolic cross-section. Journal of Glaciology, Vol.5, No.41, p.661-690.

Nye, J.F. (1969): A calculation on the sliding of ice over a wavy surface using a Newtonian viscous approximation. Proc.Roy.Soc., London, A 311, p.445-467.

Nye, J.F. (1970): Glacier sliding without cavitation in linear viscous approximation. Proc.Roy.Soc., London, A 315, p.381-403.

Ott, B. (1985): Effets de voute dans les glaciers. VAW-Mitteilung No.80 (Vischer, D., Ed.), 198 pp.

Paterson, W.S.B. (1981): The physics of glaciers. Pergamon Press Ltd., 2nd ed., 380 pp.

Paterson, W.S.B. (1986): The current state of research on hydraulic effects at the glacier bed, an introduction to the workshop. In Vischer, D. (Ed.), Hydraulic effects at the glaicer bed and related phenomena, International Workshop at Interlaken, Switzerland, VAW-Mitteilung No.90, p.4-14.

Paterson, W.S.B. (1987): Glaciology. Encyclopedia of Physical Science and Technology, Vol. 6, Academic Press Inc., p.240-263.

Raymond, C.F. (1978): Numerical calculation of glacier flow by finite element methods. Final techn.report for NSF Grant No. DPP74-19075, 21 pp.

Raymond, C.F. (1980): Temperate valley glaciers. In: Dynamics of snow and ice masses, edited by S.C.Colbeck, Academic Press, New York, p.80-139.

Reynaud, L. (1973): Flow of a valley glacier with a solid friction law. Journal of Glaciology, Vol.12, No.65, p.251-258.

Röthlisberger, H. (1968): Erosive processes which are likely to accentuate or reduce the bottom relief of valley glaciers. Extract from "Commission of Snow and Ice". General Assembly of Bern, Sept.-Oct.1967, p.87-97.

Röthlisberger, H. and Lang, H. (1987): Glacial Hydrology. In Gurnell, A.M. and Clark, M.J. (Eds.), In Glacio-Fluvial Sediment Transfer, Wiley, p.207-284.

Schwarz, H.R. (1984): Methode des finiten Elemente. B.G. Teubner Verlag, Stuttgart, 346 pp.

Schweizer, J. (1985, unpublished): Untersuchung der Spannungs- und der Geschwindigkeitsverteilung eines steilen, am Bett festgefrorenen Gletschers. Diplomarbeit an der ETH Zürich, 96 pp.

Schweizer, J. (1988): Numerische Analyse eines Hängegletschers am Liskamm (Walliser Alpen). In Vischer, D. (Ed.), Schnee, Eis und Wasser alpiner Gletscher, VAW-Mitteilung No.94, p.371-386.

Shoemaker, E.M. (1988): On the formulation of basal debris drag for the case of sparse debris. Journal of Glaciology, Vol.34, No.118, p.259-264.

Shreve, R.L. (1984): Glacier sliding at sub-freezing temperatures. Journal of Glaciology, Vol.30, No.106, p.341-347.

Sikonia, W.G. (1982): Finite-Element Glacier Dynamics Model applied to Columbia Glacier, Alaska. Geological Survey Professional Paper 1258-B, 74 pp.

Smith, G.D. and Morland, L.W. (1981): Viscous relations for the steady creep of polycristalline ice. Cold Regions Sci.& Tech., No.5, p.141-150.

Souchez, R.A. and Lorrain, R.D. (1987): The subglacial sediment system. In Gurnell, A.M. and Clark, M.J. (Eds.), Glacio-fluvial sediment transfer, Wiley, p.147-164.

Szeri, A.Z. (1987): Tribology. Encyclopedia of Physical Science and Technology, Vol.14, Academic Press Inc., p.70-95.

Vivian, R. and Bocquet G. (1973): Subglacial cavitation phe-
    nomena under the Glacier d'Argentière, Mont Blanc,
    France. Journal of Glaciology, No. 66, p.439-451.

Vögele, A. (1987): Die Anfänge der Gletscherforschung und der
    Glazialtheorie. Mitteilungen der Naturforschenden Ge-
    sellschaft Luzern, 29.Band, p.11-50.

Wagner, St. (1988, unpublished): Die Gletscherbewegung in der
    Umgebung eines Geländeknicks. Diplomarbeit an der ETH
    Zürich, 87 pp.

Weertman, H. (1957): On the sliding of glaciers. Journal of
    Glaciology, Vol.3, No.21, p.33-38.

Zienkiewicz, O.C. (1977). The finite element method. 3rd ed.,
    McGraw Hill, London, 787 pp.

List of Symbols   ,

General: symbols which are explained where they oocur are
only listed, if they appear again subsequently.

A	flow law parameter
a	amplitude of sine function
C	Clausius-Clapeyron constant
c	aeral concentration of rock fragments
A_a	apparent area of contact between ice and bed rock
A_r	real contact area between ice and bed rock
A_c	separated area
E	elasticity constant (Young's modulus)
F	contact force between rock fragment and the bed
f	shape factor
g	gravity constant
g_i	vector gravity acceleration
h	glacier thickness
i	counting index
k	wave number
$k_{i,r}$	thermal conductivity of ice, rock
L	latent heat of fusion
l	characteristic length
m	exponent in sliding law
m_i	unit normal vector
m_*	measure of roughness (Lliboutry, 1970)
N	effective pressure
$\bar{N}$	flow law parameter (Kamb, 1970)
n	flow law paramter
n_i	unit normal vector
p	pressure (general)
P_o	ice overburden pressure
P_w	water pressure
P_s	separation pressure
P_c	critical pressure
P	debris concentration
p_n	normal stress

Δp_{max}	amplitude of normal stress
p'	constant contribution of the normal stress in the case of friction
$\Delta p'$	fluctuating contribution of the normal stress in the case of friction
q	flux (general)
R	radius of rock particle
r	roughness of the glacier bed (= a/λ)
s	bed separation parameter
t	time variable
t_{ij}	stress tensor
t'_{ij}	stress deviator
t'_{II}	second invariant of stress deviator
u_i	velocity vector
u	velocity vector component
u_b	basal sliding velocity
u_d	velocity due to internal deformation
u_s	surface velocity
U_{bf}	basal sliding velocity in the case of friction
U_{bw}	basal sliding velocity in the case of bed separation
U_{bwf}	basal sliding velocity in the case of bed separation and friction
U_t	velocity at the top of the modelled section
v	velocity vector component
v_n	velocity normal to the sliding interface
W	weight
x,y,z	cartesian coordinates
y_b	transverse coordinate describing the base
α	mean inclination angle of basal surface
β	inclination angle of basal surface
Γ	constant in sliding law (Lliboutry, 1975)
δ_{ij}	Kronecker delta
$\dot{\varepsilon}_{ij}$	strain rate tensor
η	viscosity
λ	wavelength
λ_*	transition wavelength
μ	coeffient of friction

ν	Poisson's ratio
ξ	coeffient of bed geometry (Hallet, 1981)
ρ	mass density
$\sigma_{x,y}$	stress tensor component
τ	shear stress
τ_b	effective basal shear stress
τ_f	frictional drag

Acknowledgements